E12-11-108A/E12-10-006A

Target Single Spin Asymmetry Measurements in the Inclusive Deep-Inelastic $\vec{N}(e,e')$ Reaction on Transversely Polarized Proton and Neutron (^{3}He) Targets using the SoLID Spectrometer

June 2, 2014

T. Averett (Spokesperson/Contact), H. Yao (Spokesperson)
College of William & Mary, Williamburg, VA

A. Camsonne (Spokesperson)
Jefferson Lab, Newport News, VA

X. Jiang (Spokesperson)
Los Alamos National Laboratory, Los Alamos, NM

N. Liyanage (Spokesperson)
University of Virginia, Williamsburg, VA

This proposal will be submitted to the SoLID and Hall A collaborations for approval. We are grateful to the many members of these collaborations who have already expressed their support for this proposal and for the support of the SoLID transversity collaborators. In lieu of a long list of potential collaborators, this experiment is open to all members of these collaborations.

Abstract

We propose to carry out measurements of the transversely polarized target Single Spin Asymmetry (SSA) from inclusive $\vec{N}(e,e')$ scattering using transversely polarized NH_3 and ^{3}He targets in Deep-Inelastic-Scattering kinematics using 11 and 8.8 GeV electron beams. This experiment will be carried out in Hall A using the large acceptance solenoid spectrometer (SoLID). There are two approved experiments using these transversely polarized targets to measure semi-inclusive charged pion production, $\vec{N}(e,e'\pi^{\pm})$ to study the nucleon transversity distributions. This experiment will run concurrent with these two experiments using a singles trigger to collect the high statistics needed for a precise measurement. The SSA, A_{UT}, is expected to have a $\sin(\phi_S)$-dependence, where ϕ_S is the azimuthal angle of the target polarization relative to the electron plane and perpendicular to the virtual photon direction. At Born level, the asymmetry is identically zero due to time-reversal invariance and parity conservation. However, it can be non-zero when two-photon exchange is included and therefore provides fertile ground for studying this processes in the absence of a large Born contribution. The contribution to the intermediate state of the nucleon during two-photon exchange must be modeled using e.g. parton-model predictions in the DIS and predictions currently range from 10^{-4} to 10^{-2} with a positive or negative sign depending on model input and target nucleon. A recent measurement made using a 5.9 GeV beam in Hall A measured a neutron asymmetry of $(-1.09 \pm 0.38) \times 10^{-2}$ which is non-zero at the 2.89σ level. This experiment proposed here will make measurements for both protons and neutrons with statistical uncertainties of $\sim 10^{-4}$ at $Q^2 = 1.5$ GeV^2 up to $\sim 10^{-3}$ at $Q^2 = 7.5$ GeV^2 with $W > 2$ GeV and $0.05 < x < 0.65$.

We request no beam time for this measurement beyond that approved for the semi-inclusive transversity measurements. We request approval of this experiment from the Jefferson Lab PAC and the SoLID and Hall A collaborations. We request technical support from Jefferson Lab and the SoLID collaboration to optimize the singles trigger and PID to maximize electron statistics, and to achieve systematic uncertainties at the $\sim 10^{-4} - 10^{-3}$ level.

Contents

1 Introduction

1.1 Transversely Polarized Target Single Spin Asymmetry

Understanding the internal structure of nucleon and nucleus in terms of quarks and gluons, the fundamental degrees of freedom of Quantum Chromodynamics (QCD), has been and still is the frontier of subatomic physics research. QCD as a theory of the strong interaction has been well-tested by observables with a large momentum transfer in high energy experiments.

The past decade has seen a resurrection of interest in two-photon exchange in electron-nucleon scattering. This is primarily due to the realization that inclusion of the two-photon-exchange amplitude can partially reconcile the discrepancy between the Rosenbluth separation and the polarization-transfer methods for extracting the Q^2-dependence of the proton elastic form factor ratio, G_E^p/G_M^p [1–8]. As the precision of nucleon structure measurements improves, it is important to understand the dynamics of the two-photon-exchange processes. Assuming conservation of parity and time-reversal invariance, the target single-spin asymmetry (SSA) in (e, e') from a target polarized normal to the electron scattering plane is strictly zero at Born level [9], but can be non-zero when interference between one- and two-photon exchange processes is included (Fig. 2).

Consider the inelastic scattering of an unpolarized electron from a target nucleon with vector spin $\vec{S}$, oriented perpendicular (transversely polarized) to the incident electron 3-momentum $\vec{l}$, with normalization $|\vec{S}| = 1$. Requiring conservation of the electromagnetic current and parity, the differential cross section, $d\sigma$, for inclusive scattering is written as [9–11]

$$d\sigma(\phi_S) = d\sigma_{UU} + \frac{\vec{S} \cdot (\vec{l} \times \vec{l'})}{|\vec{l} \times \vec{l'}|} d\sigma_{UT} = d\sigma_{UU} + d\sigma_{UT} \sin\phi_S, \qquad (1)$$

where $\vec{l'}$ is the 3-momentum of the scattered electron, and $d\sigma_{UU}$ and $d\sigma_{UT}$ are the cross sections for an unpolarized electron scattered from an unpolarized and transversely polarized target, respectively.

The coordinates are defined according to the Trento conventions [12] as shown in Fig. 1 with the angle ϕ_S between the lepton plane and $\vec{S}$.

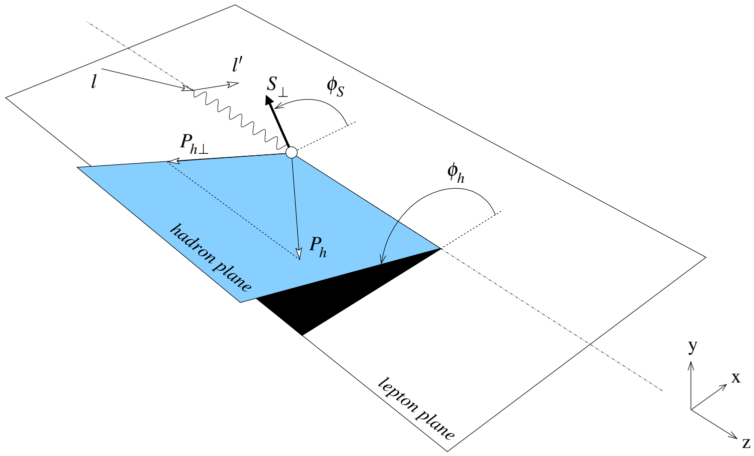

Figure 1: The definition of ϕ_S according to the Trento convention. Here, $S_\perp$ represents the spin of the target which is transverse to the virtual photon direction (z).

We define the SSA as

$$A_{UT}(\phi_S) = \frac{d\sigma(\phi_S) - d\sigma(\phi_S + \pi)}{d\sigma(\phi_S) + d\sigma(\phi_S + \pi)} = A_y \sin\phi_S. \tag{2}$$

The quantity $A_y \equiv \frac{d\sigma_{UT}}{d\sigma_{UU}}$ can be extracted by measuring the ϕ_S-dependence of $A_{UT}(\phi_S)$, or by measuring the SSA for a target polarized normal to the lepton plane.

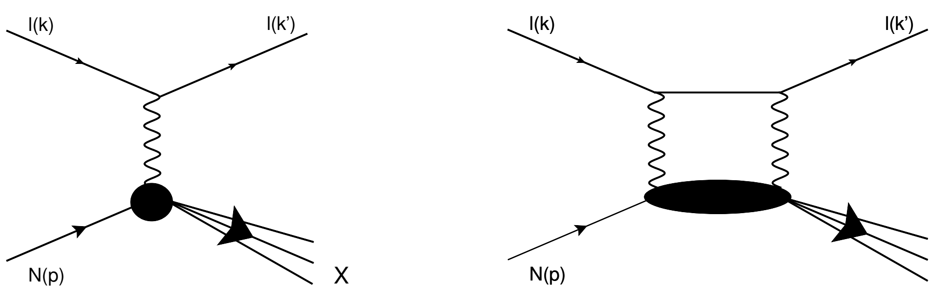

Figure 2: Interference between one- and two-photon exchange in $\vec{N}(e, e')$ allows the possibility of a non-zero target SSA. Here, l is the lepton with incident and outgoing 4-momenta k and k', respectively. N is the nucleon with initial 4-momentum p.

Considering only the one-photon-exchange amplitude, $\mathcal{M}_{1\gamma}$, we can write $d\sigma_{UU} \propto \mathcal{R}e(\mathcal{M}_{1\gamma}\mathcal{M}^*_{1\gamma})$ and $d\sigma_{UT} \propto \mathcal{I}m(\mathcal{M}_{1\gamma}\mathcal{M}^*_{1\gamma})$, where $\mathcal{R}e$ ($\mathcal{I}m$) stands for the real (imaginary) part. However time-reversal invariance requires that $\mathcal{M}_{1\gamma}$ be real and so at order α^2_{em}, $d\sigma_{UU}$ can be non-zero but $d\sigma_{UT}$ must be zero. When one includes the (complex) two-photon-exchange amplitude, $\mathcal{M}_{2\gamma}$, the contribution to the asymmetry from one- and two-photon interference is $d\sigma_{UT} \propto \mathcal{I}m(\mathcal{M}_{1\gamma}\mathcal{M}^*_{2\gamma})$ which can be non-zero at order α^3_{em}. The two-photon exchange process forms a loop with the nucleon intermediate state and contains the full response of the nucleon (see Fig. 2).

1.2 Summary of Existing Measurements and Theory for A_y

1.2.1 Proton Asymmetry in the Resonance Region

Here we summarize the existing data from polarized proton targets. For protons, the first measurement of A^p_y was done in 1968 at CEA [14]. Electrons were scattered from an alcohol/water target containing protons with an average polarization $\sim 20\%$. Three invariant photon-hadron masses were studied, W =1236, 1512 and 1688 MeV, with $Q^2 = 0.2 - 0.7$ GeV^2. Results were consistent with zero at the $4\times\ 10^{-2}$ level. In 1969 a measurement at SLAC [15] was made using both e^- and e^+ scattering in the resonance region with $Q^2 = 0.4 - 1.0$ GeV^2. A butanol target provided protons with a polarization of $\sim 20\%$. Results were consistent with zero at the few $\times 10^{-2}$ level.

A theoretical calculation for A^p_y at $W = 1232$ MeV [10] treated the intermediate state as purely elastic and predicted $A^p_y \sim 0.75 \times 10^{-2}$ at $Q^2 = 0.6$ GeV^2.

1.2.2 Theoretical Predictions in DIS

There are two parton-model predictions for the two-photon exchange contribution to A_y for protons and neutrons in DIS. The first, by A. Afanasev *et al.* [11] assumes the scattering is dominated by two-photon exchange with a single quark. Two possible contributions that may give a non-zero asymmetry due to higher-twist effects are presented. The first possibility is a quark-helicity-conserving interaction which gives a non-zero asymmetry when the active quark is allowed to interact with the spectator system.

The authors argue that the other possibility, in which the quark helicity flips due to interaction with QCD vacuum fields, is the dominant contribution. These interactions are effectively described by a constituent quark mass times $\sum_f e_f^3 h_f(x, Q^2)$ where e_f is the charge of a quark with flavor f and $h_f(x)$ is the quark transversity distribution. They predict $A_y^n \sim 10^{-4}$ and $A_y^p \sim -2 \times 10^{-4}$ at $x \sim 0.3$ and $Q^2 = 2.0$ GeV^2. See Figure 3.

In the second prediction, A. Metz *et al.* [13] argue that the DIS asymmetry is dominated by the process in which one of the photons couples to an active quark and the other couples to one of the quarks in the spectator di-quark system. The interaction with the di-quark system is related to the quark-gluon-quark correlators, T_F^f, for quarks of flavor f. For the proton they predict an asymmetry with magnitude $< 10^{-2}$ that crosses zero in the mid-x range. For the neutron, the case is more interesting. The magnitude of A_y^n is predicted to be $\sim 10^{-2}$, but is negative when the T_F are obtained using the Sivers distributions from semi-inclusive DIS (SIDIS) and positive when the T_F are extracted from hadron-hadron collisions when a final state meson is detected (referred to as KQVY). This sign disagreement is currently one of the important puzzles in hadronic spin physics [13]. Results are shown in Figure 4. For reference, note that Metz *et al.* use a different sign convention which means that their asymmetries should be multiplied by (-1) for consistency with the Trento convention.

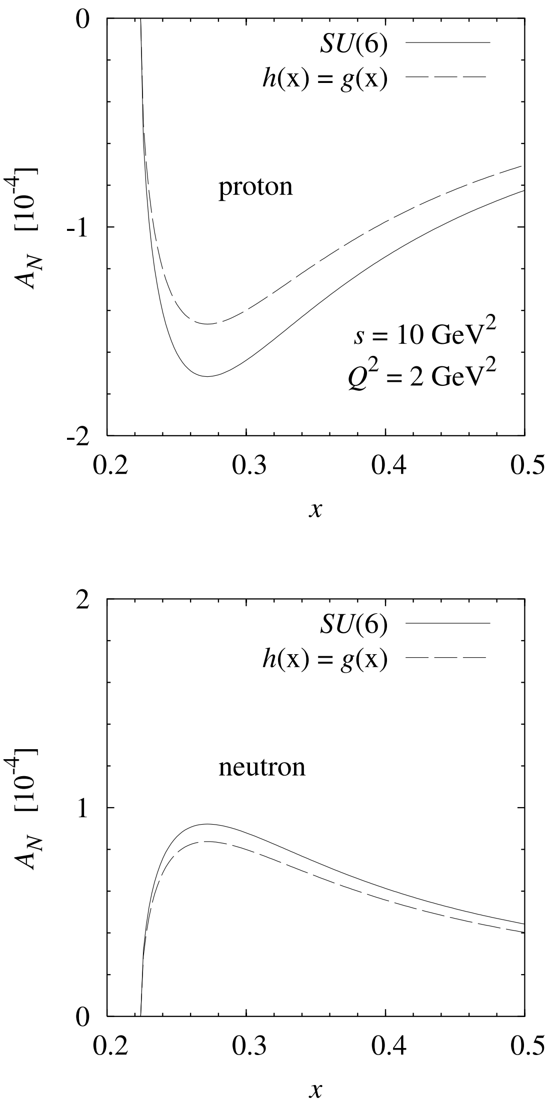

Figure 3: Model predictions from two-photon exchange for the target normal asymmetry A_N (A_y) in DIS kinematics for proton (upper) and neutron (lower) from Afanasev *et al.* [11]. In this model it is assumed that the primary contribution comes from exchange of the two photon with a single quark that is interacting with the remainder of the nucleon.

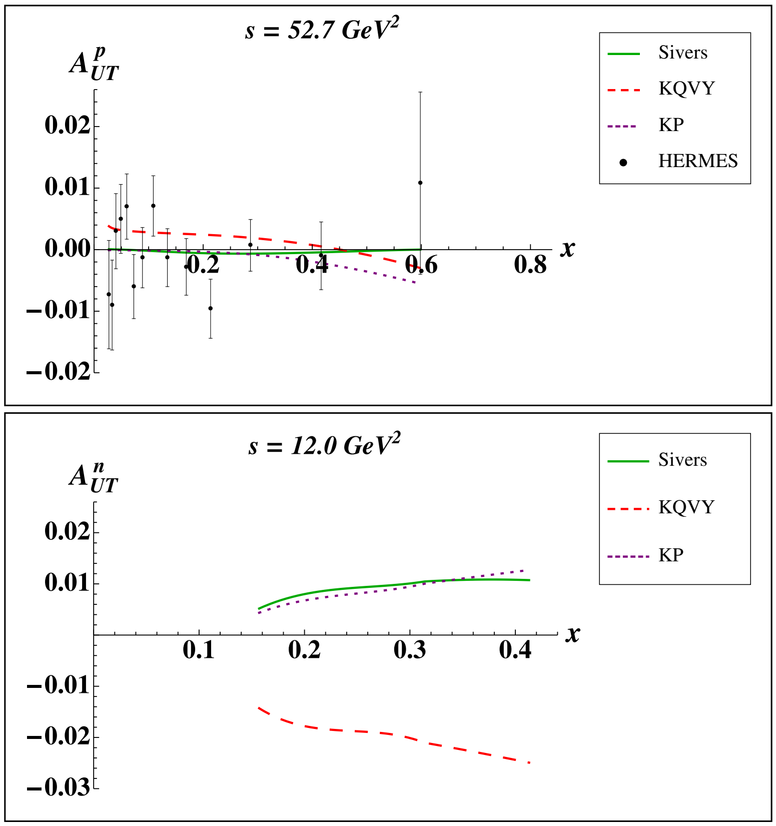

Figure 4: Model predictions from two-photon exchange for the target normal asymmetry A_{UT} (A_y) in DIS kinematics for protons (upper) and neutrons (lower) by Metz *et al.* [13]. Here it is assumed that the asymmetry is dominated by the process where one photon is exchanged with a single quark and the other interacts with the remaining di-quark system. The sign of the prediction depends on the choice of model input and is an important open question in this field. Note that due to the use of a different sign convention, the asymmetries shown here should be multiplied by (-1) for consistency with the Trento convention.

An additional contribution to $d\sigma_{UT}$ at $\mathcal{O}(\alpha_{em}^3)$ may arise from interference between real photon emission (bremsstrahlung) by the electron and the hadronic system. The two-photon exchange contribution and bremsstrahlung interference processes are show in Figure 5 [11]. The authors point out that for scattering from a point-like particle, the amplitudes are real (non-absorptive) and this contribution is zero. In a paper by M. Schlegel [16] a parton model formalism for calculating the contribution to A_{UT} from both diagrams in Figure 5 is given. Contributions from the bremsstrahlung diagrams are argued to be negligible except for a possible contribution from a hard fermionic pole which has not yet been calculated. The compelling result of this paper is a complete, well-behaved parton model formalism that may be used to predict the contributions of both pieces. This provides fertile ground for measurements of A_y to be used to study multi-parton correlations. We look forward to future theoretical predictions using this model. In summary, a measurement of A_{UT} provides direct access to nucleon structure including multi-parton correlations without experimental suppression from a dominant Born contribution.

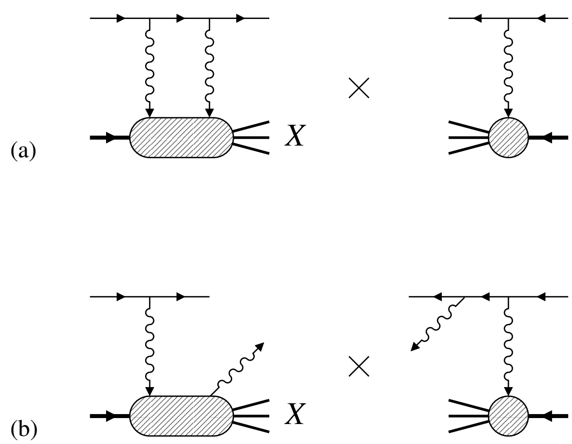

Figure 5: QED processes contributing to the transverse target spin dependence of the inclusive eN cross section at $\mathcal{O}(\alpha^3)$. (a) Interference of one-photon and two-photon exchange. (b) Interference of real photon emission (bremsstrahlung) by the electron and the hadronic system. Figure taken from Afanasev *et al.* [11].

1.2.3 Proton DIS Measurement at HERMES

The only measurement of A_y^p using deep-inelastic scattering (DIS) was made at DESY by the HERMES collaboration [17]. Both e^- and e^+ with energy 27.6 GeV were scattered from a polarized hydrogen target with average polarization $\sim 75\%$. Particles were detected over $0.007 < x_B < 0.9$, $0.25 < Q^2 < 20$ GeV^2 and $\phi_S = 0 - 2\pi$. Results for A_y^p for Q$^2 > 1$ GeV^2 are consistent with zero at the $\sim 10^{-3}$ level. See Figure 6.

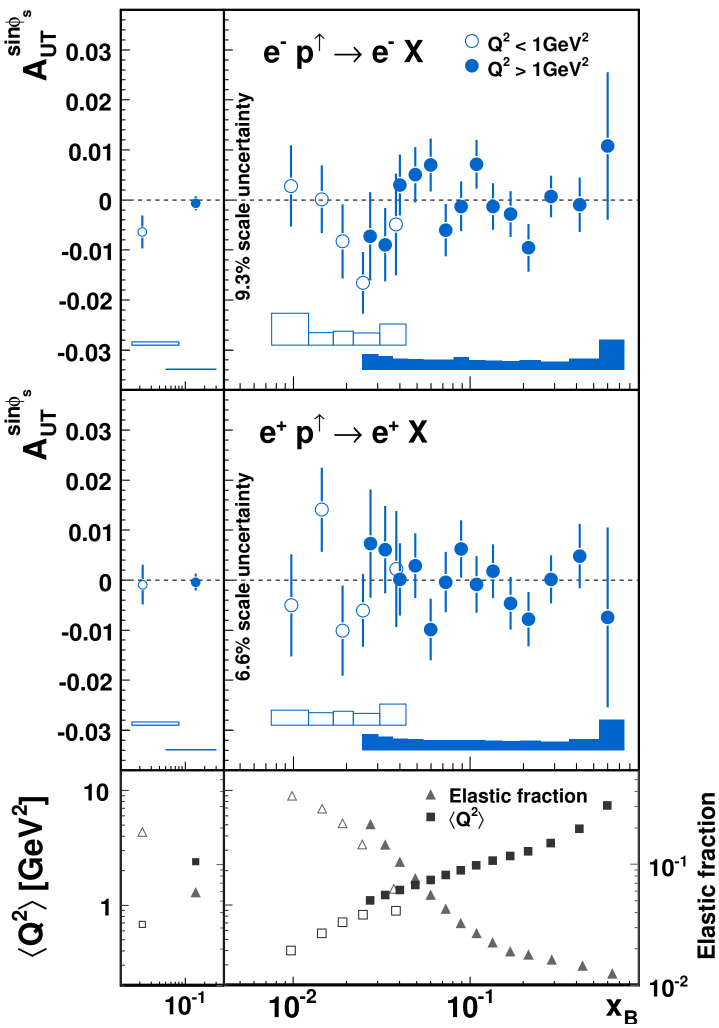

Figure 6: The x dependence of the $\sin\phi_S$ amplitudes, $A_{UT}^{\sin\phi_S}$ ($= A_y^p$) measured with an electron beam (top) and a positron beam (center). The open (closed) circles identify the data with $Q^2 < 1$ GeV^2 ($Q^2 > 1$ GeV^2). The error bars show the statistical uncertainties, while the error boxes show the systematic uncertainties. The asymmetries integrated over x are shown on the left. Bottom panel: average Q^2 vs. x from data (squares), and the fraction of elastic background events to the total event sample from a Monte Carlo simulation (triangles) [17].

1.2.4 Recent Neutron DIS Measurement at Jefferson Lab

Jefferson Lab experiment E07-013 was a measurement of the neutron SSA, A_y^n, in DIS that was made in 2012 using a transversely polarized ^{3}He target and two independent spectrometers in Hall A [18]. This will hereafter be referred to as the "6 GeV A_y^n measurement". The ϕ_S-dependent asymmetries were measured using inclusive scattering of unpolarized electrons from a ^{3}He target polarized either vertically ($\phi_S \sim \pm 90°$) or transversely ($\phi_S \sim 0°,\ 180°$) in the lab frame. A_y was obtained by fitting the ϕ_S dependence according to Eqn. 2. The nuclear ground state of ^{3}He is dominated by the configuration in which the spins of two protons are anti-aligned, which means that the spin is mostly carried by the neutron, effectively providing a polarized neutron target. Note that the results presented below for this measurement used a coordinate system similar to Figure 1 but with the the$z$-axis along the direction of $\vec{k}$. The transformation between the two sets of coordinates is straightforward.

An electron beam with energy 5.889 GeV and average current 12 μA was incident on polarized ^{3}He gas with density $\sim$ 10 amg contained in a 40 cm-long cylindrical aluminosilicate glass cell. The beam was rastered in a 3×3 mm^2 pattern to reduce the possibility of cell rupture and localized de-polarization. Polarization of the ^{3}He nuclei was achieved via Spin-Exchange Optical Pumping (SEOP) with a hybrid alkali-metal mixture of Rb and K [19]. The polarization direction was reversed every 20 minutes using adiabatic fast passage nuclear magnetic resonance (NMR). With each spin-flip, the NMR signals were used to measure the relative polarization. Absolute calibration was done periodically throughout the run using electron paramagnetic resonance [20]. The average polarization was 55% with a 5% relative uncertainty. The total luminosity downstream of the target was measured during each 20-minute target polarization state using eight Lucite/PMT detectors placed symmetrically around the beam line. The average luminosity asymmetry for the experiment was $(38 \pm 12) \times 10^{-6}$ which is negligible compared to our measured raw asymmetries of $\sim 10^{-3}$.

Scattered electrons were detected using the Hall A BigBite detector package [21] at $+30°$ (beam-right) and the left Hall A High Resolution Spectrometer (LHRS) at $-16°$ [22]. The BigBite package includes a dipole magnet for momentum separation, 3 sets of multi-wire drift chambers for track reconstruction, and a lead-glass electromagnetic calorimeter for particle identification (PID) with pre-shower and shower layers sandwiching a scintillator plane for providing timing information. The useful momentum coverage of BigBite was $0.6 < p < 2.5$ GeV with an average solid angle acceptance of 64 msr. The corresponding ϕ_S coverage is $\sim 60°$ for each target polarization configuration. The LHRS consists of two sets of drift chambers for tracking, two scintillator planes for the trigger, and gas Cherenkov and lead-glass shower detectors for PID. The central momentum of the LHRS was 2.35 GeV with a momentum coverage of $\pm$ 4.5%. The solid angle acceptance was $\sim$ 6 msr with $\sim 7°$ ϕ_S coverage. Optics for both detectors were calibrated using elastic e^- scattering from hydrogen and multi-foil carbon targets. Angular reconstruction in both detectors was calibrated using a sieve slit placed in front of each spectrometer. The angular resolution in BigBite was < 10 mrad and the the resolution of the reconstructed momentum was $< 1\%$.

Raw asymmetries for each data bin were formed as

$$A^{e^-}_{raw}(\phi_S) = \frac{1}{P_{target}} \frac{Y^{\uparrow}_{raw}(\phi_S) - Y^{\downarrow}_{raw}(\phi_S + \pi)}{Y^{\uparrow}_{raw}(\phi_S) + Y^{\downarrow}_{raw}(\phi_S + \pi)} \tag{3}$$

where the raw yields, $Y^{\uparrow(\downarrow)}_{raw}$, are the number of particles, N, observed in the target spin "up" ("down") state that pass all data cuts for electrons, normalized by accumulated charge, Q, and DAQ livetime, LT:

$$Y^{\uparrow(\downarrow)}_{raw} = \frac{N^{\uparrow(\downarrow)}_{raw}}{Q^{\uparrow(\downarrow)} \cdot LT^{\uparrow(\downarrow)}} = \frac{N^{\uparrow(\downarrow)}_{e^-} + N^{\uparrow(\downarrow)}_{\pi^-} + N^{\uparrow(\downarrow)}_{e^+}}{Q^{\uparrow(\downarrow)} \cdot LT^{\uparrow(\downarrow)}}. \tag{4}$$

The terms $N_{\pi-}$ and N_{e+} represent pion and pair-produced electron backgrounds that pass the good-electron cuts and P_{target} is the target polarization. The ϕ_S angle is defined for the spin up state, and changed by 180° ($\phi_S + \pi$) when the target spin was flipped.

The dominant background passing the data cuts in BigBite were photo-induced electron-positron pairs. The positrons were cut from the data by requiring particles with negative charge. However, the pair-produced electrons are indistinguishable from the desired DIS electrons. A direct measurement of the pair-produced electron contamination was made by reversing the polarity of the BigBite magnet and calculating the positron yield under conditions identical to the normal data collection. Since photons are mostly produced from neutral pion decay, the contamination decreased with increasing momentum, see Table 1. This also explains why this type of background in the LHRS (central momentum of 2.35 GeV) is negligible. Negative pions were also a source of contamination. Their contributions to the BigBite data were accounted for by fitting the pre-shower energy spectrum. Likewise, the positron data sample was contaminated by positive pions. The positive pion contamination was estimated based on the negative pion contamination. A GEANT-based Monte Carlo simulation of the BigBite spectrometer was used to study the differences between the π^+ and π^- contaminations. Data from the LHRS were relatively free of background contamination due to the choice of kinematics and exceptional PID.

Due to the large acceptance of the BigBite spectrometer, asymmetries for each type of background particle (A^{π^-}, $A^{e^+}_{raw}$, and A^{π^+}) were obtained from the data in the same way as $A^{e^-}_{raw}$ but with different selection cuts: i) the positrons were selected using the same cuts as electrons except for the particle charge; ii) the pions were selected using the same cuts as electrons/positrons except for requiring a pre-shower energy deposition under 150 MeV. Corrections were made to the asymmetry via:

$$A^{e^-} = \frac{A^{e^-}_{raw} - f_1 A^{\pi^-} - f_4\,(1-f_3)\,\frac{A^{e^+}_{raw} - f_5 A^{\pi^+}}{1-f_5}}{1 - f_1 - f_4\,(1-f_3)}, \tag{5}$$

where the coefficients, f_i, give the fractions of mis-identified particles and are defined as:

$$\begin{aligned} f_1 &= Y^{\pi^-}_{neg}/(Y^{e^-}_{neg} + Y^{\pi^-}_{neg}) \\ f_3 &= Y^{\pi^+}_{pos}/(Y^{e^+}_{pos} + Y^{\pi^+}_{pos}) \\ f_4 &= (Y^{e^+}_{pos} + Y^{\pi^+}_{neg})/(Y^{e^-}_{neg} + Y^{\pi^-}_{neg}) \\ f_5 &= Y^{\pi^+}_{neg}/(Y^{e^+}_{neg} + Y^{\pi^+}_{neg}). \end{aligned} \tag{6}$$

The *pos* and *neg* subscripts indicate the polarity of the BigBite magnet (standard running conditions are *neg*).

A small quantity of unpolarized N_2 was used in the ^{3}He target-cell to improve the efficiency of the optical pumping. The asymmetry was corrected by a dilution factor defined as:

$$\eta_{N_2} \equiv \frac{1}{1 + \left(\frac{\rho_{N_2}}{\rho_{^3\mathrm{He}}}\right)\left(\frac{\sigma_{N_2}}{\sigma_{^3\mathrm{He}}}\right)} \tag{7}$$

where ρ are the densities and σ are the unpolarized cross-sections for each gas. The ratio of densities is taken from the target cell filling data. The cross-section ratio is determined experimentally by inelastic scattering from a reference cell filled with known densities of either N_2 or ^{3}He. The dilution factors for BigBite measured for T1 and T6 triggers agree with each other. The final dilution was determined by combining results from T1 and T6 according to their statistical contribution, giving $\eta \sim 0.9$ for all kinematics with an uncertainty of $\sim 2\%$. The dilution factor for the LHRS was determined to be 0.851 ± 0.018. The ^{3}He asymmetries from BigBite T1, T2 and T6 triggers were extracted independently and were consistent with each other within the statistical uncertainties for each bin. The final ^{3}He asymmetries were obtained by combining the results from the T1, T2 and T6 asymmetries according to their statistical contribution.

Neutron asymmetries were obtained from the ^{3}He asymmetries using the effective polarizations of the proton and neutron in polarized ^{3}He using [23],

$$A_y^{^3\mathrm{He}} = (1 - f_p) P_n A_y^n + f_p P_p A_y^p \tag{8}$$

Here, $P_n = 0.86^{+0.036}_{-0.02}$ ($P_p = -0.028^{+0.009}_{-0.004}$) is the effective neutron (proton) polarization [24].

The proton dilutions of ^{3}He for BigBite, $f_p = \frac{2\sigma_p}{\sigma_{^3\mathrm{He}}}$, were measured for the T1 and T6 triggers using the yields from unpolarized hydrogen and ^{3}He targets and are consistent with each other. The final dilutions, which varied between $0.75 - 0.82$, with uncertainties of $0.02 - 0.08$, were determined by combining the T1 and T6 results according to their statistical contribution. Neutron asymmetries were calculated separately for each trigger type and combined according to their statistical contributions. The proton dilution for the LHRS was 0.715 ± 0.007. A value of $A_y^p = (0 \pm 3) \times 10^{-3}$ was used in Eqn. 8 based on the HERMES measurements [17]. External radiative corrections were applied to both the BigBite and LHRS data using a Monte Carlo simulation that included detailed modeling of geometry and material in the target and spectrometers. No correction was made on the asymmetries since the radiative corrections to the two-photon exchange process are not yet available and the phase space of this measurement is limited.

The dominant systematic uncertainty for BigBite is from background contamination, the largest of which is from pair-produced electrons, see Table 1. The π^- contamination in the T6 triggers ranges from 0.5 to 2.0% (rel.) from the lowest to highest W bin, respectively. The uncertainties on the contamination are $\sim 0.5\%$, which were estimated using the difference between information from the Monte Carlo simulation and contamination estimation

Detector	W GeV	x	Q^2 GeV^2	$A_y^n \pm$ (stat) $\pm$ (sys) ($\times 10^{-2}$)
BigBite	1.72	0.65	3.98	$-0.55 \pm 1.81 \pm 0.36$
BigBite	2.17	0.46	3.24	$-3.87 \pm 1.55 \pm 0.58$
BigBite	2.46	0.34	2.65	$-3.89 \pm 0.96 \pm 0.53$
BigBite	2.70	0.24	2.08	$-1.08 \pm 1.18 \pm 0.69$
BigBite	2.89	0.17	1.58	$-3.84 \pm 2.00 \pm 2.42$
LHRS	2.54	0.16	1.05	$-0.64 \pm 0.41 \pm 0.09$

Table 1: Kinematics and results for neutron asymmetries with statistical and systematic uncertainties. The BigBite spectrometer was set at a fixed angle and central momentum and data were divided into the five kinematic bins.

based on data. The uncertainties associated with backgrounds contribute to both the asymmetries and dilution factors. The final results were extracted taking into account the full correlation of these uncertainties. Other BigBite systematic uncertainties include the detector acceptance eq (1.2×10^{-4}), detector response drift (9×10^{-5}), and livetime asymmetry (6×10^{-5}). For the LHRS, systematic uncertainties include the livetime asymmetry (6×10^{-5}) and tracking efficiency (7×10^{-5}). The correction to the LHRS asymmetry due to pair-produced electrons is 1.56 $\times10^{-4}$ with a 100% relative uncertainty. Systematic uncertainties from the polarized target include target polarization and misalignment (5%), and luminosity fluctuations (1.2×10^{-5}).

The neutron A_y results are presented in Table 1 and are shown in Fig. 7. The asymmetry is generally negative and non-zero across the measured kinematic range. At the largest value of W, the systematic uncertainty is quite large due to the uncertainty in the pair-produced electron contamination. In order to evaluate how much the data disfavors the zero-asymmetry hypothesis in the DIS region, the average asymmetry was calculated for the data with $W > 2.0$ GeV. Because the systematic uncertainties of the BigBite points are mostly due to background contamination, they were assumed to be fully correlated, and uncorrelated with the LHRS point. The final average neutron asymmetry in the DIS region and its total experimental uncertainty are determined to be $(-1.09 \pm 0.38) \times 10^{-2}$, which is non-zero at the 2.89σ level. The data are in good agreement with the two-photon exchange prediction by A. Metz *et al.* [13], $A_y^n \sim -10^{-2}$, that uses model input from the semi-inclusive DIS Sivers distribution.

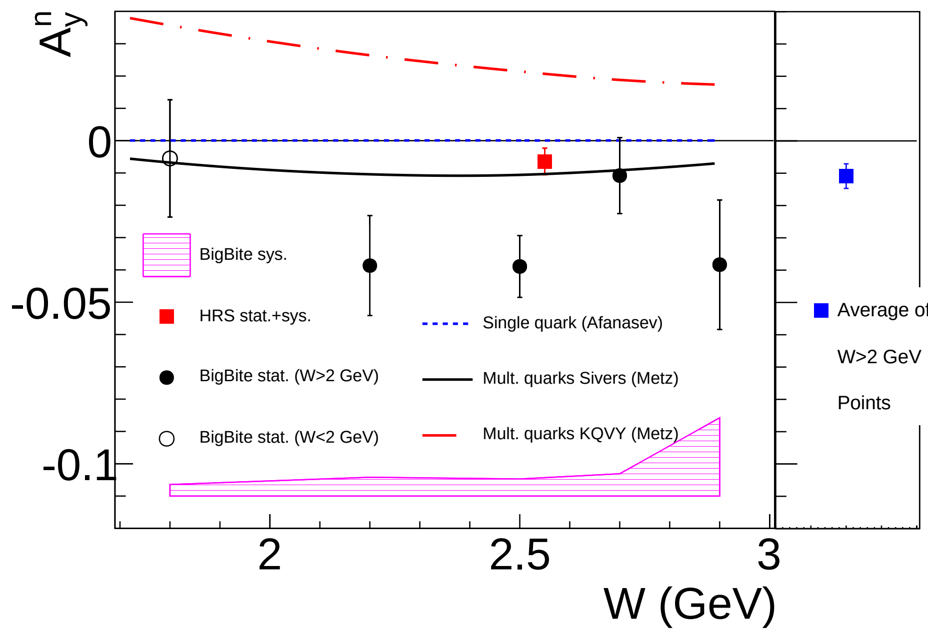

Figure 7: Neutron asymmetry results (color online). **Left panel:** Solid black data points are DIS data ($W > 2$ GeV) from the BigBite spectrometer; open circle has $W = 1.72$ GeV. BigBite data points show statistical uncertainties with systematic uncertainties indicated by the lower solid band. The square point is the LHRS data with combined statistical and systematic uncertainties. The dotted curve near zero (positive) is the calculation by A. Afanasev *et al.* [11], The solid and dot-dashed curves are calculations by A. Metz *et al.* [13] (multiplied by -1). **Right panel:** The average measured asymmetry for the DIS data with combined systematic and statistical uncertainties.

1.3 Overview of the Proposed Experiment

We propose to make precision measurements of the target single spin asymmetry (SSA) in the inclusive deep-inelastic $\vec{N}(e, e')$ reaction during the two approved SIDIS (transversity) experiments that will measure the semi-inclusive reaction $\vec{N}(e, e'\pi^{\pm})$ using polarized proton (NH_3) and neutron (^{3}He) targets and the SoLID spectrometer in Hall A [25, 26].

The layout of the SoLID-SIDIS experiments are shown in Fig. 8 and Fig. 9. For the experiment proposed here, we will run concurrently with the SIDIS measurements using the same target and spectrometer configurations.

For the proton measurement, a 3 cm long upgraded NH_3 target transversely polarized will be used with a 100 nA electron beam with energies of 8.8 and 11 GeV. For the neutron measurement, polarized ^{3}He gas is contained in a 40 cm long cylindrical glass cell. The beam current will be 15 μA with energy 8.8 and 11 GeV.

Because the asymmetry is predicted to be as small as 10^{-4}, precision measurements require both a high luminosity and a large acceptance detector to maximize statistics. Azimuthal acceptance covering 2π is needed to accurately determine the ϕ_S dependence of A_{UT}. The goal is to determine A_y for both proton and neutron with a statistical precision of $10^{-4} - 10^{-3}$ (kinematic dependent) over a broad range of x and $1.5 < Q^2 < 7.5$ GeV^2 ($0.05 < x < 0.65$, $W > 2$ GeV) by measuring the ϕ_S-dependence of A_{UT}. Systematic uncertainties will be kept to the $\sim 10^{-4} - 10^{-3}$-level.

The detector for this experiment with be the SoLID spectrometer proposed for 5 previous experiments including the transversity measurements mentioned above. It is a large acceptance solenoidal detector designed to measure at high rate over a broad kinematic range allowing one to study reactions where the cross sections and/or symmetries are small such as large Q^2 DIS studies of nucleon structure as well as parity-violating DIS where extremely high rate is necessary to make precision measurements of very small asymmetries. The spectrometer will be made using the CLEO magnet with essentially two detector systems, one at forward scattering angles and one for larger scattering angles, to be described in the next section. The singles trigger rate in the detector will be as large as 80-100 kHz (DAQ limited). Tracking will be accomplished using a 6 plane GEM detector system. Particle ID (PID) will be accomplished with light and heavy gas Cherenkov detectors as well as segmented Shashlyk-type electromagnetic calorimeters. Taking advantage of the 2π azimuthal acceptance, the $8 - 24^{\circ}$ polar acceptance, the

0.4-11 GeV momentum acceptance and the high-rate DAQ, this is the ideal detector for this type of measurement.

2 The SoLID Spectrometer

This section gives an overview of the relevant parameters for the SoLID spectrometer. These requirements were taken from the recent SoLID pre-CDR document [27]. Here we attempt to emphasize the requirements from the SIDIS sections of that document that are relevant for the measurements proposed here. No additional requirements beyond optimizing the singles trigger have been added to the current SoLID design. A schematic view of the detector is shown in Figure 8.

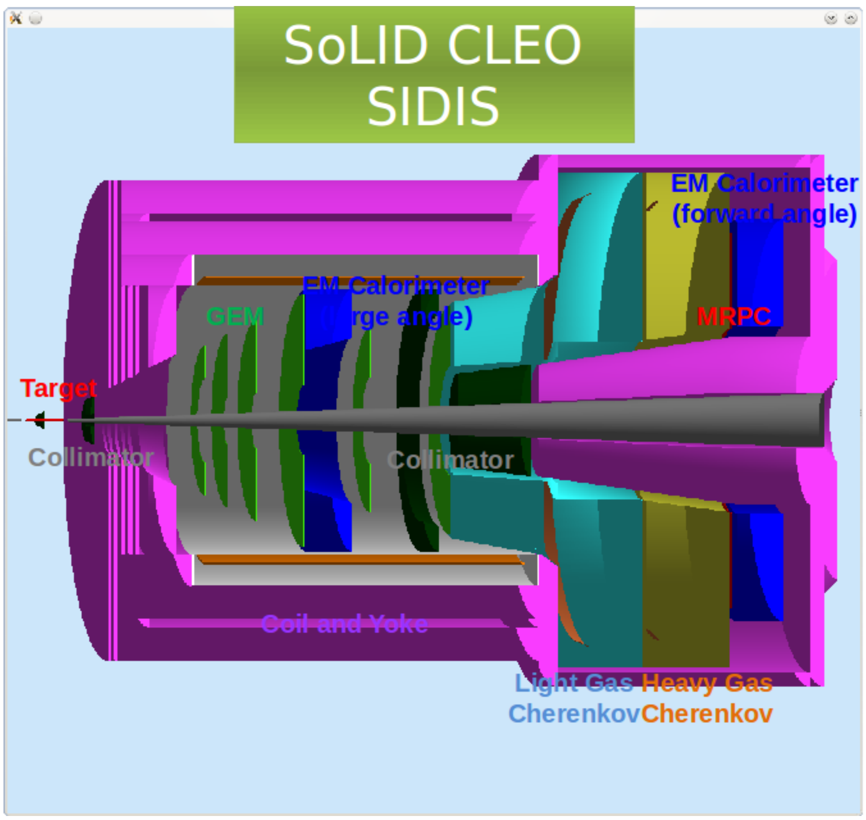

Figure 8: The experimental layout of the SoLID SIDIS based on the CLEO magnet. The scattered electrons are detected by both forward-angle (FA) and large-angle (LA) detectors. The leading pions are detected by the forward-angle detector only. The polarized ^{3}He (or NH_3) target will be placed upstream in front of the spectrometer entrance.

2.1 Summary of SoLID Design

The minimum requirements of the base equipment for SoLID are summarized below and also listed in Table 2.

- Magnet: Outer diameter is 3 meters (to fit in Hall A), inner diameter is 1 meter and length is greater than 3 meters. Field strength is greater than 1.35 Tesla and integrated BDL is 5 Tesla-meters. Acceptance in azimuthal angle (ϕ) is 2π, in polar angle (θ) is 8 to 24°. Momentum range is 1-7 GeV, and momentum resolution (combined with 100-micron tracking resolution) is 2%. Fringe field at the front end after endcap (shielding) is less than 5 Gauss (for polarized target operation).

- GEM Tracking Chambers: Six planes with total area 37 m^2, total number of channels 165K. Tracking efficiency is greater than 90%. Radial position resolution reaches 0.1 mm. Works in high rate environment.

- EM Calorimeter: Shashlyk sampling (lead-scintillator/fiber) calorimeter. Total 1800 modules of shower (18 radiation length) and 1800 preshower (2 radiation length), with an area of 100 cm^2 for each module. In front of them are 300 pieces of scintillator paddle detectors (SPDs) with thickness of 5 mm. Energy resolution is $10\%/\sqrt{E}$. Reaches $50:1\pi$ suppression with electron efficiency better than 90%. Reaches $5:1$ photon suppression. Radiation hard (gain decreasing less than 20% after 400 KRad). Combined EC and Cherenkov for PVDIS trigger rate to be below 600 KHz (20 KHz/sector).

- Light Gas Cherenkov: 2-meter long of 1-atm CO_2 gas and 1-meter long with 1-atm C_4F_8O (65%) mix with N_2 (35%). 60 mirrors and 270 PMTs. Total area is 20 m^2. Number of photo-electrons larger than 10 and with electron efficiency greater than 90%, π suppression is greater than 500 for momentum less than 4 GeV. Works in moderate field up to 200 Gauss ($<$ 100 Gauss after Mu-metal shielding). Combined EC and Cherenkov for PVDIS trigger rate to be below 600 kHz (20 KHz/sector).

- Heavy Gas Cherenkov: 1-meter long 1.5-atm C_4F_8O gas, 30 mirrors, 480 PMTs. Total area is 20 m^2 (active 8.5 m^2) number of photo-electrons greater 10. With an efficiency for π greater than 90%, Kaon suppression is greater than 10:1. Works in moderate field up to 200 Gauss (< 100 Gauss after Mu-metal shielding)

- MRPC: 50 super-modules, each 3 MRPC modules. 1650 strips and 3300 readout channels, covers an area of 10 m^2. Provides timing resolution better than 100 ps. Kaon suppression 20:1 for momentum from 2.5 to 7 GeV. Photon suppression 10:1. Works at a high rate up to 10 KHz/cm^2.

- DAQ: 282 FADC sampling at 250 MHz. 32 high-speed pipeline VME switched Series (VXS) system. 30 GEM Scalable-read-out system (SRS). Can handle trigger rate of 100 KHz for SIDIS with event size of 2.6 KBytes.

These requirements result from the summary of the detector requirements of all approved SIDIS experimental programs as in Table 3. The key parameters of the approved programs relevant to this proposal are in Table 4. The experimental setup for SoLID-SIDIS is given in the next subsections.

2.2 Experimental Requirements

The layout of the SoLID-SIDIS experiment is shown in Fig. 8 and Fig. 9. The entire detector system consists of two parts: the forward-angle detectors and the large-angle detectors. At forward angle, there are five layers of GEM detectors inside the coils upstream of the gas Cherenkov counter. The first three of the five layers are shared with the large angle detectors. A 2.04 m long light gas Cherenkov counter, is used to discriminate the scattered electrons from the produced pions. A 90 cm long heavy gas Cherenkov counter is placed after the light gas Cherenkov counter to separate kaons and protons from the pions at momenta larger than 2.5 GeV. One layer of Multi-gap Resistive Plate Chamber (MRPC) is placed after the heavy gas Cherenkov counter to provide timing information. The calorimeter detectors will be used for electron/pion separation, especially at high momentum. To cover the large electron scattering angles, there are four layers of GEM detectors placed inside the coils, with the last three layers shared with the forward angle detectors. A "Shashlyk"-type calorimeter will also be placed inside the coils with a low energy background absorber after the large-angle calorimeter. Another absorber will be placed close to the beam line to protect the forward detectors from low energy backgrounds.

Table 2: Summary of Minimum Requirements of SoLID Base Equipment

Equipment	dimension/description	description	performance, eff	performance, rej	conditions
Magnet	OD 3m, ID 1m, L> 3m	B> 1.35 T, BDL> 5 T-m	2π, 8 to 24° / 22 to 35°	P: 1-7 GeV, Res 2%	Fringe field < 5 G
GEMs	6 planes / 5 planes	Total 37 m^2, Chan 165K	Track Eff > 90%	Posi res 100μm	high rate
EM Calorimeter	1800 × 100 cm^2	18 RL + 2 RL +5 mm SPD	E res 10%, eff> 90%	50:1 π, 5:1 γ	rad hard
Light Cherenkov	2m CO2/ 1m C4F8O/N2	60 mirr, 270 PMTs, 20 m^2	γ-e > 10, Eff> 90%	π 500:1 < 4.5/3.2 GeV	100 G field
Heavy Cherenkov	1m 1.5 atm C4F8O	30 mirr, 480 PMTs, 20 m^2	γ-e > 10, Eff> 90%	K 10:1 2.5-7 GeV	100 G field
MRPC	50 × 3 modules, 10 m^2	1650 strips, 3300 chan.	Time res < 100 ps	K 20:1 < 2.5 GeV, γ 10:1	high rate
DAQ	282 FADC @ 250 MHz	32 pipeline VXS, 30 SRS	Trig 100 KHz × 2.6 KB	Trig 30 × 20 KHz × 48 KB	high noise

Table 3: Detector Summary for this proposal (based on SIDIS requirements).

Experiments	SSA-^{3}He	SSA-Proton
Target Length	^{3}He 40 cm	NH_3 3 cm
Target Polarization Target Spin Flip	∼60% ≤20 mins	∼70% ≤4 hours
GEM Tracking Chambers	6 chambers	6 chambers
E&M Calorimeter	Forward + Large angle	Forward + Large angle
Light Gas Cherenkov	2 m long	2 m long
Heavy Gas Cherenkov	1 m long	1 m long
MRPC (TOF)	100 ps resolution	100 ps resolution
Target Polarimetry	∼ 3%	∼ 3%
DAQ	Singles trigger	Singles trigger

Table 4: Summary of Key Parameters for this proposal (based on SIDIS requirements).

Experiments	SSA-^{3}He	SSA-Proton
Reaction channel	(e, e')	(e, e')
Approved number of days	125	120
Target	^{3}He	NH_3
Unpolarized luminosity ($cm^{-2}s^{-1}$)	$\sim 10^{37}$	$\sim 10^{36}$
Momentum coverage (GeV/c)	0.8-7.0	0.8-7.0
Momentum resolution	∼2%	∼2%
Polar angle coverage (degrees)	7.5-24	7.5-24
Polar angle resolution	0.6 mr	0.6 mr
Azimuthal angle resolution	5 mr	5 mr
Trigger type	Singles e^-	Singles e^-
Backgrounds	$(e, \pi^\pm)$, $(e, e^\pm$ (non-DIS)) (e,γ), (e,p)	$(e, \pi^\pm)$, $(e, e^\pm$ (non-DIS)) (e,γ), (e,p)
Major requirements	Radiation hardness Target Spin Flip High Singles Trigger Rate PID	Shielding of *line-of-flame* Target spin flip High Singles Trigger Rate PID

The polar angular coverage for the forward-angle detectors ranges from 7.5° to 14.8° and the momentum coverage extends from 0.8 GeV/c to 7.0 GeV/c. The total subtended solid angle is about 95 msr for this range of momentum. Six layers of the GEM detectors are placed inside the coils and will be used as tracking detectors. Five of them provide for the forward-angle detection tracking system. A combination of an electromagnetic calorimeter, gas Cherenkov counters, and a layer of Multi-gap Resistive Plate Chamber (MRPC) will be used for electron and pion identifications. The large-angle detectors polar angle coverage ranges from 15.7° to 24°. They are mainly used for electron detection in a momentum range of 3.5-6.0 GeV/c where the expected π^-/e ratio smaller than 1.5. The "Shashlyk"-type calorimeter should be sufficient to provide the desired pion rejection. Four layers of GEM detectors will be used as tracking detectors. The total subtended solid angle is about 280 msr for the momentum range.

2.2.1 Polarized ^{3}He Target

Jefferson Lab experiment E12-10-006 [25] is designed to measure the target single spin asymmetries through the semi-inclusive deep-inelastic scattering (SIDIS) $(e, e'\pi^{\pm})$ with the SoLID spectrometer and the transversely polarized ^{3}He target. Note that experiment E12-11-007 [28] will measure single and double pin asymmetries using a longitudinally polarized ^{3}He target and while not directly contributing to the measurements presented here, will provide valuable information for understanding our systematic uncertainties. The standard Hall A polarized ^{3}He target will be used in its transverse mode. A higher than 60% target polarization with a faster than 20 minutes target spin flip is expected at the full polarized luminosity of 10^{36} cm^{-2} s^{-1}, which is corresponding to the unpolarized luminosity of 10^{37} cm^{-2} s^{-1}. The target polarization is expected to be limited by the magnetic field gradient in the target region, which is dominated by the leakage field from the SoLID magnet. Therefore, the design of the magnet yokes is important to achieve the required target polarization. As shown in Fig. 8 and Fig. 9, the target will be located about 80 cm upstream of the front yoke. Target collimators will be placed close to the end caps of the 40 cm long target in order to reduce backgrounds generated from both endcaps. The expected kinematic coverage includes $0.1 < x < 0.6$ which comprises the majority of the valence quark region; and 1.5 GeV$^2 < Q^2 <$ 7.5 GeV^2.

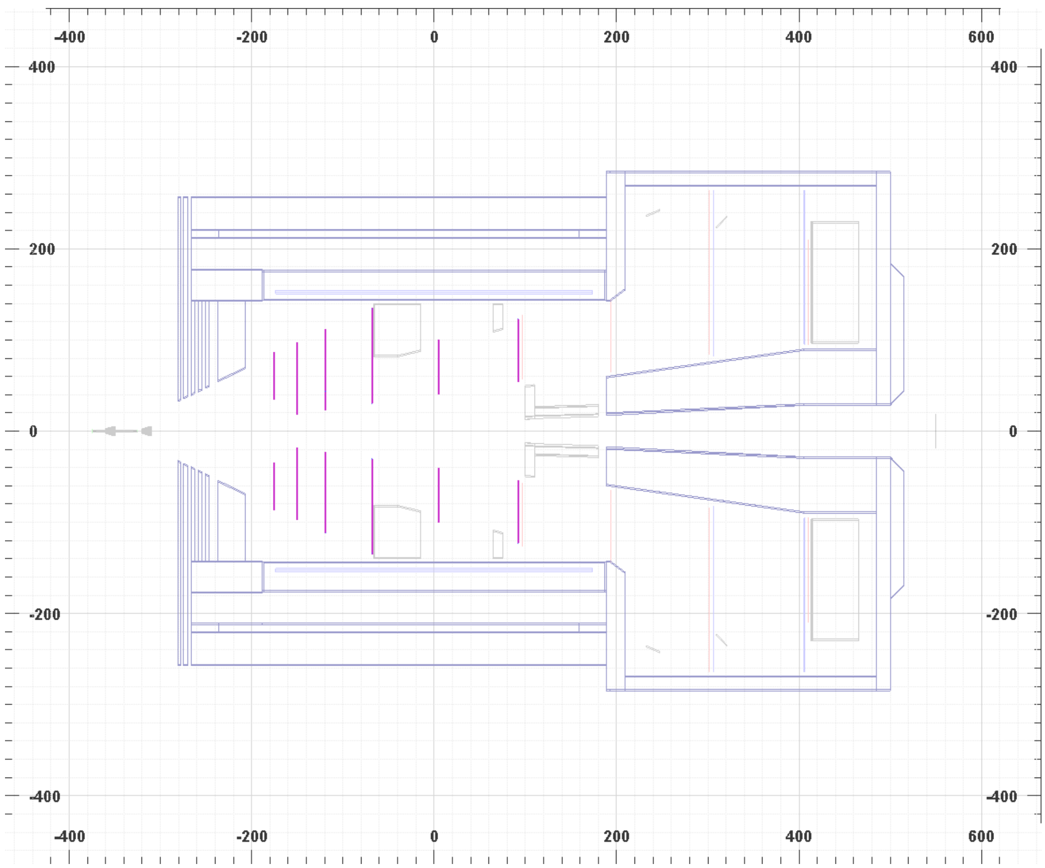

Figure 9: A 2D representation of the experimental layout of SoLID SIDIS.

2.2.2 Polarized NH_3 Target

The E12-11-108 [26] is designed to measure the single/double spin asymmetries through the semi-inclusive deep-inelastic scattering (SIDIS) $(e, e'\pi^{\pm})$ with the SoLID spectrometer and a transversely polarized proton target. The overall luminosity in this case is smaller compared to that of using the polarized ^{3}He target. An improved version of the JLab/UVa/SLAC polarized NH_3 target shown in Fig. 10 will be used. The main upgrade is to replace the aging Helmholtz-coil magnet with a new magnet and to have a fast spin-flip capability with the AFP technique to minimize the systematic uncertainty in the single spin asymmetry measurement. In order to satisfy the requirements of phase space coverage, the new design will further allow both transverse and longitudinal direction to have a nominal forward opening of more than $\pm 25°$, while maintaining the same maximum field (5 Tesla) and a uniform field region in the center. The target polarization is required to be higher than 70% with the spin flip every hour.

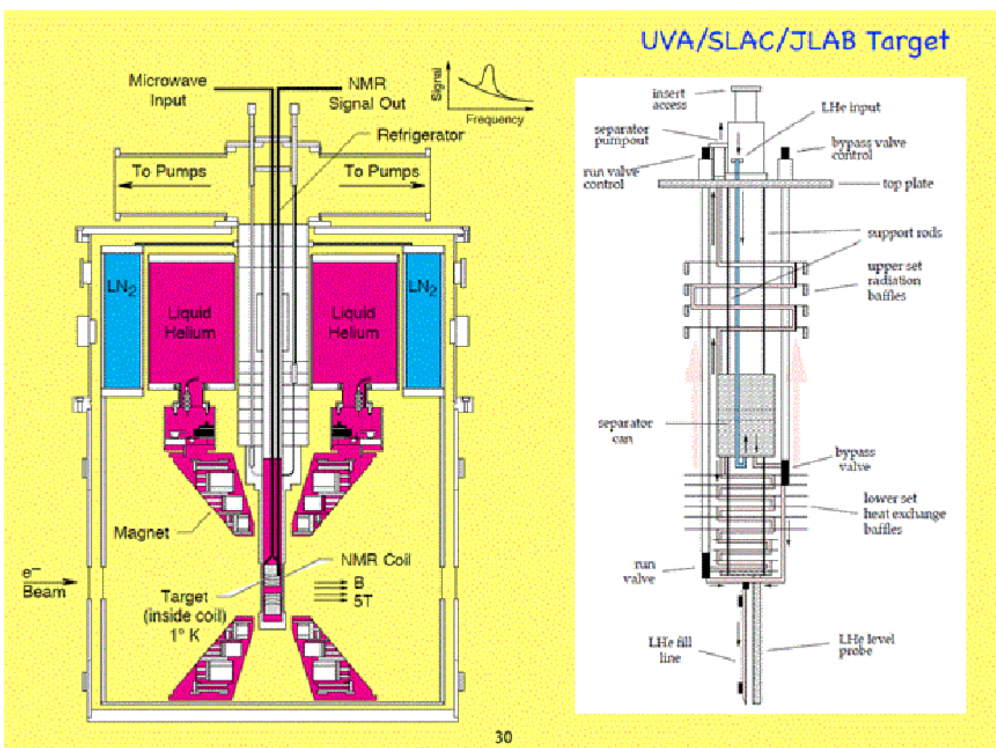

Figure 10: Current JLab/UVa/SLAC polarized target system.

Due to the large magnetic field in the transverse direction, this experiment suffers from a different kind of background compared to the low field polarized ^{3}He experiment, known as *line-of-flame*. The main feature of such a background is that a very high rate of charged particles with momentum range between 1-2 GeV will be localized in a very narrow region of the acceptance. Fig 11 shows this background on all six GEM planes in the SoLID. The GEM chambers in regions outside of the *line-of-flame* location see a background rate of less than 1.0 KHz/mm^2, whereas the regions inside have much higher rates. In order to handle this background and avoid damage to the apparatus, detector sectors in the direct line-of-sight of this *line of flame* will be removed or turned off during the proton experiment.

2.2.3 Particle Identification

In order to achieve the proposed precision in the asymmetries, the negative pion contamination in the electron sample needs to be controlled to below 1%. At forward angle, it is achieved by a combination of an electromagnetic calorimeter and a 2.04 m light gas Cherenkov detector. At large angle, the electromagnetic calorimeter alone will be enough to provide the required pion rejection, since the expected pion to electron ratio is small.

For the measurements proposed here, we are only interested in the single electron events but will need the same level of precision PID as SIDIS to eliminate background particles. For reference, SIDIS will identify pions (forward angle detector only) by a combination of time-of-flight (TOF) and a heavy gas Cherenkov detector. With the expected 100ps TOF resolution from the MRPC, backgrounds from kaons and protons can be eliminated to the $< 1\%$ level in pion events. Because the experiment proposed here seeks to measure singles electron events at the 10^{-4} level, it will greatly benefit from the ability of SoLID to carefully measure the rates and asymmetries from hadronic background events. Background contaminations were the large systematic uncertainty in the 6 GeV A_y^n measurement due to relative poor particle ID.

For this experiment, it is also necessary to remove electron events that result from pair production from π^0 decay. This was our largest background in the 6 GeV A_y^n measurement due to the inability to cleanly separate these event from the good electron sample. We expect to be able to reduce this background to below 1% primarily by removing events with a correlated e^+-e^- pair. We will also be able to directly be able to measure the contamination and asymmetry of these events with SoLID as part of the singles trigger.

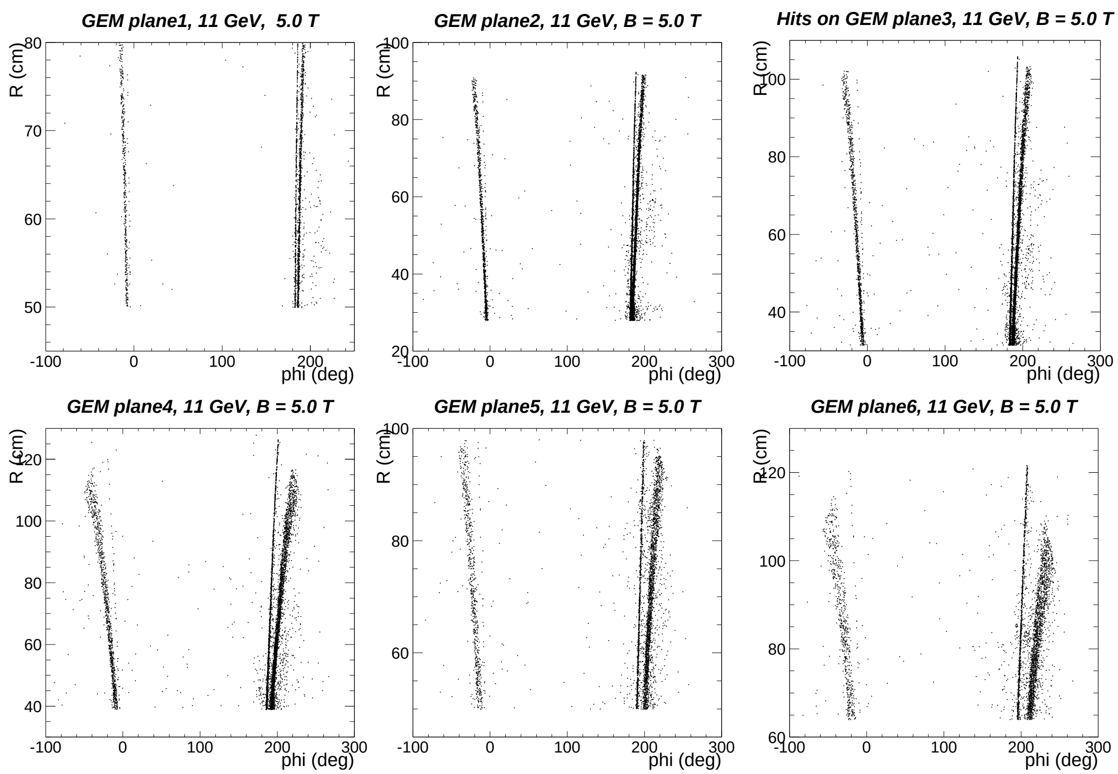

Figure 11: GEANT3 simulation results of background with NH_3 target field ON. The x-axis is the azimuthal angle in lab frame. The y-axis is the radius of GEM chambers (1-6). Narrow regions of high rate (compared to rest of the acceptance) are clearly seen as a function of azimuthal angle ϕ.

2.2.4 Resolution Requirement

The extraction of the single spin asymmetries in $N(e, e')$ relies on measuring the ϕ_S angular dependence in each kinematic bin in x and Q^2. Since the kinematics of interest are in the deep-inelastic-scattering (DIS) region, the requirements on the resolution of the reconstructed kinematic variables are modest. Consistent with the requirements for SIDIS we require a better than a few percent momentum resolution, a better than 1 mr polar angular resolution, a better than 10 mr azimuthal angular resolution, and a 1-2 cm reconstructed vertex resolution would satisfy the needs of these experiments. Fig. 12 shows the expected momentum and angular resolution for different polar angles and momentum ranges. The position resolution of the GEM chambers is assumed to be 100μm, and the angle between the u/v readout strips is assumed to be 10°. Furthermore, the effects of multiple scattering due to the finite thickness of the GEM chambers and the air in the SoLID spectrometer are taken into account. The average momentum resolution, the average polar angular resolution, and the average azimuthal angular resolutions are about 2%, 0.6 mr, and 5 mr, respectively.

2.2.5 DAQ Requirement

The SIDIS experiment relies on a coincidence between an electron and pion. With conservative thresholds, this trigger can be easily handled by the DAQ system that is planned. It is desirable however for SIDIS to be able to take all singles triggers to optimize statistics and best understand background events. The SIDIS collaboration is working to achieve this goal, which is also the goal for the measurement proposed here. Under the expected luminosity conditions, which are largest for the polarized ^{3}He target experiment, the expected singles trigger rate is $\sim$ 100 kHz with the thresholds described below. At present the maximum trigger rate that the DAQ can handle is $\sim$ 80 kHz. For the NH_3 measurements, we expect to have a singles trigger rate below the DAQ limit but this is not true for the ^{3}He experiment. The trigger rates were calculated through a GEANT simulation with a combination of the Whitlow [29], the QFS [30], and the Wiser [31] codes.

The electron trigger for the forward angle detector will be formed by a coincidence between the gas Cherenkov detector, the EM calorimeter, and the scintillator detector. Considering the kinematic information of the scattered electrons from the DIS process (e.g. $Q^2 > 1$ GeV^2), a position dependent

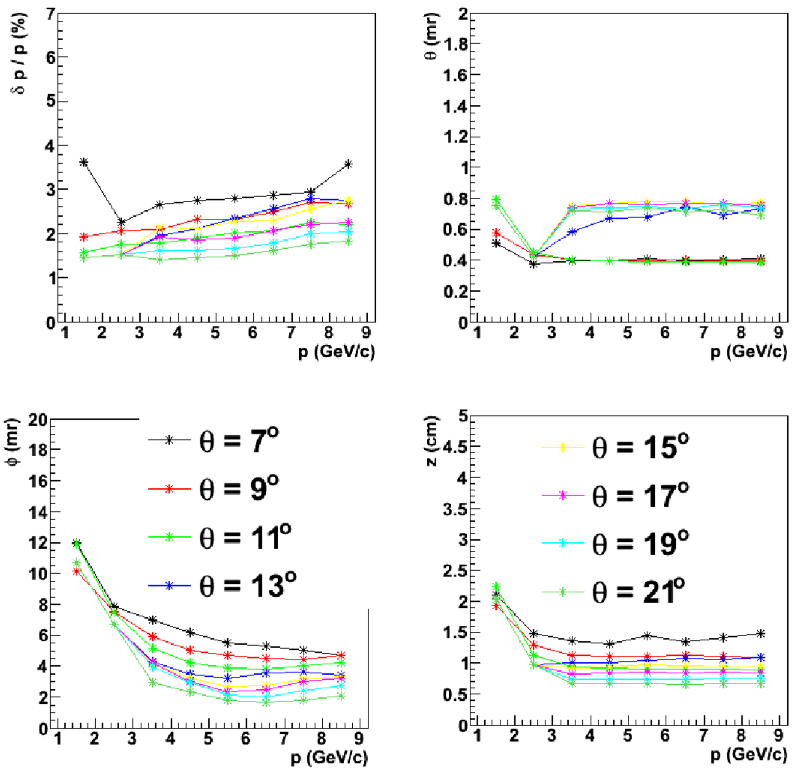

Figure 12: The expected momentum, angular and interaction vertex resolution for SoLID. The position resolution of the GEM chambers is assumed to be 100 μm. The angle between u/v readout strip is assumed to be 10 degrees.

energy threshold with a low limit at 0.8 GeV and high limit at 3.0 GeV in the EM calorimeter could significantly reduce the trigger rate. The expected total trigger rate is 120 kHz (^{3}He) and $\sim$ 70% of these are good electron events.

The electron trigger for the large angle detectors will be provided by the EM calorimeter with an energy threshold of about 3 GeV. Such a trigger would be sensitive to both high energy electrons and high energy photons (mostly from the π° decay). With the scintillator plane detector being incorporated into the trigger, the high energy photon triggers can be significantly suppressed. The total expected trigger rate is about 18 kHz (^{3}He) with approximately 26% good electron events.

We will also install additional higher threshold singles triggers to provide cleaner, lower statistics samples of electrons to help us understand our backgrounds.

2.3 SoLID Simulation

Development of the SoLID spectrometer requires the detailed evaluation of different solenoidal fields, optics from those fields, backgrounds from multiple sources, possible detector and baffle geometries, detector responses, and tracking. Overall, a figure-of-merit must be calculated for different configurations for quantitative comparison. It is also necessary that such simulations be done in a coherent fashion and validated as well as possible. Because details of the design have not been finalized, it must also be flexible enough to be quickly adapted to different configurations.

Initial simulations for SoLID were done using a combination of GEANT3 and COMGEANT. However, these are FORTRAN based and GEANT3 is no longer actively maintained. The decision was made to offer a modern design based on GEANT4 [32] to handle particle propagation and interactions. This is a well-supported framework and offers a variety of physics packages, such as simulation of low-energy electromagnetic backgrounds. However, the detector geometries, how magnetic field maps are specified, input parameters, and output formats must all be developed on top of this framework. Furthermore, software for post-processing, such as tracking, also must be developed separately and integrate into the analysis flow efficiently. Because this is being done with a new simulation package, it is necessary to also compare and reconcile the output between GEANT3 and GEANT4.

To accomplish all these goals, we have adopted a simulation suite, GEMC, which was successfully developed and employed for similar CLAS12 simulations [33]. It utilizes GEANT4 and includes facilities for external event generators, output to a compact style similar to that utilized by JLab data acquisition systems, and a flexible framework to specify arbitrary detector geometries. A framework for specifying sensitive detectors, processing particle hits, and generating output is also included. The geometry and sensitive detector types are read in at run type allowing for easy modification of designs. Advanced visualization abilities are available, which provides a useful debugging tool.

Magnetic field maps for GEMC can be produced using the Poisson Superfish package [34] developed at LANL or TOSCA [35]. The POISSON package allows for the calculation of azimuthally symmetric magnetic fields (relevant for the solenoidal spectrometer). Because both the optics and the fields in the detector regions are relevant, accurate optimization of the iron yoke is important. More detailed field maps produced by TOSCA can be used for more advanced stages of design should it become necessary.

2.3.1 Framework

The overall framework design is based on a modular philosophy which is general enough to allow many different software components to interact with each other. This needs to encompass ideas such as external event generators, ROOT analysis scripts, raw hit digitization, and tracking analysis. A schematic is given in Fig. 13.

GEMC and generally GEANT4 provide the predominant simulation component in modeling secondary physics processes (such as multiple scattering) and propagation through a magnetic field. Physics generators provide information on the initial particle type, position, and momentum to the simulation for each event. These can take more than one form and we allow for general text file input and internal generators within GEMC. Magnetic field maps are described over a grid using text files. GEMC allows for various coordinate systems to be used in the grids and handles all interpolation and lookup.

Geometries and detectors are described externally in a SQL database. The specific detector response-types are assigned within the SQL database tables, but the details of how events are processed and sent to output are hardcoded within GEMC. To avoid the need for active development in GEMC to tailor our needs to that simulation, GEMC is built as a library and linked to a version developed specifically within the SoLID collaboration. This gives

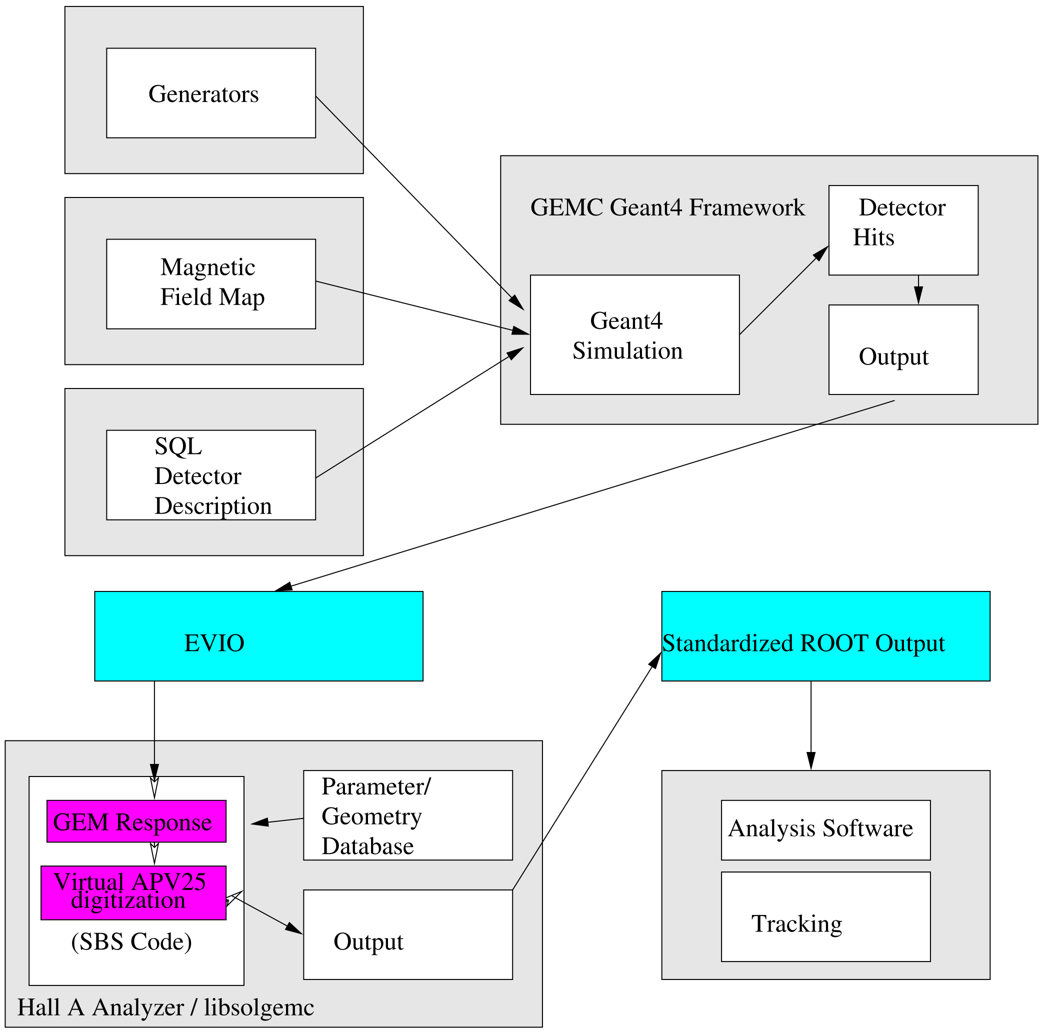

Figure 13: Schematic of the simulation and software framework.

access to all of the functionality within GEMC, but allows us to modify and add components as we need them without interference to the CLAS development.

Output from GEMC is through EVIO, which is a binary format developed at Jefferson Lab. Libraries are available to provide decoding. These files can be converted to ROOT files through available tools or used by higher level analysis packages, such as the detector digitization.

Presently, a library exists to do the digitization for GEMs, (other detector systems are planned for the future) which produces a standard ROOT file with tree objects and operates within the Hall A analyzer framework. This provides generic C++ class objects for representing detectors and useful parameter database tools. These can be read by the Hall A tree-search code (or potentially any other tracking code base) to do tracking simulations.

2.3.2 Generators

Beyond the physics included in GEANT4, several generators have been implemented to study specific processes. The interface between the generator and GEMC is the LUND format (or an extension of it), which is a text-based file containing event-by-event information of the initial particle configuration. These generators allow for an extended target and randomly sampled position to simulate a fast-rastering system. The generators implemented presently are

- Deep inelastic scattering cross sections from the CTEQ6 parton distribution fits [36].
- Charged and neutral pion production based on empirical fits to SLAC data [37] using the Weizsäcker-Williams approximation.
- Elastic scattering from protons and neutrons based on dipole parameterizations.

Additional generators are planned, which includes extending the present generators to include initial radiative and multiple-scattering effects. Additionally, self-analyzing hyperon decay processes are a potential systematic and must be evaluated as well. Background rates for processes included in GEANT4 can be evaluated by simulating sufficient numbers of individual electrons passing through the target.

3 Polarized Targets

There are five approved SoLID experiments. Two semi-inclusive DIS experiments (E12-10-006 and E12-11-007) use a polarized ^{3}He target with the achieved performance. One SIDIS experiment (E12-11-108) uses a transversely polarized proton (NH_3) target. The following subsections will describe the polarized ^{3}He target, the polarized proton (NH_3) target

3.1 Polarized ^{3}He Target

The polarized ^{3}He target is based on the technique of spin-exchange optical pumping of hybrid Rb-K alkali atoms. Such a target was used successfully in the recently completed SIDIS experiments at 6 GeV [38] with a 6-GeV electron beam at JLab. See Figure 14. Three sets of Helmholtz coils provide a 25 Gauss holding field for any direction, supporting polarization in the transverse or longitudinal direction. Target cells were 40-cm long with density of about 10 amg (10 atm at 0°). The luminosity was about 10^{36} nuclei/s/cm with a beam current of 15 μA. An in-beam polarization of up to 60% was achieved. Both achieved luminosity and figure-of-merit are the world-best so far. Two kinds of polarimetry, NMR and EPR (paramagnetic-Resonance), were used to measure the polarization of the target. The precision for each method was about 5% (relative) and the methods agreed well within uncertainties.It is expected to be able to reach 3% with the planned improvements.

Frequent target polarization direction reversal is needed to minimize target-spin-correlated systematic uncertainties. The fast target spin reversal was achieved in a few seconds for the 6 GeV SIDIS experiment by using RF AFP technique. The frequency of the spin reversal was kept to 20 minutes to minimize the polarization loss due to AFP. The additional polarization loss due to frequent spin reversal was kept at $< 10\%$ (relative). The above quoted maximum in-beam polarization achieved for the 6 GeV experiment (up to 60%) included the loss due to spin reversal. A new method using field rotation for spin reversal was tested and a nearly no polarization-loss result was achieved and will resulting in an improved performance. It will allow to have more frequent (a few minutes instead of 20 minutes) spin reversal to help further improve the target-spin-correlated systematics.

The upstream endcap plate will keep the magnetic field and its gradients under control in the target region. In this design, the absolute magnetic field

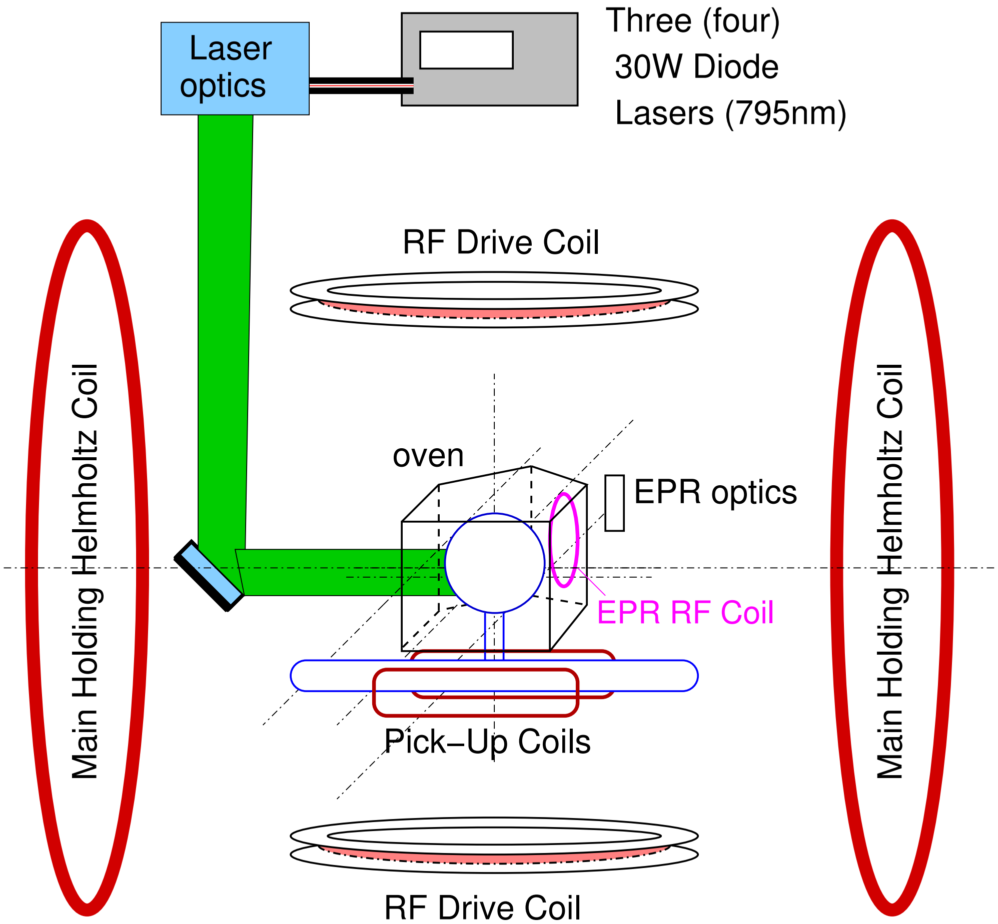

Figure 14: Schematic representation of the existing Hall A polarized ^{3}He target system. Large Helmholtz coils provide a uniform $\sim$ 25 G magnetic field that serves as the polarization axis for the ^{3}He. Spin-Exchange Optical Pumping is used to polarize the gas in an aluminosilicate glass cell. Only one of three sets of Helmholtz coils are shown.

strength in the target region is about a few Gauss with field gradients 50 mG/cm. Correction coils around the target will further reduce field gradients to the desired level of 30 mG/cm.

A collimator, similar to the one used in 6 GeV experiment, will be placed next to the target cell window to minimize the target cell contribution to the total events.

In addition to the polarized ^{3}He target, the current target system has a multi-foil ^{12}C target for spectrometer optics study, a BeO target for beam tuning and a reference target cell system, which allows to have different target gases, hydrogen, deuterium, ^{3}He and nitrogen, be used to measure unpolarized cross sections, for calibration and dilution study.

Upgrades are planned for other polarized ^{3}He experiments before the SoLID experiments. These upgrades are not required for the SoLID experiments but will benefit them.

3.2 Transversely Polarized Proton Target for SoLID

The SoLID collaboration proposes to measure single spin asymmetries in the semi-inclusive, deep-inelastic $(e, e'\pi^{\pm})$ reaction using a transversely polarized proton target. The target to be used is the dynamically polarized ammonia target that has been used at SLAC and at Jefferson on numerous occasions [39]. Its last use was in 2012 for the g_2^p/G_E^p experiments, which took place in Hall A [40]. Proton luminosities of 10^{35} cm^{-2}s^{-1} have been achieved with this target, in conjunction with electron beam currents up to 100 nA. In order to meet requirements of the SoLID measurements however, a new superconducting magnet must be procured, as discussed below.

Dynamic nuclear polarization (DNP) has been used to polarize solid targets for nuclear and particle experiments for more than four decades. To realize DNP, a paramagnetic species is implanted into the target material, either by dissolving a stable radical into the material (if the latter is liquid at room temperature), or by producing radicals directly within the material using ionizing radiation. The unpaired electrons are highly polarized by cooling the sample to a low temperature and exposing it to a high magnetic field. For example, at the 1 K and 5 T operating conditions of the JLab target, the electron polarization is -99.8%. Off-center microwave saturation of the radicals Electron Spin Resonance (ESR) frequency is used to transfer this polarization to nearby nuclear spins, with one or more mechanisms, such as the solid effect, thermal mixing or the cross effect, being responsible for the polarization transfer. Spin diffusion then transports the nuclear polarization throughout the bulk of the sample. The polarization may be positive or negative, depending upon whether the microwave frequency is below or above the ESR frequency. In well-designed systems, proton polarizations exceeding 95% [41] and deuteron polarizations approaching 90% [42] have been achieved.

Frozen ammonia (NH_3) has been the target material of choice for electron beam experiments at Jefferson Lab. Proton polarizations in excess of 90% are routinely achieved in ammonia, and it has a relatively high ratio of polarizable-to-nonpolarizable nucleons (17.6%). Additionally, ammonia displays a very high resistance to radiation damage, and simply warming the material to about 100 K for a few minutes can largely repair the damage that does occur. Prior to the experiment, paramagnetic radicals (chiefly NH_2) are created within the ammonia by irradiating the material (under liquid argon) with an electron beam. For convenience, this irradiation is typically done off site, and the material is then stored under liquid nitrogen until required for the experiment. The JLab target system, as utilized in Hall A, is shown in Fig 15. It consists of a 5 T split-coil superconducting magnet, a ^{4}He evaporation refrigerator with a cooling power of about 1 W at 1 K, and a target insert containing two samples of frozen ammonia along with additional targets for background and dilution studies. These reside in a purpose-built, evacuated scattering chamber with thin windows around its perimeter for beam entrance and exit. Equipment outside the chamber includes a large set of vacuum pumps for the evaporation refrigerator, microwave electronics for polarizing the target sample, and a NMR system for measuring its polarization. Liquid helium is provided to the target from a nearby 500 L dewar.

Before its use in the g_2^p/G_E^p experiments, numerous upgrades were made to the polarized target in order to improve its performance, reliability, and safety:

- An entirely new refrigerator was constructed at JLab according to the safety regulations dictated by 10 CFR 851;
- The quench-relief piping system for the superconducting magnet was upgraded to replace leaking rubber seals with copper gaskets, and also made compliant to 10 CFR 851;
- The pumping system and controls were overhauled;

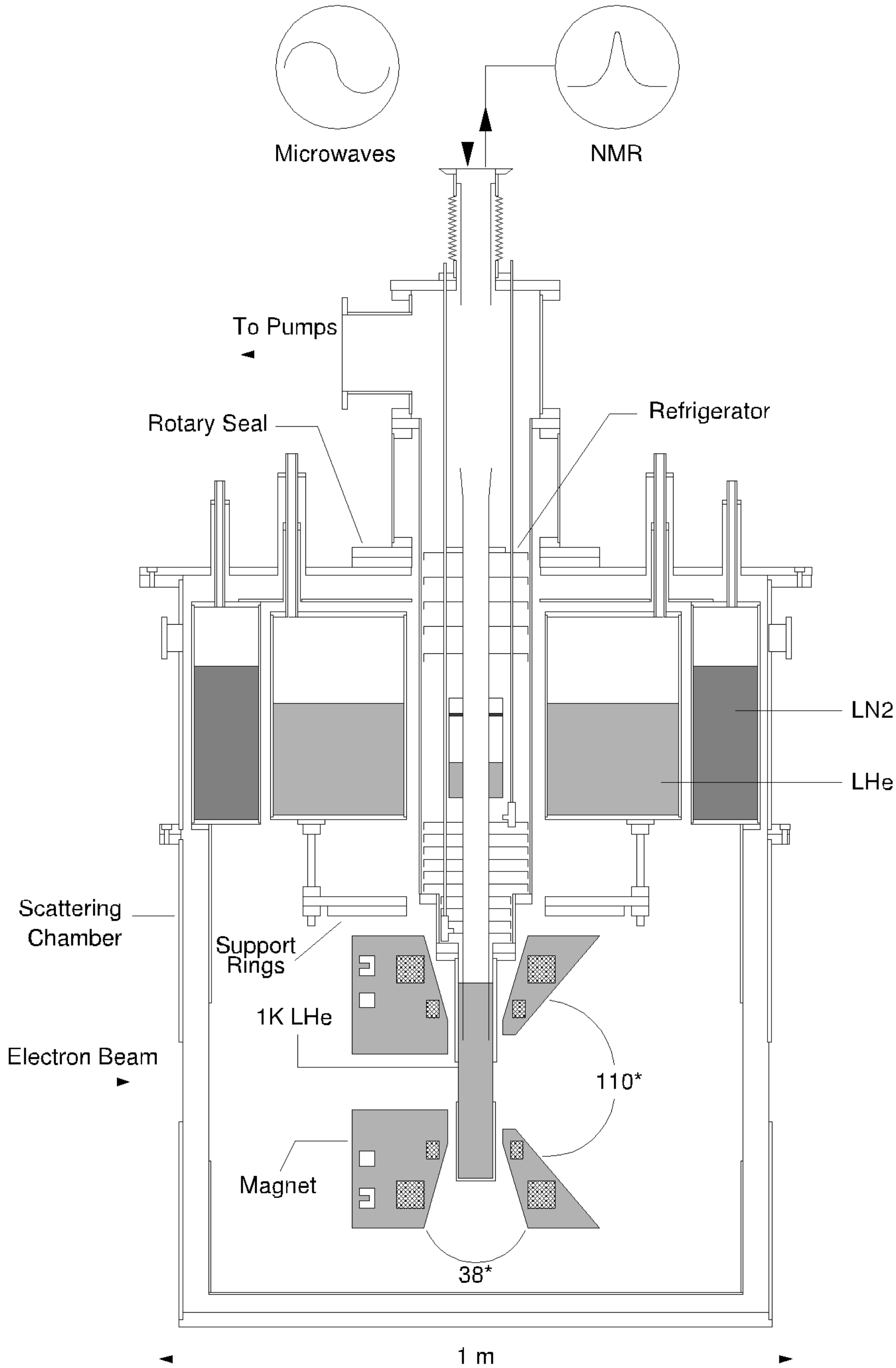

Figure 15: The dynamically polarized target, as utilized in Hall A. The cryostat can rotate 90° about the vertical axis, thus providing either longitudinal or transverse polarization with respect to the electron beam. The longitudinal orientation is shown.

- A more robust sample insert and motion mechanism were constructed to address problems that were encountered in previous experiments;

- A new rotary vacuum seal was implemented that significantly reduces the time required to rotate the magnet between its longitudinal and transverse orientations. With the new seal, there is no longer a need to disconnect the refrigerator pumping line, nor remove and replace the sample insert;

- The 5 T magnet suffered irreparable damage during the final systems tests, and was replaced with a similar magnet removed from the Hall B polarized target [43].

It should be noted that both the original and Hall B magnets were primarily designed to provide longitudinal polarization, while still permitting limited use for transverse polarization. As such, each magnet possesses an opening angle of $100°$ ($\pm 50°$) in the direction parallel to the magnetic field, compared to only $\pm 17°$ perpendicular to it (see Fig. 15). Because the SoLID proposal requests transverse polarization with an opening angle $\pm 25°$ or greater, a new magnet will be necessary.

Oxford Instruments (manufacturer of both the Hall B and original magnet) has performed a detailed feasibility study and concludes that they can build a 5 T split-coil magnet with both a $\pm 25°$ split angle and the homogeneity required for DNP [44]. The SoLID collaboration and JLab Target Group will work alongside the eventual vendor to ensure the magnet can be easily incorporated into the existing JLab cryostat. This will greatly reduce the time and cost required to field a transversely polarized target for SoLID.

4 Beamline Instrumentation

4.1 Beam Chicane for the NH_3 Target

In this experiment the polarization direction of the proton target will be held transverse to the beam direction. The strong magnetic field of the target will create a non-negligible deflection of the electron beam. To ensure the proper transport of the beam into the downstream exit beam pipe, a chicane will be employed. Two chicane magnets will be used for this purpose. The first one will be located 10m upstream of the target and this will bend the beam out of the horizontal plane to vertically down. The second magnet which will be located about 4m upstream of the target will bend back the beam at an angle that will compensate the 5 Tesla target field. We will choose the bend angle such that the beam will pass through the exit beam pipe after interacting with the target. A GEANT3 simulation was performed to optimize the bend angle. The simulations included physics processes such as synchrotron radiation and Bremsstrahlung. Fig. 16 shows an event display for the 11 GeV beam. Beam position monitors will be used before and after the chicane for the proper transport of the beam. They will also be used in determining the beam positions at the target.

4.2 Beam Charge Monitors

Typically low beam currents (up to 100 nA) are used for the polarized proton target to reduce the depolarization effects and any significant changes to the density. The standard Hall-A BCM cavities are linear down to 1 μA. An upgrade of the beam diagnostic elements such as BCM, BPM and Harps were done for the g_2^p experiment (E08-028) in Hall-A, which uses the polarized proton target. The upgrades allowed us to measure the beam charge and positions up to 50 nA current. In order to calibrate the beam charge a tungsten calorimeter was used to provide an absolute calibration of the Hall A BCM with an accuracy of better than 2%.

4.3 Slow and Fast Raster

The existing Hall-A faster raster has a 2 mm x 2 mm pattern and and will be used for both the NH_3 and ^{3}He targets to minimize depolarization (and prevent ^{3}He cell rupture). In addition a slow raster will be added tocover a

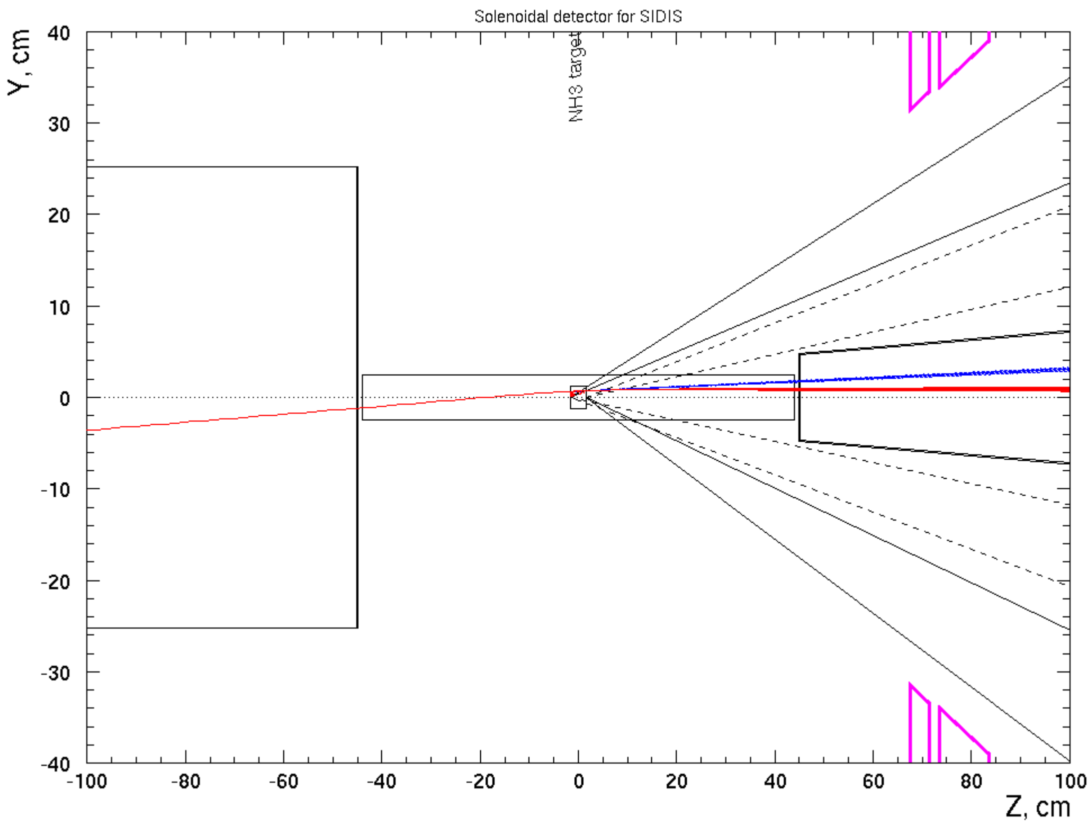

Figure 16: Event display of the beam transport at the target region with the initial bend of the beam before hitting the target. The red color denotes the 11 GeV beam and the blue color denotes the uncharged particles (mostly bremsstrahlung photons). The NH_3 target field direction is pointing into the page.

circle of 20 mm diameter for NH_3. This is done in order to uniformly cover most of the surface of the target cell which has a 25 mm diameter.

4.4 BPM

The standard Hall A BPMs, including the upgrades done for low current running, are sufficient for these experiments and have been successfully used with these polarized targets in the past. BPM calibration can be done by Harp scans using the existing scanners.

4.5 Luminosity Monitors

During the 6 GeV running era in Hall A, a set of 6 PMT's with attached lucite pieces were arranged symmetrically about the downstream beam line to monitor the relative luminosity and beam quality, as well as look for false asymmetries. During the 6 GeV A_y^n measurement, these monitors were sensitive to false asymmetries at the $\sim 4 \times 10^{-5}$ level. We plan to use these or similar detectors to again monitor the luminosity for changes or false asymmetries in addition to monitoring the overall luminosity using SoLID itself.

5 Kinematics and Rates

5.1 Acceptance and Kinematic coverage

SoLID (Figure 8) will have a magnet designed to have optimized geometry such that it will have acceptance at forward polar angles (FA) between 8°and 14.7°, and between 14.7°and 24°for large angles (LA). See Figure 17. The momentum acceptance is $0.7 - 11$ GeV for forward angles and $0.4 - 11$ GeV for large angles as shown in Figures 18 and 19.

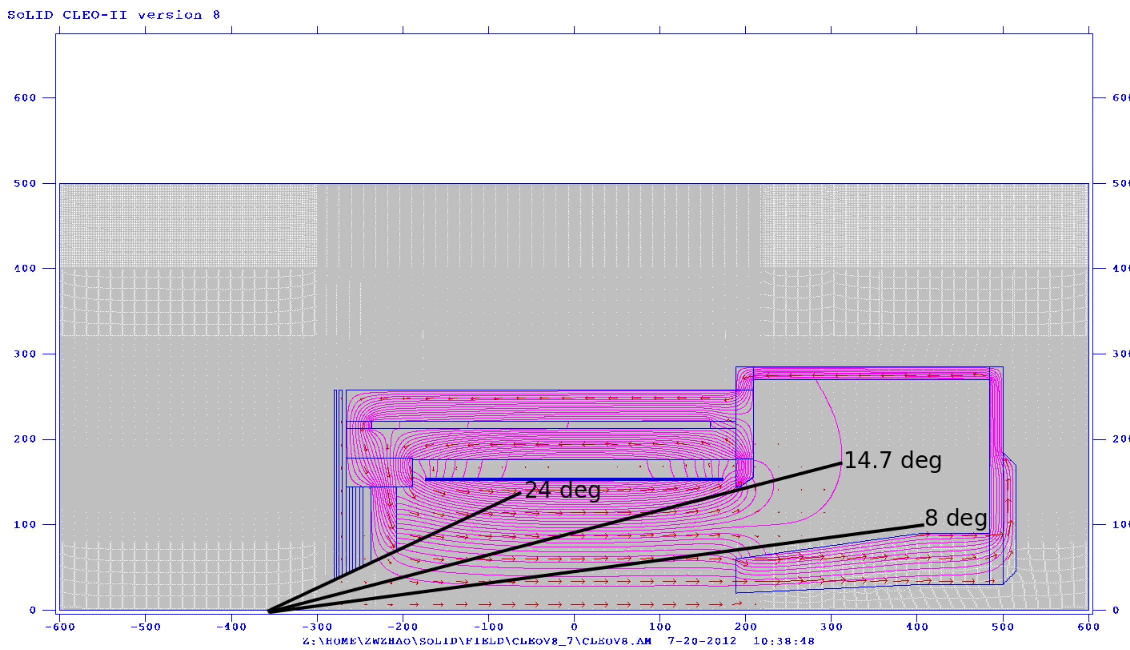

Figure 17: Angular acceptance of SoLID. Forward angle $(8° - 14.7°)$ and Large angle $(14.7° - 24°)$

A very important experimental issue associated with the strong (5 T) field from the NH_3 target is known as the "line of flame" and is clearly seen in our simulations, where extremely high backgrounds are seen in highly localized areas as shown in Figure 11. One way to get around this issue is to "remove" certain areas of the detectors where "line of flame" passes through as shown in Fig. 20 by turning off part of the detectors. The other way is to add collimators in the target region to block these high rate regions more efficiently. While the simulation results show that the θ angular distribution of acceptance extends to both smaller and larger angles, the acceptance of ϕ at forward angle decreases by 30% and at large angle by 20%. Reconstruction of angles is more important which can be addressed by careful simulations of the optics before the experiment and calibration during the experiment. Optics studies based on Monte Carlo simulations have been completed recently for the g_2^p/G_E^p experiment employing also the transversely polarized NH_3 target in Hall-A, and a careful optics study with beam is being planned for the these experiments.

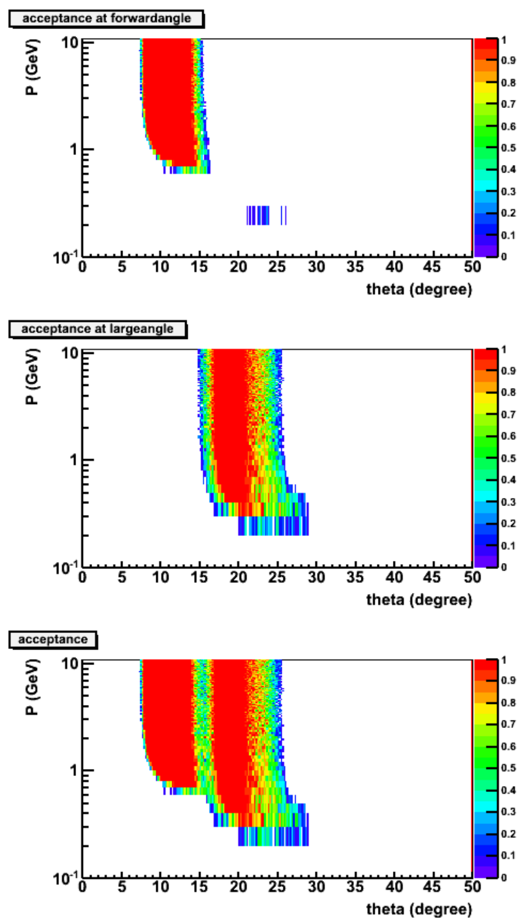

Figure 18: Acceptance (momentum vs. polar angle) for negative particles for forward angle (top), large angle (middle) and combined (bottom).

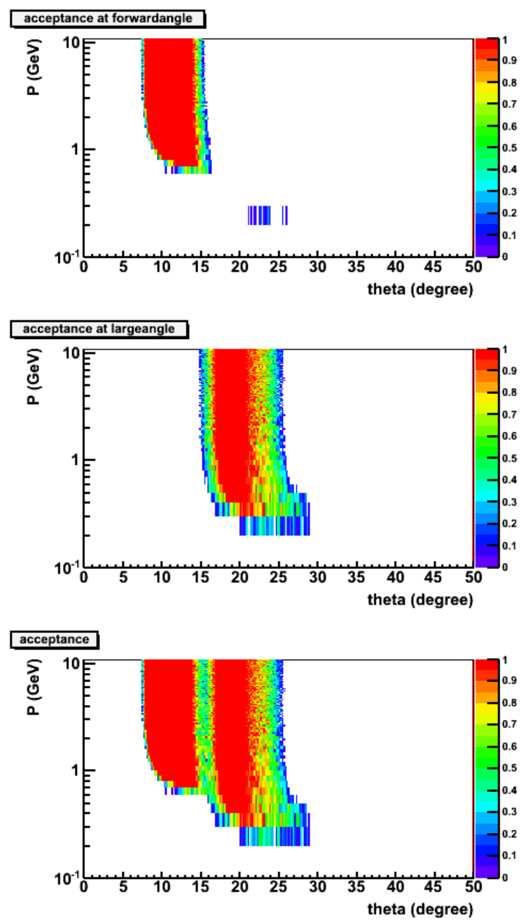

Figure 19: Acceptance (momentum vs. polar angle) for positive particles for forward angle (top), large angle (middle) and combined (bottom).

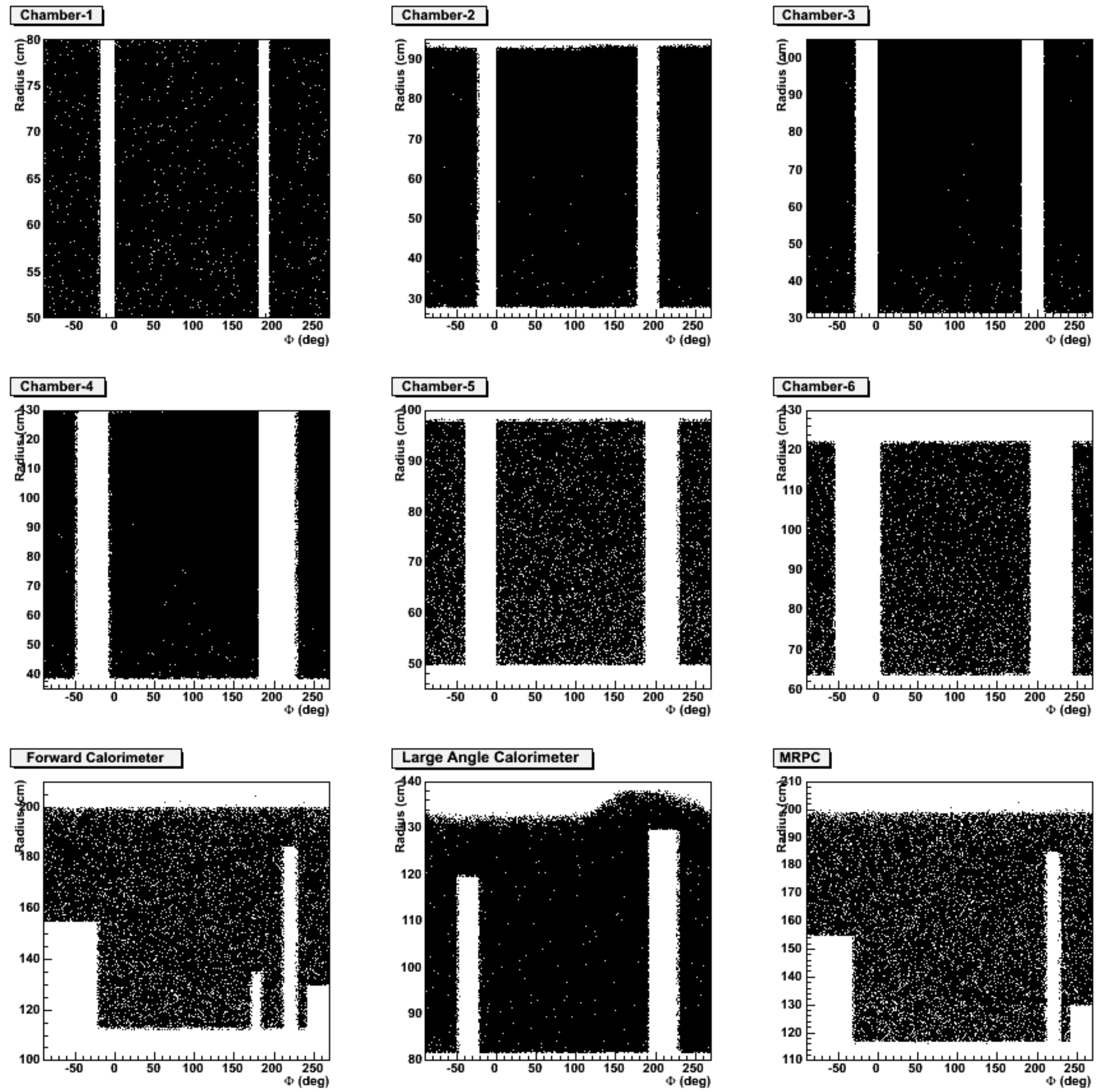

Figure 20: Cuts shown in detector acceptance to remove "line of flame". The top six panels show the acceptance on GEM chambers. The 7th and 8th panel shows the acceptance on forward and large angle calorimeters. The last panel shows the acceptance of MRPC.

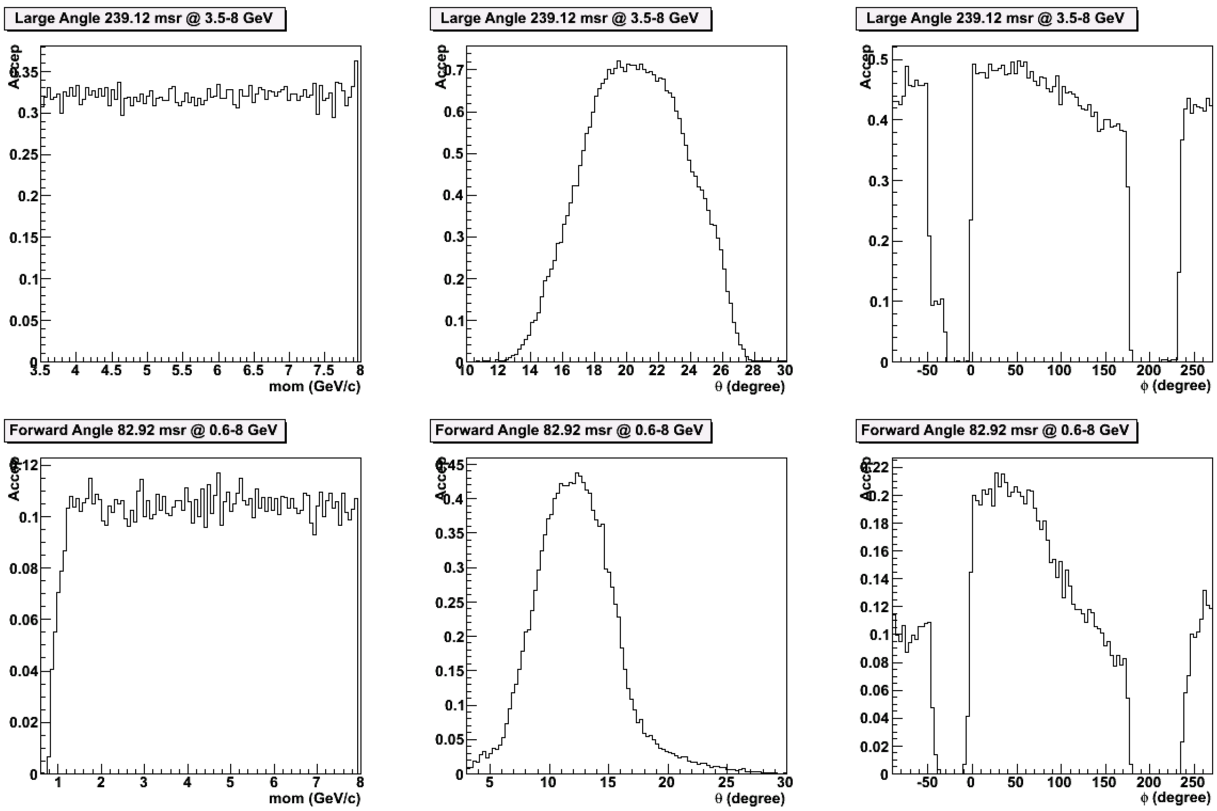

Figure 21: GEANT3 simulation results of electron acceptance with NH_3 target field on with certain area removed to avoid "line of flame". Top and bottom panels show the acceptance of large and forward angle detection, respectively. The total solid angle in the accepted momentum range are also listed.

After accounting for the lost acceptance due to the "line of flame" in the NH_3 data, and applying (DIS) kinematic cuts, $Q^2 \geq 1$ GeV^2 and W ≥ 2 GeV, the full kinematic coverage is $x = 0.06$ - 0.7, $Q^2 = 1.0$ - 9.0 GeV^2, W = 2.0 - 4.5 GeV. Figures 22 and 23 show the coverage in Q^2 vs. x for NH_3 at 11 and 8.8 GeV beam energy. Figures 24 and 25 show the coverage in Q^2 vs. x for ^{3}He at 11 and 8.8 GeV beam energy.

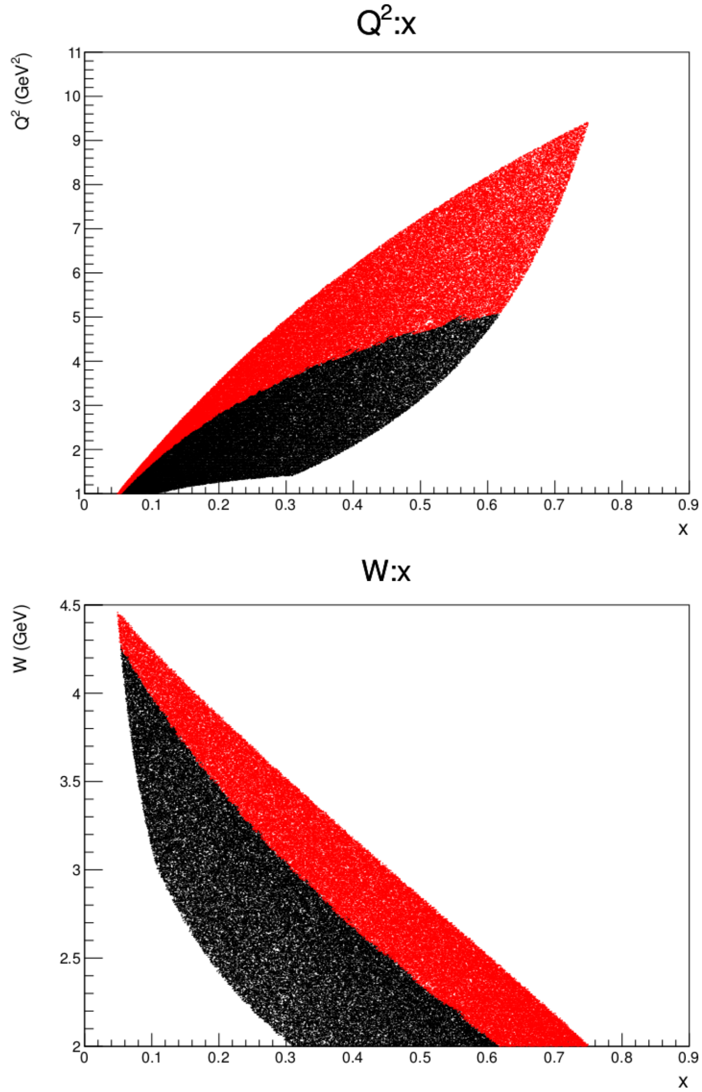

Figure 22: Kinematic coverage for an 11 GeV electron beam with a polarized NH_3 target and "line of flame" cut. The upper plot is Q^2 vs. x. The lower plot is W vs. x. Black (red) is for forward (large) angle.

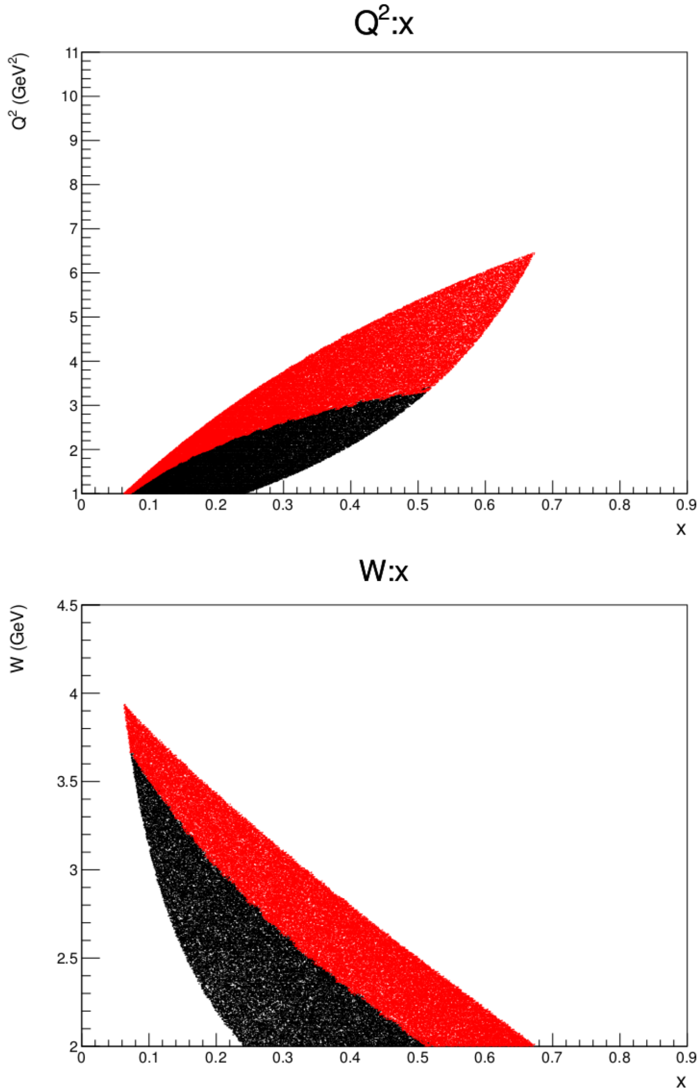

Figure 23: Kinematic coverage for an 8.8 GeV electron beam with polarized NH_3 target and "line of flame" cut. The upper plot is Q^2 vs. x. The lower plot is W vs. x. Black (red) is for forward (large) angle.

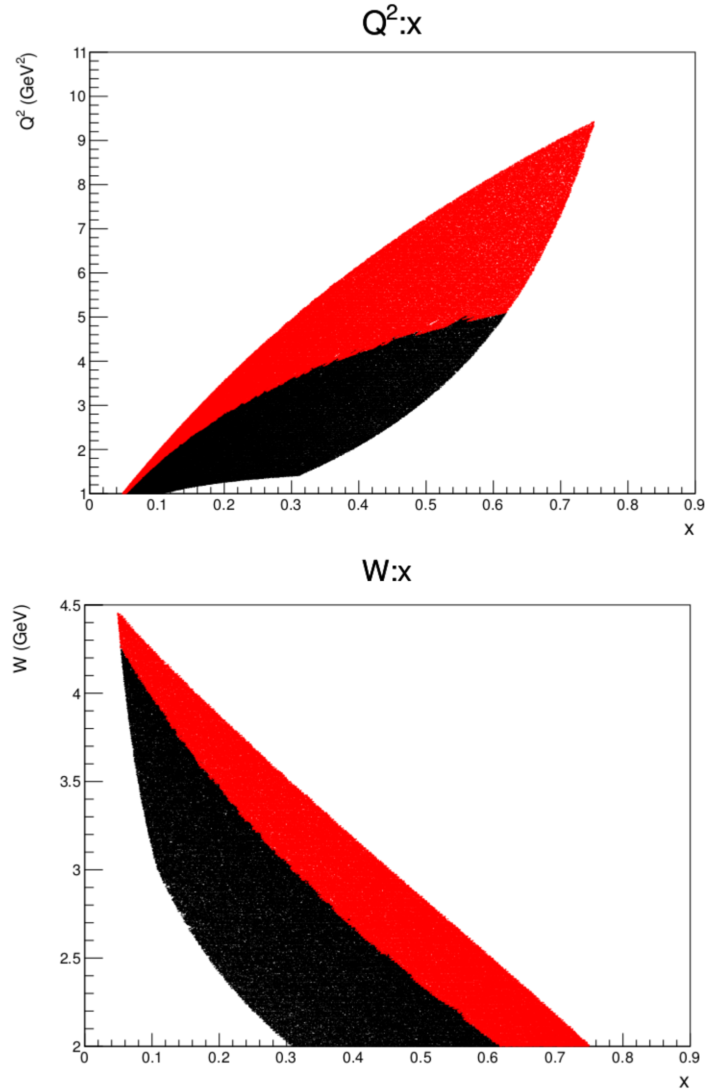

Figure 24: Kinematic coverage for an 11 GeV electron beam with polarized ^{3}He target. The upper plot is Q^2 vs. x. The lower plot is W vs. x. Black (red) is for forward (large) angle.

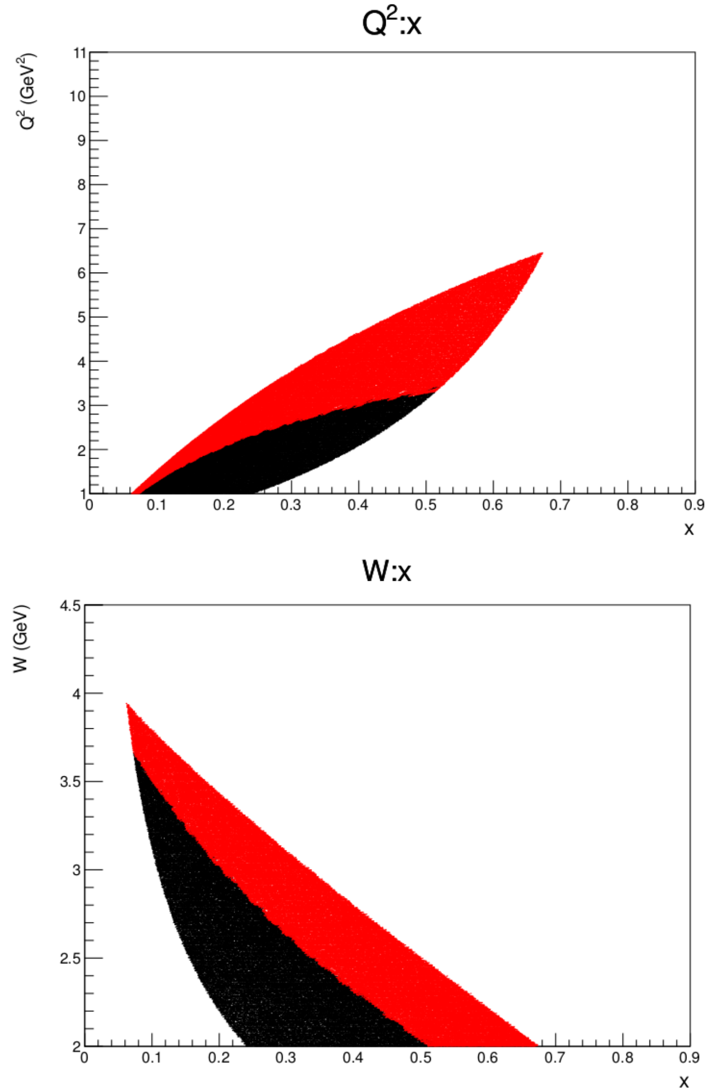

Figure 25: Kinematic coverage for an 8.8 GeV electron beam with polarized ^{3}He target. The upper plot is Q^2 vs. x. The lower plot is W vs. x. Black (red) is for forward (large) angle.

5.2 Rate Estimates

5.2.1 Simulation and Cross Section Model

All simulations were done with a slightly modified version of the GEMC [33] software developed at Jefferson Lab. GEMC uses a GEANT4.95 [32] backend to simulate all particle tracking through and interaction with materials and geometries. A framework for specifying sensitive detectors, processing particles hits, and generating output is also included. The geometry and sensitive detector types are read in at run time allowing for easy modification of designs. Advanced visualization abilities are available, which provides a useful debugging tool. The events are generated by the eicRate simulation package [45] developed by Seamus Riordan. The eicRate program can generate e^- DIS, elastic and $\pi^\pm$,π^0, $K^\pm$, K_s and proton events. Particles are generated including photons and electrons from the low energy EM process (GEANT4), DIS electrons (CTEQ6 PDF), and hadrons (WISER fit). The hadron events are given by the WISER fits in the eicRate which is higher than the global world data. According to the 6 GeV transversity π data, the pion rate from eicRate should be lower by 40%.

5.2.2 Experimental Input

For the NH_3 target, we have a we have assumed a beam current of 100 nA and a target length of 3 cm with a mixture of solid NH_3 and liquid ^{4}He. For the ^{3}He target we assume a beam current of 15 μA and a 40 cm length of ^{3}He gas at a density of 10 amg. The details for the target and beam information can be found in Table 5.

	^{3}He	NH_3+^{4}He
Z	2	7+3+2=12
N	1	7+0+2=9
Density (g/cm^3)	1.345e-3	0.917(NH_3)*0.5+0.145(^{4}He)*0.5=0.531
Length (cm)	40	3
raster (cm×cm)	0.5×0.5	2×2
Position(cm)	(0,0,-350)	(0,0,-350)
I	$15\mu A$	100 nA
Energy (GeV)	11	8.8, 11
Luminosity (target) (Hz/cm^2)	1e37	1e36

Table 5: Basic information about target and beam.

Because we are going to run concurrently with the transversity experiments, we will be using the same beam time as those experiments. See Tables 7 and 6. For the NH_3 target, we will take 94 days of total beam time with 82.5 days for beam on a transversely polarized NH_3 target and 4 days with a longitudinal target polarization to study the systematics of A_{UL} contamination. An additional 7.5 days will be used for dilution measurements, optics, and detector calibrations. There will be an overhead time of 26 days for regular target annealing which does not need an electron beam. This overhead time can be shared with other regular activities such as detector maintenance, etc. Some of this target annealing activities can also be arranged to coincide with the scheduled accelerator maintenance activities in order to reduce overhead time.

For the ^{3}He measurement, we will use 85 days of total beam time with 69 days for beam on the transversely polarized ^{3}He target and 3 days on a longitudinally polarized target. A total of 13 days are dedicated measurements with hydrogen, deuterium and nitrogen gas and optics targets. A total target overhead time of 5 days is needed.

	Time (Hour)	Time (Day)
Trans. Pol. ^{3}He at 11 GeV	**1152**	**48**
Trans. Pol. ^{3}He at 8.8 GeV	**504**	**21**
Long. Pol. ^{3}He at 11 GeV	48	2
Long. Pol. ^{3}He at 8.8 GeV	24	1
Reference cell runs optics and detector check	72	3
Dedicated Hydrogen run	120	5
Dedicated Deuterium run	120	5
Target Overhead: spin rotation, polarization measurement	120	5
Total Time Request	**2040 + 120**	**85 +5**

Table 6: Details of beam time for ^{3}He target at 11 and 8.8 GeV. The beam current is 15 μA.

	Time (Hour)	Time (Day)
Trans. Pol. NH_3 at 11 GeV	**1320**	**55**
Trans. Pol. NH_3 at 8.8 GeV	**660**	**27.5**
Long. Pol. NH_3 at 11 GeV	60	2.5
Long. Pol. NH_3 at 8.8 GeV	36	1.5
Dilution measurements	36	1.5
Optics and detector calibration	144	6
Target overhead regular annealing	624	26
Total Time Request	**2256+624**	**94+26 days**

Table 7: Details of beam time for NH_3 target at 11 and 8.8 GeV. The beam current is 100 nA.

5.2.3 PID and Kinematic Cuts

Pion electro- and photo-production are a significant background for this experiment and for SIDIS. The π^-/e^- ratio from the polarized ^{3}He target are shown in Fig. 26.

The requirements for the singles trigger are listed below and are optimized to remove as much of the pion (and other background) contamination as possible while providing the largest possible rate of good electron events. For forward angle we require a minimum energy deposited in the EM calorimeter , that varies with polar angle, in coincidence with the gas Cherenkov detector. For the large angle, we require a minimum energy deposit in the EM calorimeter. These requirements form the singles trigger. The details are given here:

- **The FAEC (Forward-Angle Electron Calorimeter) Trigger Thresholds:** A cut on the deposited energy, E_f, vs. θ is applied for the forward calorimeter (FAEC). To summarize, we use $E_f \geq 4$ GeV at $\theta \leq 8°$, $E_f \geq 3$ GeV for $8° < \theta \leq 10°$, $E_f \geq 2$ GeV for $10° < \theta \leq 12°$ and $E_f \geq 1$ GeV for $12° < \theta$. This cut is quite tight compared to the EC cut used in the GEMC simulation which utilizes the EC radius. So the final rate will be slightly lower and more conservative than the one from the transversity experiments, about 90%.

- **The LAEC (Large-Angle Electron Calorimeter) Trigger Threshold:** For the large angle calorimeter (LAEC), to reduce large background particles like π^-, we will set a high energy threshold of ~ 3 GeV on the calorimeter.

- **Gas Cherenkov Detectors:** The momentum thresholds for the gas Cherenkov detectors are listed in Table 8. For the forward angle events we require the Cherenkov detector to fire in coincidence with the FAEC.

5.2.4 Rates and Backgrounds

Based on the simulation parameters given above, the rate for the highest luminosity (^{3}He) running are given in Table 9. In this case the total trigger rate is above the expected 80 kHz DAQ limit. For calculating statistical uncertainties we impose a maximum rate of 80 kHz on the singles trigger. Of course, if improvements are made in the DAQ rate capability, we will benefit from the increase in events counted.

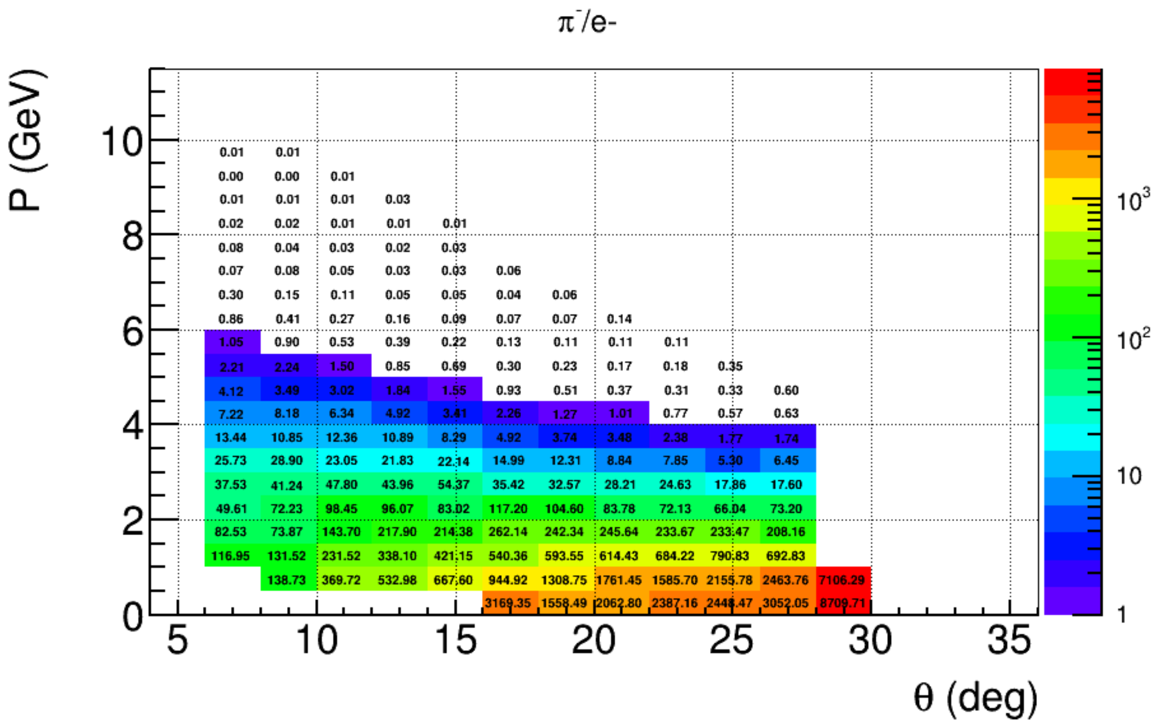

Figure 26: The π^-/e^- ratio for the SIDIS experiment with a 15 μA beam on a 40 cm ^{3}He target. The momentum and polar angles are at the vertices in the target where particles are created.

	Light GC (forward)	Heavy GC (large)
gas	CO_2	C_4F_8O
n	1.0004	1.00135
pressure(atm)	1	1.5
length(m)	1.05	1
p.e for e^-	5	25
P_{π^-}(GeV)	4.8	2.2
P_{K^-}(GeV)	17	7.7
P_{proton}(GeV)	33	14

Table 8: The properties of the gas Cherenkov detector in SoLID.

	e^-	$e^-(\pi^0)$	$\gamma(\pi^0)$	hadron	Total
FA rate (kHz)	90	16.75	1.32	18.7	127
LA rate (kHz)	4.7	0.16	0.8	12.4	18

Table 9: Contributions to the singles electron trigger rates in the forward (FA) and large (LA) detectors. From left to right they are: good electrons, electrons from pair production in π^0 decay, photons from π^0 decay, and hadrons.

Using the good electron rates from above, we then require $W > 2$ GeV and $Q^2 > 1$ GeV^2 to select DIS events. Figures 27 and 28 for the NH_3 target, and Figures 29 and 30 for the ^{3}He target show the final good DIS electron rates binned by x and Q^2. From these rates we can obtain the expected statistical uncertainties in our measurements.

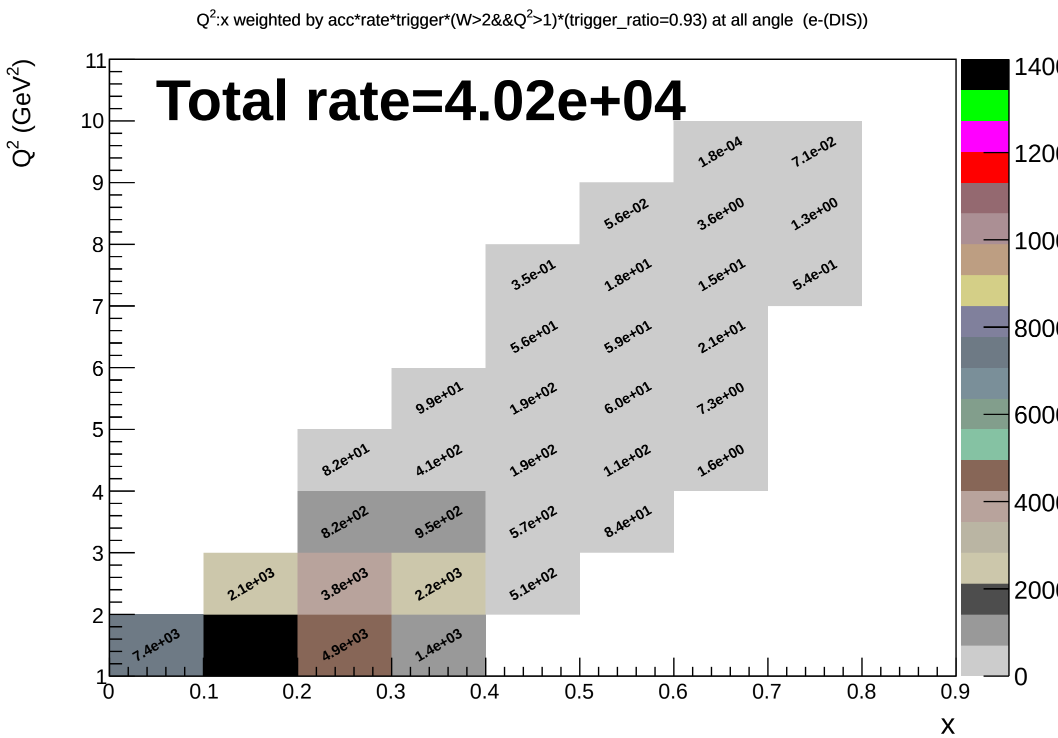

Figure 27: Good electron rates (after PID and DIS cuts) in each Q^2 vs x bin for the NH_3 target for an 11 GeV electron beam. Units for rates are Hz.

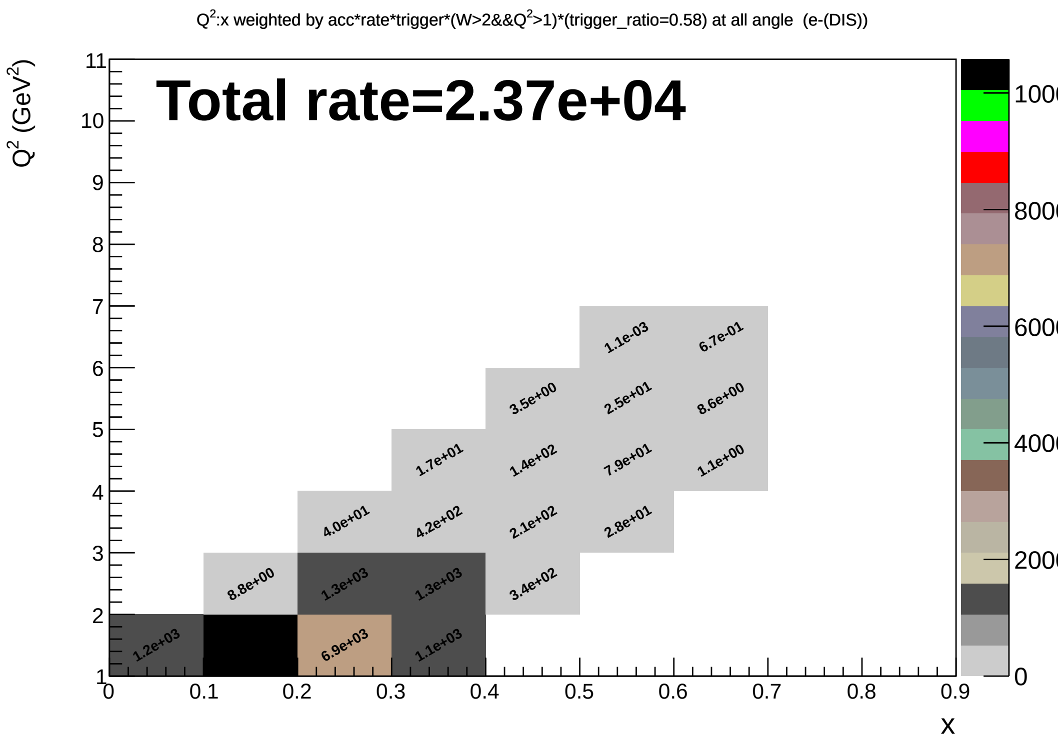

Figure 28: Good electron rates (after PID and DIS cuts) in each Q^2 vs x bin for the NH_3 target for an 8.8 GeV electron beam. Units for rates are Hz.

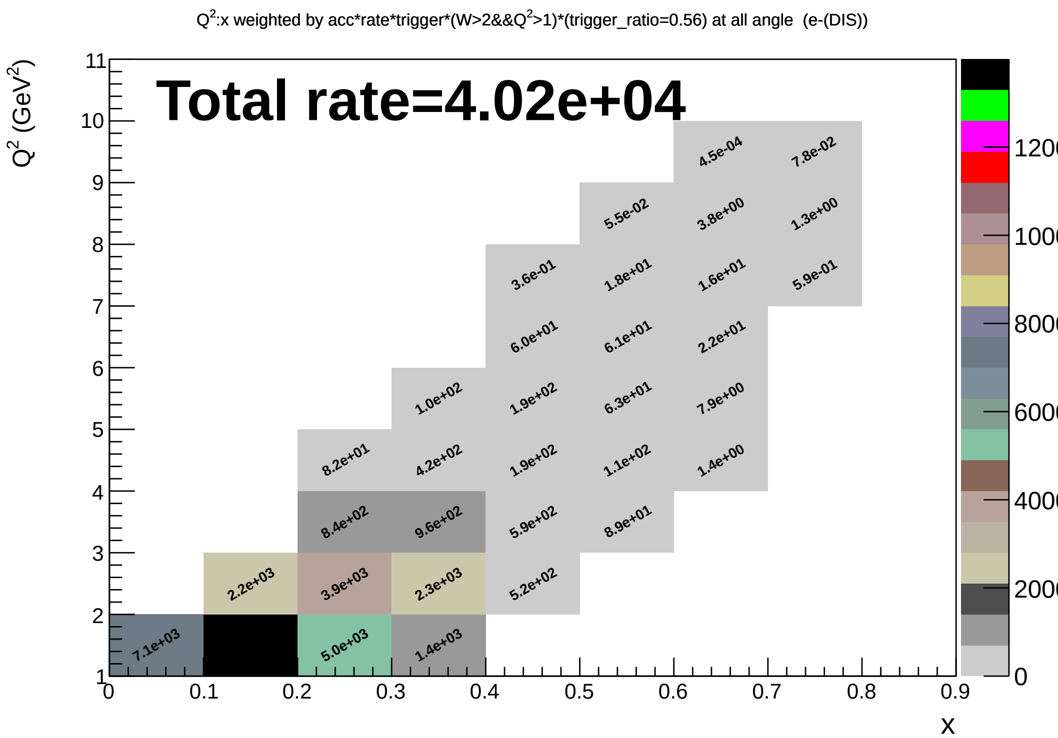

Figure 29: Good electron rates (after PID and DIS cuts) in each Q^2 vs x bin for the ^{3}He target with an 11 GeV electron beam. Units for rates are Hz.

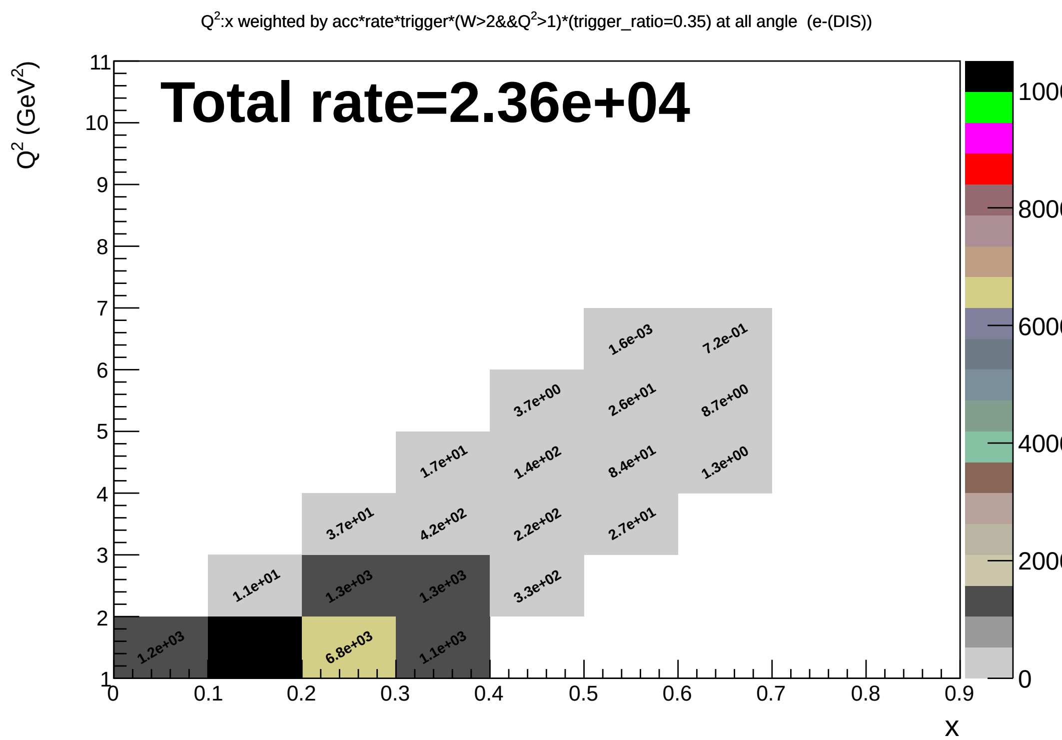

Figure 30: Q^2 vs x for the ^{3}He target with an 8.8 GeV electron beam. Rates are given for each x and Q^2 bin after PID and DIS cuts. Units for rates are Hz.

6 Systematic Uncertainties

Because the statistical uncertainties in each kinematic bin for the fully corrected (physics) $A_{UT}(\phi_S)$ are expected to be $\sim 10^{-4} - 10^{-3}$, corresponding to raw asymmetries of $\sim 10^{-5} - 10^{-4}$, systematic uncertainties must also be under control at this level where possible. In this section we estimate the expected contributions to the systematic uncertainties.

The large azimuthal angular coverage plays an important role in reducing the systematic uncertainties in the raw asymmetries because it will all us to study sector by sector variations in luminosity and detector efficiency. The target spin will frequently be flipped by 180° which will further help us to quantify false asymmetries due to luminosity or detector related anomalies. High quality PID will be important for reducing uncertainties due to background contamination. Systematic uncertainties will also arise from uncertainty in the target polarizations, dilution factors and radiative corrections. For ^{3}He, there is also an uncertainty due to the extraction of the neutron asymmetry from the measured ^{3}He asymmetry.

6.1 The Experimental Observable

In this experiment, we will form the (raw) target SSA $A_{UT}(\phi_S)$ directly as:

$$A_{UT}(\phi_S) = \frac{1}{f\ P_t} \frac{N^+(\phi_S) - N^-(\phi_S)}{N^+(\phi_S) + N^-(\phi_S)} \tag{9}$$

where f and P_t are the dilution factor and target polarization and the $N^\pm$ are the luminosity-normalized yields at each ϕ_S bin for the target spin "normal" (+) or "reversed" (-). The relative luminosity will be monitored by various spectrometer singles rates and downstream luminosity monitors. In Eq. 9, the major systematic uncertainties are from false asymmetries due to time-dependent uncertainties in luminosity and detector efficiency. The time-independent part of these uncertainties will cancel in first order in the asymmetries.

To extract the physics asymmetry, A_y, we will fit the measured $A_{UT}(\phi_S)$ (corrected for backgrounds and radiative effects) as a function of ϕ_S and divide by the average target polarization and dilution factors. The dilution factors are needed to extract the proton or neutron data from the measured yields that include scattering from unpolarized nucleons.

6.2 Target Spin Flip and ϕ Coverage

The direction of the target polarization as measured in the laboratory frame will be flipped by 180° periodically to allow measurement of the SSA. However, the large number of spin flips that will be made will also allow us to study time-dependent detector efficiencies and luminosity asymmetries. For one simple example, the combined event rate in two detector channels at the same θ but separated by $\phi = 180°$ should remain constant regardless of target orientation. Many such quantities can be monitored for time dependent rate changes due to the high segmentation of the detector.

NH_3 Target: Due to the strong target magnetic field (5T) for the NH_3 measurements, it is difficult to rotate the target field direction to realize the spin reversal. One possible method is to use RF spin flip with the adiabatic-fast-passage (AFP) technique. The most current information on the efficiency of AFP spin-flip for NH_3 is in a proceedings paper from a recent workshop [46] in which it is expected to be about 50% for the condition at 5T/1K. With its spin-up (recovering) time of about 20 minutes, if we keep the spin flip (pair) frequency to be every two-hours, the net effect will be a loss of about 10% of the polarization. Combining the spin-flip effect together with the beam depolarization, the average in-beam polarization with spin flip will be roughly 70%. This concept will be tested by the polarized target group at UVa for both NH_3 and ND_3 targets.

^{3}He Target: In the 6 GeV A_y^n experiment, the target SSA was measured by flipping the ^{3}He spin every 20 minutes using AFP and an average target polarization of $\sim 60\%$ was achieved. Based on this performance, we plan to flip the target polarization direction every 20 minutes (40 minutes per pair).

6.3 False Asymmetries

For the NH_3 measurement there will be 990 spin flip pairs when transversely polarized. For the ^{3}He measurement, there will be 1720 spin flip pairs. We expect to control the systematic uncertainties in both detection efficiencies and luminosity to less than 1% in each pair. These give a false asymmetry of $\sim 3 \times 10^{-4}$ in the raw asymmetries.

6.4 Determining ϕ_S

There are systematic uncertainties in finding ϕ_S due to the uncertainty in the target polarization direction and the uncertainty in the reconstructed electron azimuthal scattering angle. We assume an uncertainty of $\pm 0.2°$ in each target orientation which is relevant for comparing and combining the measured asymmetries from each of the two different target directions. When the scattered electron in is the plane of the target polarization, the asymmetry should be exactly zero. This means that the asymmetries measured in each bin for the two different target orientations will have a relative uncertainty of $\sim \pm 2 \times 10^{-5}$ due to target misalignment. For the detected electron, we assume each particle detected will have an uncertainty in ϕ_S of $\pm 0.2°$ due to the detector resolution and tracking reconstruction. We assume that this is uncorrelated for each measured track. Because each bin in ϕ_S will contain $\sim\geq 10^{-6}$ events, the uncertainty on the average value of ϕ_S for each bin will be negligible. By the same reasoning, the uncertainty in the average reconstructed polar angle in each bin is negligible. Based on these estimates we assume the total systematic uncertainties due to the uncertainties in the observed ϕ_S and θ angles is negligible.

6.5 Azimuthal Angular Asymmetry in A_{UL}

In the lab frame, the targets are transversely polarized with respect to the beam direction. However, in the definition of A_{UT}, the S_T is defined as the transverse polarization with respect to the virtual photon direction, which has a small angle with the z-axis. Therefore, there will be a small S_L (longitudinal) polarization component. When the target spin is flipped, the S_L will also flip. Thus there will be a false asymmetry from the S_L contamination. The average S_L values are 0.1 and 0.15 with 11 GeV and 8.8 GeV incident beam energies, respectively, and are exactly calculable from kinematics. Theory says that A_{UL} is exactly zero which means we can make a precise correction for this S_L component. We do not expect a significant systematic uncertainty due to this correction. In addition, data will be taken with longitudinally polarized targets to measure A_{UL} directly. (This also serves as another technique to look for false asymmetries.)

6.6 Background Contributions

The 6 GeV A_y^n experiment [18] measured the raw SSA for $\vec{N}(e,\pi^{\pm})$ to be (magnitude)$< 0.04 \pm 0.005$. Based on the detector performance expected from the SoLID Pre-CDR report, the pion efficiency will be better than $\sim 10^{-3}$ below 4 GeV. The calorimeters have pion efficiency $\sim 10^{-2}$ except at the lowest momentum. We will assume an overall rejection of $\sim 10^{-4}$ for all particles with momentum above 2 GeV where the π/e ratio is $\leq 10^{-2}$. In this case, pions will contribute approximately 4×10^{-4} to the systematic uncertainty on the raw A_{UT}. For particles with momentum below 2 GeV, this number will increase. Another background comes from mis-identified electrons that come from e^+/e^- pair production from neutral pion decay. During the 6 (5.5) GeV measurement, the contamination from pair-produced electrons after cuts on the data was $> 10\%$ for $E' < 1.8$ GeV but dropped quickly to well below 1% for $E' > 2.7$ GeV. The measured raw positron asymmetry was $\sim 0.01 \pm 0.01$. These large contaminations were due to the inability to distinguish these events from good electrons in the BigBite spectrometer. For the SoLID spectrometer, we expect to reduce the contamination from this background to the 10^{-2} level by rejecting triggers with coincident positron and electron events consistent with pair production. Under this assumption, the expected contribution to the raw asymmetry from pair produced electron events is $\sim 10^{-4}$. We believe these background estimates are conservative.

6.7 Target Polarization

The systematic uncertainty corresponding in the magnitude of the target polarization is limited by the ability to do an absolute calibration. For NH_3 the calibration is done by measuring the known non-enhanced (thermal equilibrium) polarization at ≈ 1.5 K. The uncertainty in the polarization is expected to be $\sim 3\%$ (rel.). Another correction related to the polarized NH_3 target comes from the relatively small polarization of the ^{14}N nuclei which must be applied to the measured asymmetries. We do not expect a large systematic uncertainty from the ^{14}N.

For ^{3}He, the calibration can be done by measuring the known thermal equilibrium polarization of the protons in a cell filled with purified water and also by measuring the frequency shift of the alkali metal hyperfine splittings in the presence of the polarized gas. These techniques are well-understood and are the mainstay of the Hall A polarized ^{3}He target. The uncertainty in the polarization is expected to be $\sim 3\%$ (rel.).

6.8 Dilution Factors

Both targets contain unpolarized material that contributes to the total rates. For the NH_3 target these are primarily nitrogen, helium and aluminum and the dilution factor is ~ 0.13. To study the target dilutions we will take several different sets of data in both elastic and DIS including empty cell (with ^{4}He/windows/shielding etc.) runs and solid target runs such as ^{12}C and CH_2. Typically, with this target, ^{12}C data is used to approximate the nitrogen contribution to the dilution. There is an associated quantity known as the packing fraction which specifies the fraction of the volume of the target cell occupied but he NH_3 crystals. This is typically $\sim 0.5 - 0.6$ and is part of the input needed to obtain the packing fraction. There were many studies done on the extraction of dilution factor from the previous experiments which typically achieved a relative uncertainty of 5%, dominated by the uncertainty in the packing fraction.

For the ^{3}He target, the dilution comes from a small amount (~ 0.1 amg) of N_2 gas used to aid the SEOP process. This dilution factor can be measured by using an identical glass "reference" cell which may be evacuated or filled with H_2 or N_2 gas. Measurements at both elastic and DIS kinematics are useful to disentangle the contributions to the dilution factor. The dilution factor is expected to be ~ 0.85 with an expected relative uncertainty of 2% based on previous experiments.

6.9 Neutron Results from ^{3}He

To extract the asymmetries for the neutron, we must model the effective polarization of the neutron in a polarized ^{3}He nucleus. The formalism is described in equation 8. The dilution from the proton events is ~ 0.8 with an uncertainty of $\sim 5\%$ (rel.).

6.10 Radiative Corrections

External (unpolarized) radiative effects can be calculated using the formalism of Mo & Tsai [47] with model input from global fits to world DIS data. The uncertainty in these corrections is expected to contribute a 2% (rel.) uncertainty in the physics asymmetries. Because there is currently no model for the radiative corrections to the asymmetry, no estimate of these corrections is given at this time.

6.11 Systematic Uncertainty Budget

The systematic uncertainties are summarized in Tables 10 and 11 .

Sources	Type	δA_y^{raw}	δA_y^{phys}
False Asymmetries	absolute	3×10^{-4}	3×10^{-3}
Background Subtraction	absolute	4×10^{-4}	4×10^{-3}
Target Polarization	relative	3%	3%
Dilution Factor	relative	5%	5%
Radiative Correction	relative	2%	2%

Table 10: Systematic uncertainties on the proton asymmetries for the proposed NH_3 experiment.

Sources	Type	δA_y^{raw}	δA_y^{phys}
False Asymmetries	absolute	3×10^{-4}	1×10^{-4}
Background Subtraction	absolute	4×10^{-4}	1×10^{-3}
Target Polarization	relative	3%	3%
Dilution Factor	relative	2%	2%
Radiative Correction	relative	2%	2%
Neutron Extraction	relative	5%	5%

Table 11: Systematic uncertainties on the neutron asymmetries for the proposed ^{3}He experiment.

7 Projected Results

The expected statistical precision of the results in this experiment are shown in this section. Good electrons were counted after using the cuts defined in the section 5.2.2, including the partial loss in the azimuthal coverage due to "line of flames" for the NH_3 target and the acceptance effect from the GEMC simulation. For the ^{3}He results, we assume a maximum DAQ rate of 80 kHz.We assume the dilution factors are 0.13 for the NH_3 target and 0.85 for the ^{3}He target. The target polarizations are 70% for the NH_3 target and 60% for the ^{3}He target. There is another "dilution" factor due to extracting the neutron from the ^{3}He target which is ~ 0.8.

Statistical uncertainties were calculated in three dimensional phase space (ϕ_S, x, Q^2) for $0.05 < x < 0.75$ and $1.5 < Q^2 < 9.5$ GeV^2. For plotting purposes, a token value of $|A_y| = 10^{-2}$ was used for all results. As a way of summarizing the expected statistical precision, we combine the data for $A_{UT}(\phi_S)$ from all values of x at a given Q^2, which are shown in Figures 31 and 32 for NH_3, and Figures 33 and 34 for ^{3}He. Fitting these results for $A_{UT}(\phi_S)$ we obtain the statistical uncertainties for A_y shown in Figures 35 and 36 for NH_3, and Figures 37 and 38 for ^{3}He. Detailed results for $A_{UT}(\phi_S)$, and A_y versus Q^2, separated into individual bins in x are shown in Appendix A.

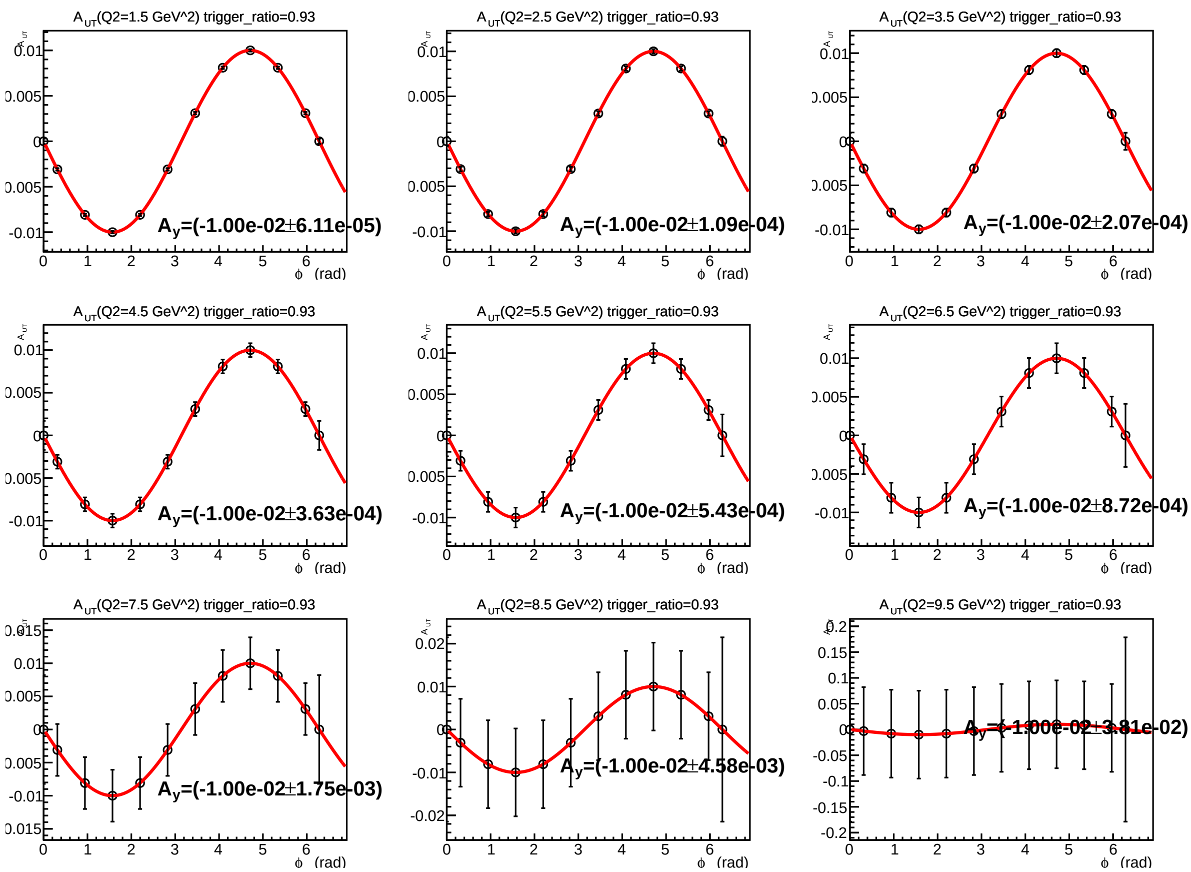

Figure 31: Expected uncertainties in A_{UT} vs. ϕ_S at different Q^2 at 11 GeV for the NH_3 target. For each plot, the data over all values of x was combined. An arbitrary amplitude of 10^{-2} was chosen for the asymmetry.

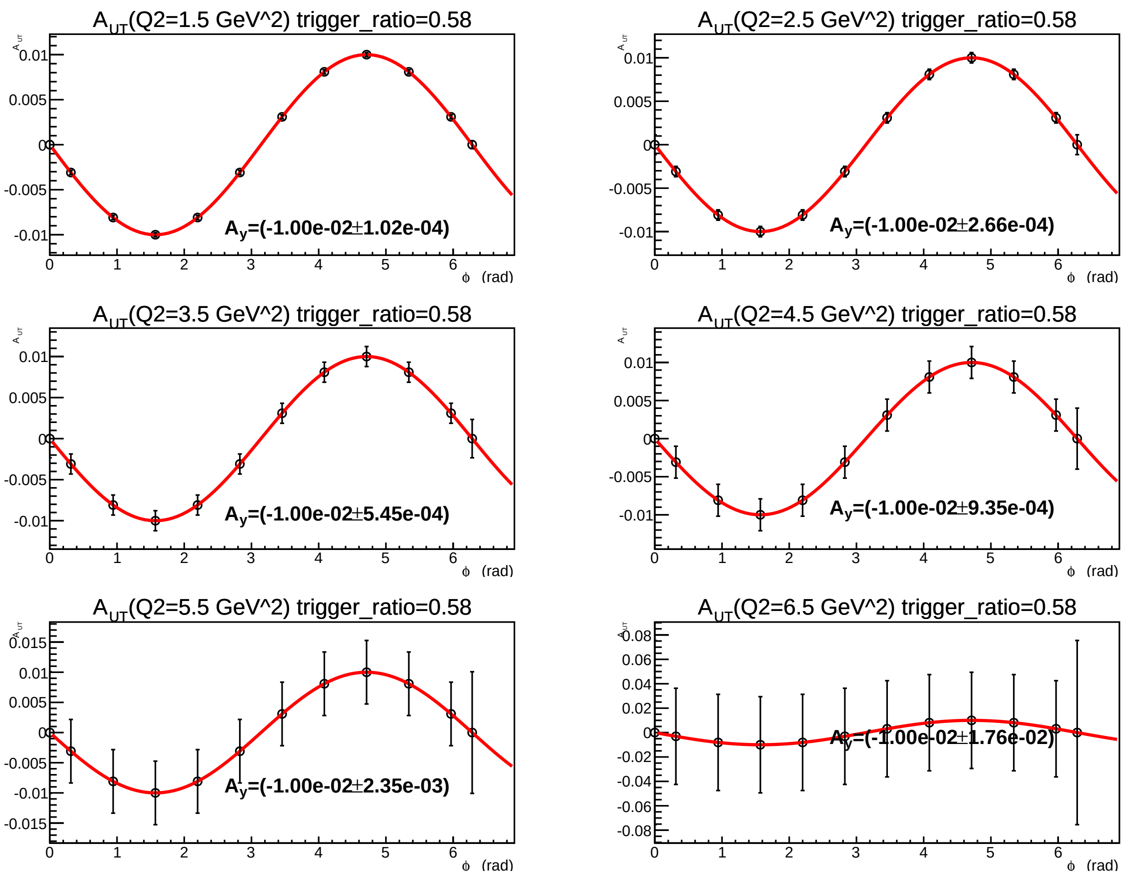

Figure 32: Expected uncertainties in A_{UT} vs. ϕ_S at different Q^2 at 8.8 GeV for the NH_3 target. For each plot, the data over all values of x was combined. An arbitrary amplitude of 10^{-2} was chosen for the asymmetry.

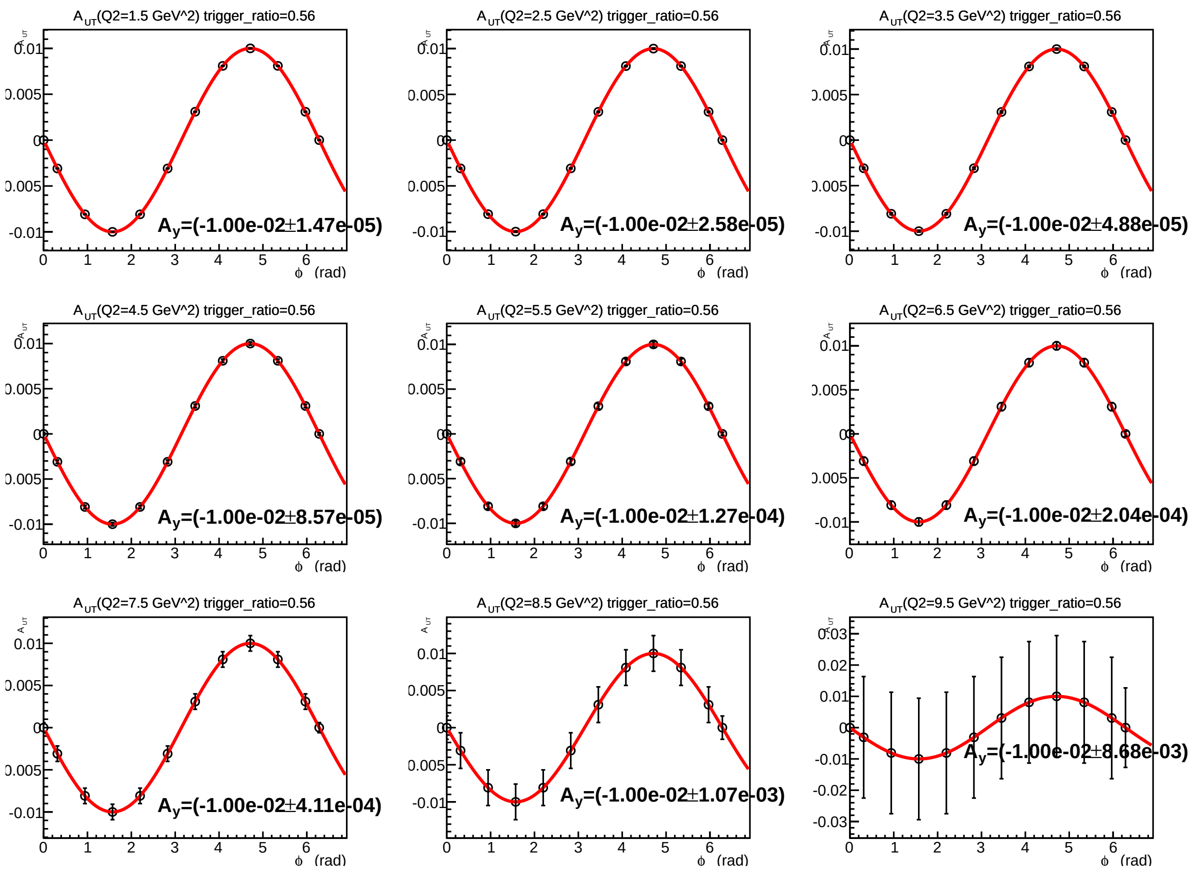

Figure 33: Expected uncertainties in A_{UT} vs. ϕ_S at different Q^2 at 11 GeV for the ^{3}He target. For each plot, the data over all values of x was combined. An arbitrary amplitude of 10^{-2} was chosen for the asymmetry.

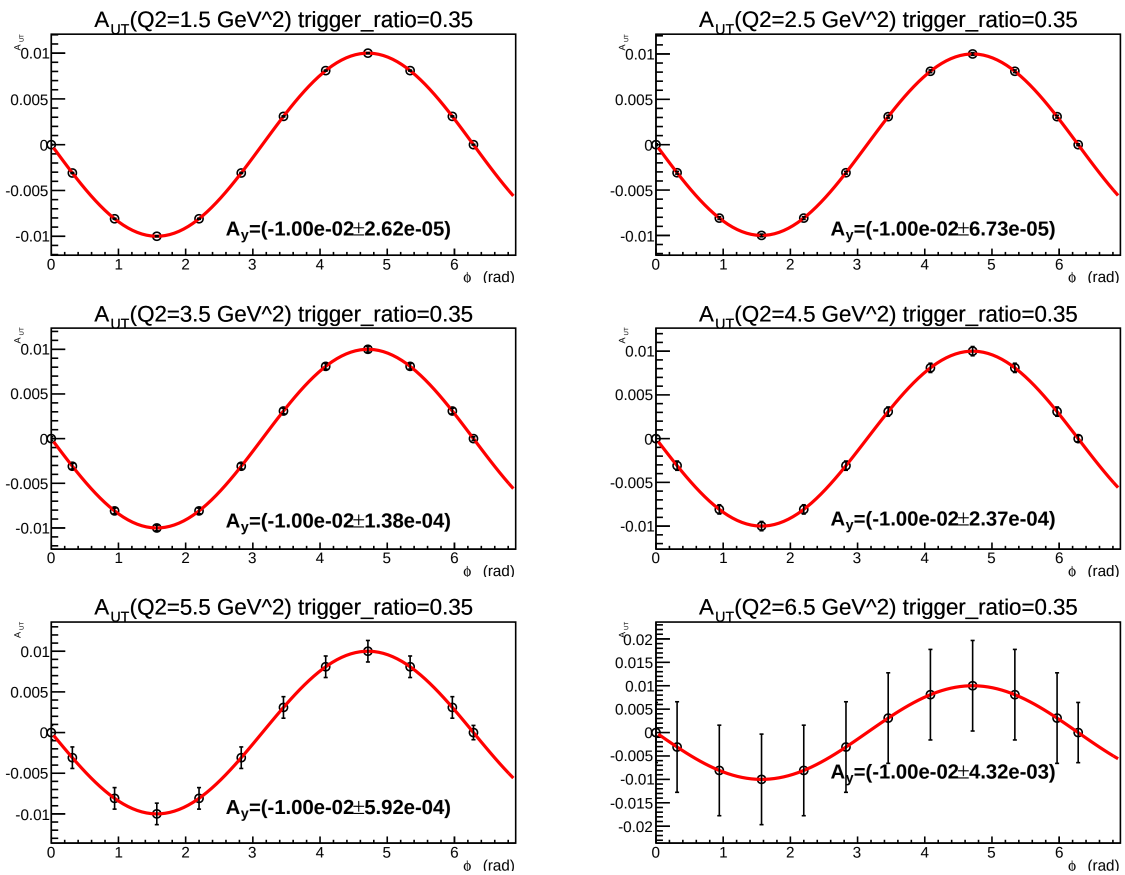

Figure 34: Expected uncertainties in A_{UT} vs. ϕ_S at different Q^2 at 8.8 GeV for the ^{3}He target. For each plot, the data over all values of x was combined. An arbitrary amplitude of 10^{-2} was chosen for the asymmetry.

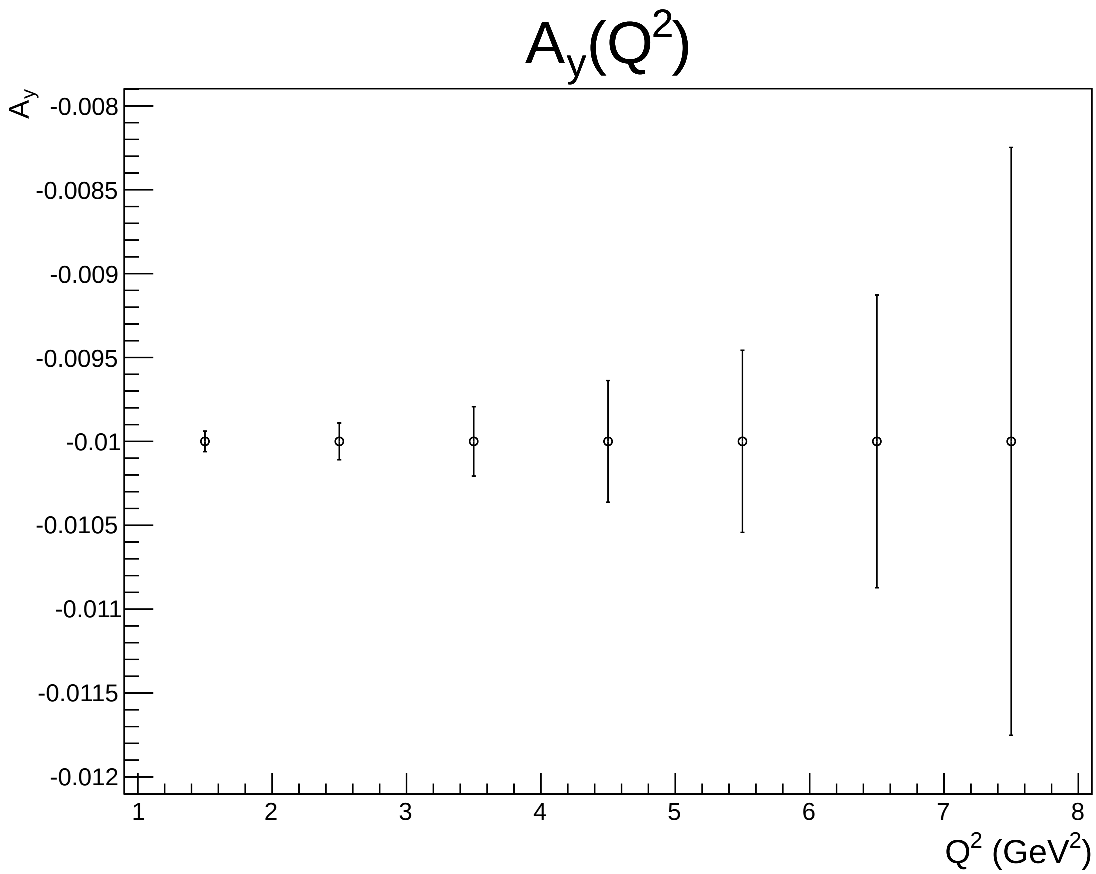

Figure 35: Expected statistical uncertainties in A_y vs Q^2 at 11 GeV for the NH_3 target. At each Q^2 data at all x were combined. An arbitrary value for A_y of 10^{-2} was used.

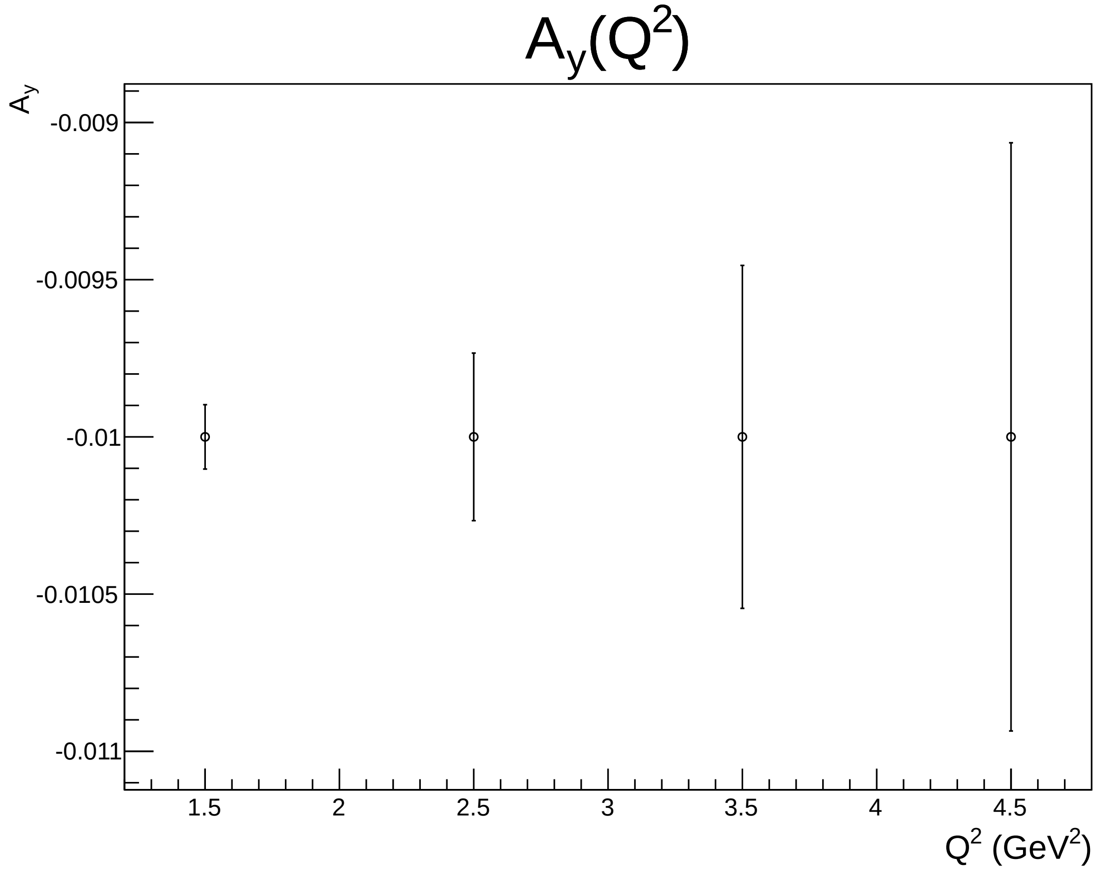

Figure 36: Expected statistical uncertainties in A_y vs Q^2 at 8.8 GeV for the NH_3 target. At each Q^2 data at all x were combined. An arbitrary value for A_y of 10^{-2} was used.

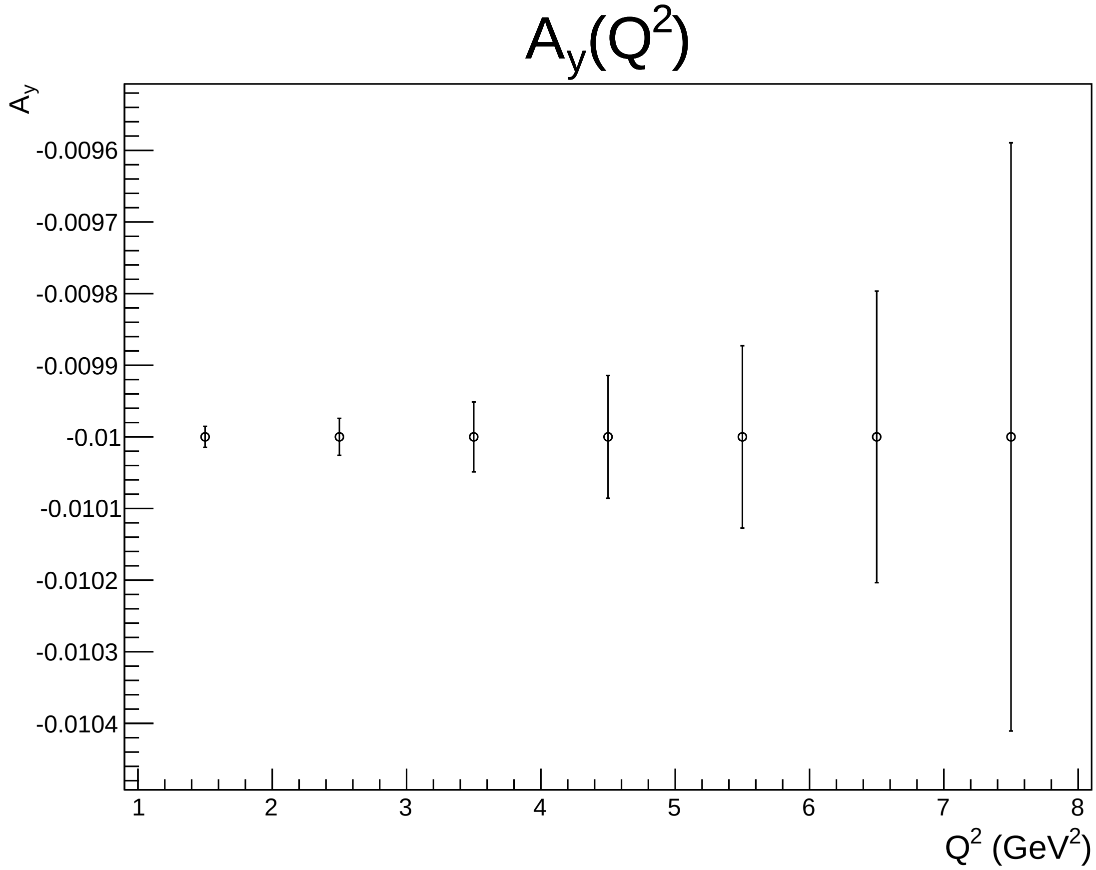

Figure 37: Expected statistical uncertainties in A_y vs Q^2 at 11 GeV for the ^{3}He target. At each Q^2 data at all x were combined. An arbitrary value for A_y of 10^{-2} was used.

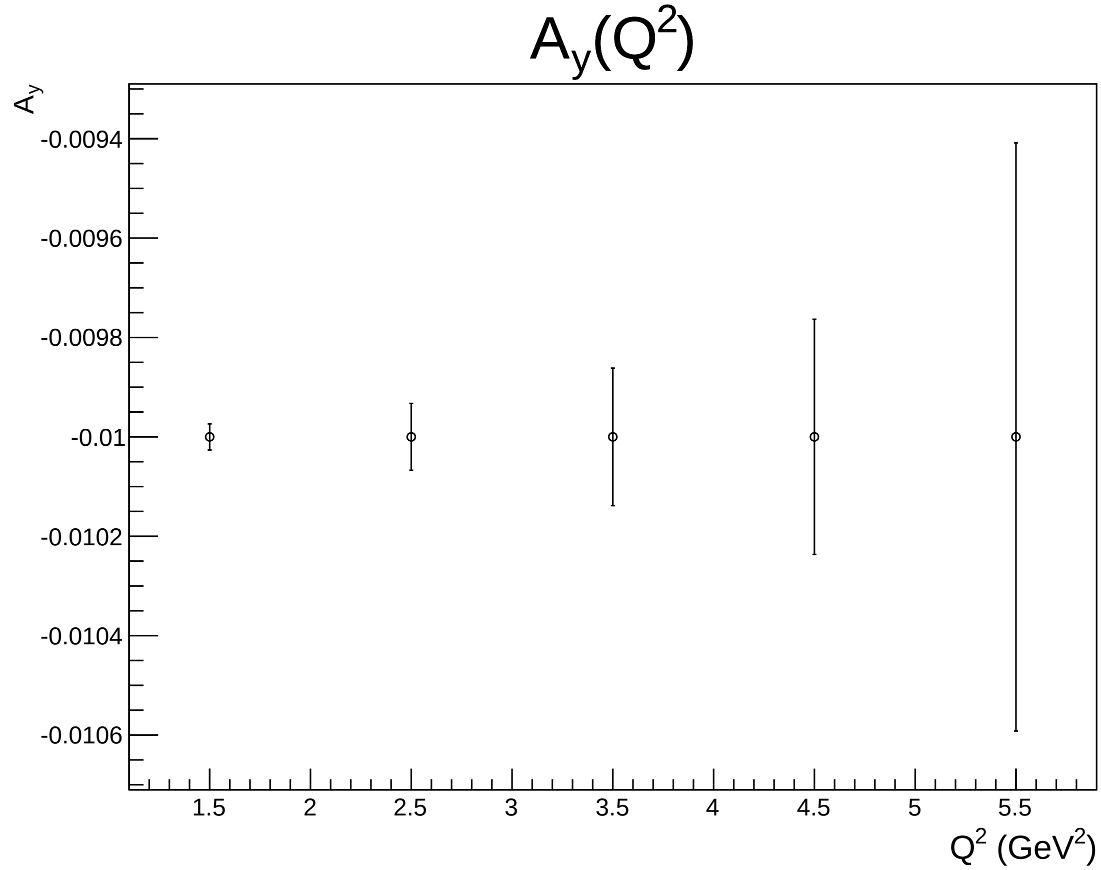

Figure 38: Expected statistical uncertainties in A_y vs Q^2 at 8.8 GeV for the ^{3}He target. At each Q^2 data at all x were combined. An arbitrary value for A_y of 10^{-2} was used.

7.1 Conclusion and Summary

From the above plots one can see that measurements of $A_{UT}(\phi_S)$ and A_y in a large number of x and Q^2 bins ($1.5 < Q^2 < 7.5$ GeV^2, $0.05 < x < 0.65$, $W > 2$ GeV) will be obtained for both proton and neutron. The statistical uncertainties of $10^{-4} - 10^{-3}$ (kinematic dependent) with similar expected systematic uncertainties will provide information on the transverse target single spin asymmetry at a level never before achieved. The level of precision will allow us to definitively discriminate between various parton model predictions for the nucleon intermediate state in two-photon exchange. It will provide an answer to the important sign mis-match in the neutron predictions using either the Sivers or KQVY input for guark-gluon correlations. Finally, these measurements provide a new opportunity to access the dynamics of the nucleon beyond the non-interacting parton level without the significant contribution from Born scattering that is typically present in nucleon structure measurements.

By optimizing the singles triggers and PID, and by focusing on minimizing systematic uncertainties, we can complete the proposed measurements during the already approved SoLID transversity experiments without the need for additional beam time. Our experience with the first-ever neutron measurement at 6 GeV has prepared us for this measurement and subsequent analysis.

8 Appendix A

Here we give the expected statistical uncertainties in $A_{UT}(\phi_S)$ at fixed values of Q^2 and specific ranges of x.

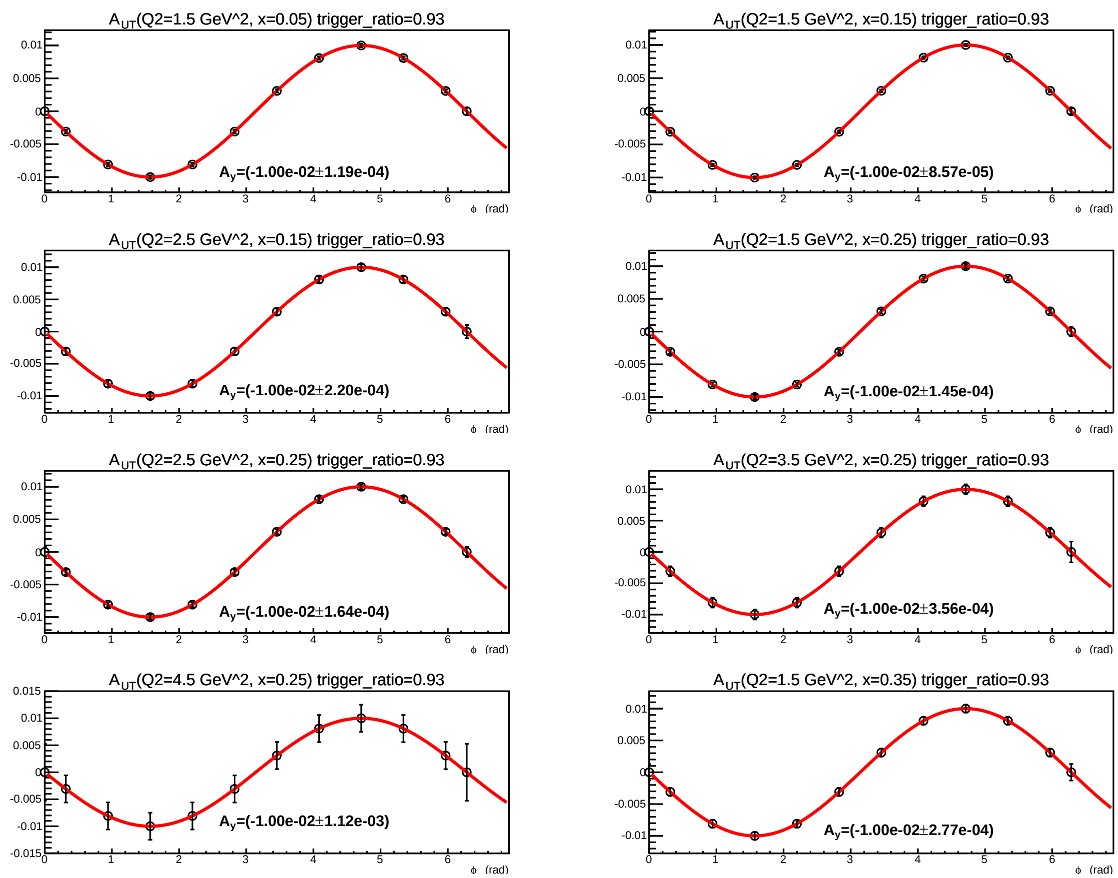

Figure 39: A_{UT} at different Q^2 and x for the NH_3 target at 11 GeV. Here $0.05 < x < 0.35$.

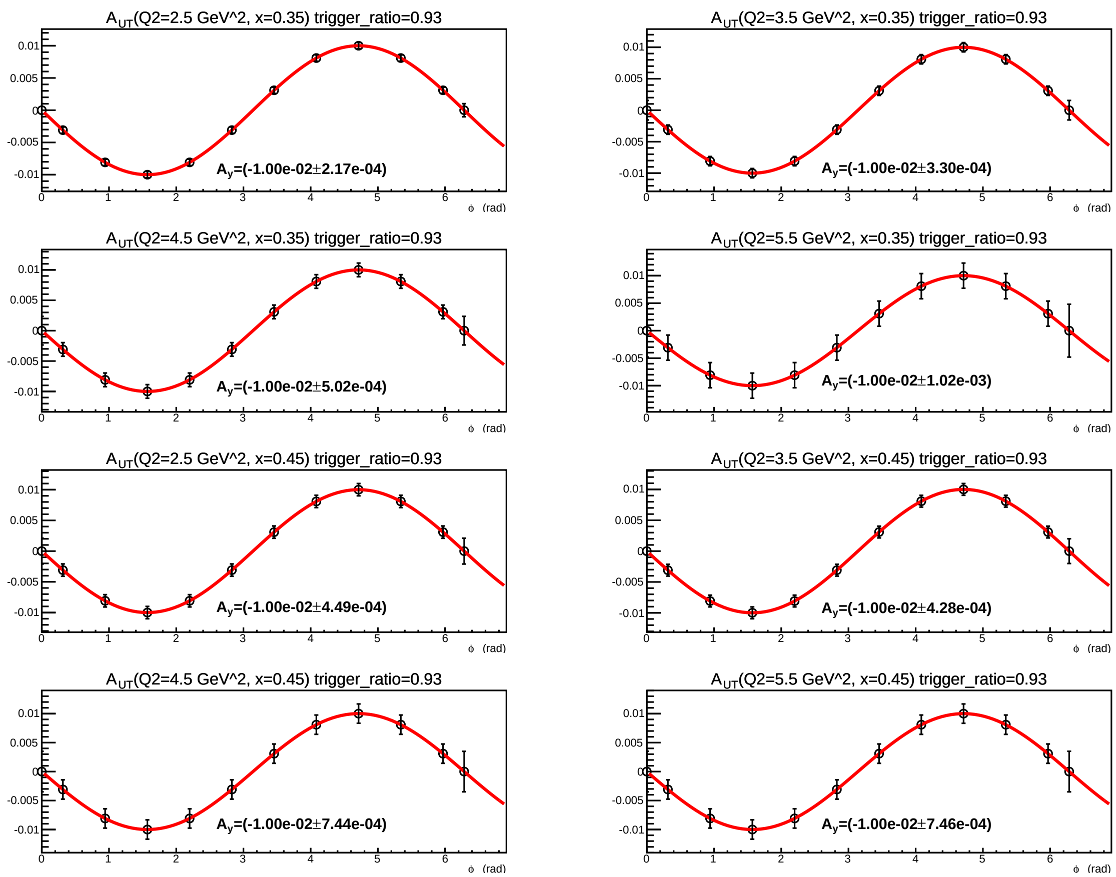

Figure 40: A_{UT} at different Q^2 and x for the NH_3 target at 11 GeV. Here $0.35 < x < 0.45$.

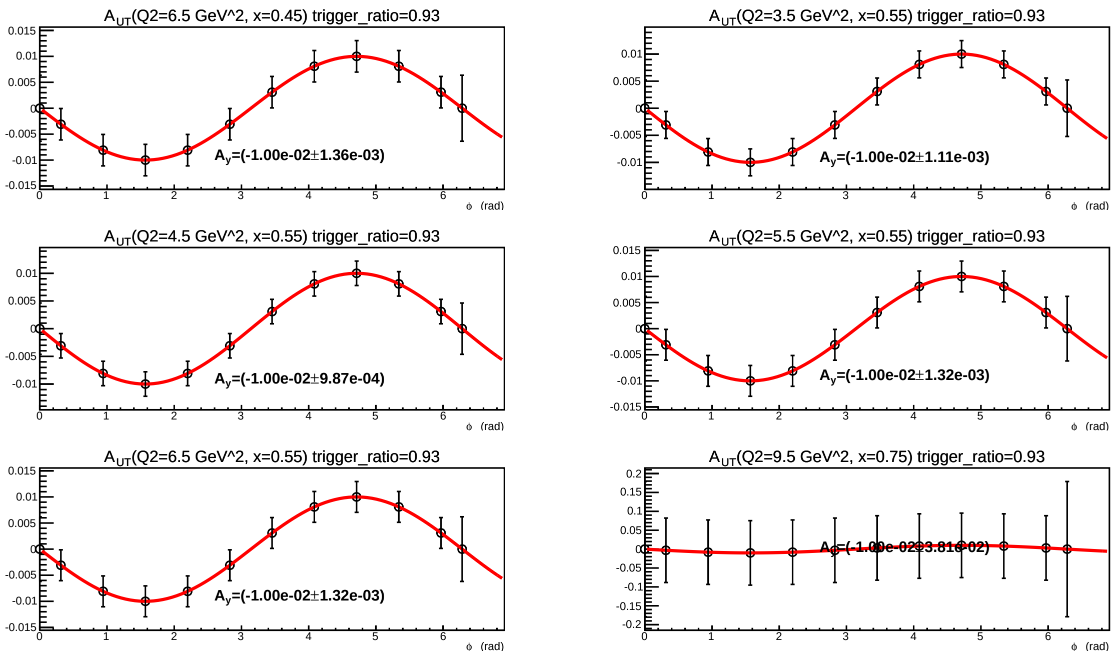

Figure 41: A_{UT} at different Q^2 and x for the NH_3 target at 11 GeV. Here $0.45 < x < 0.75$.

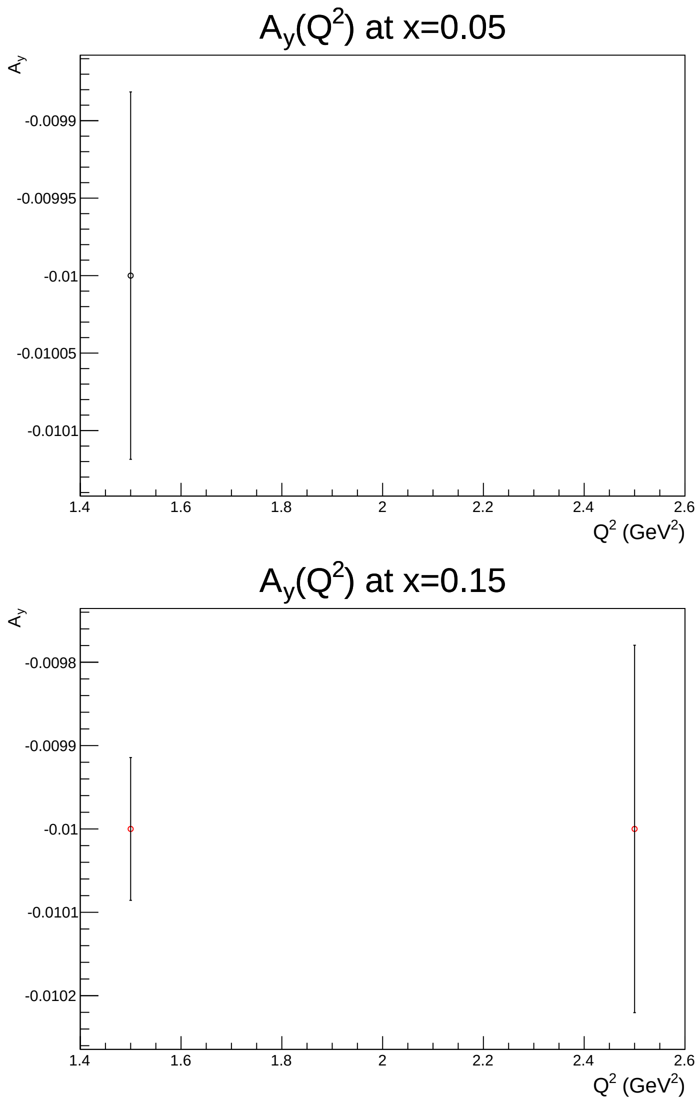

Figure 42: A_y vs Q^2 at $x = 0.05$ and 0.15 for the NH_3 target at 11 GeV.

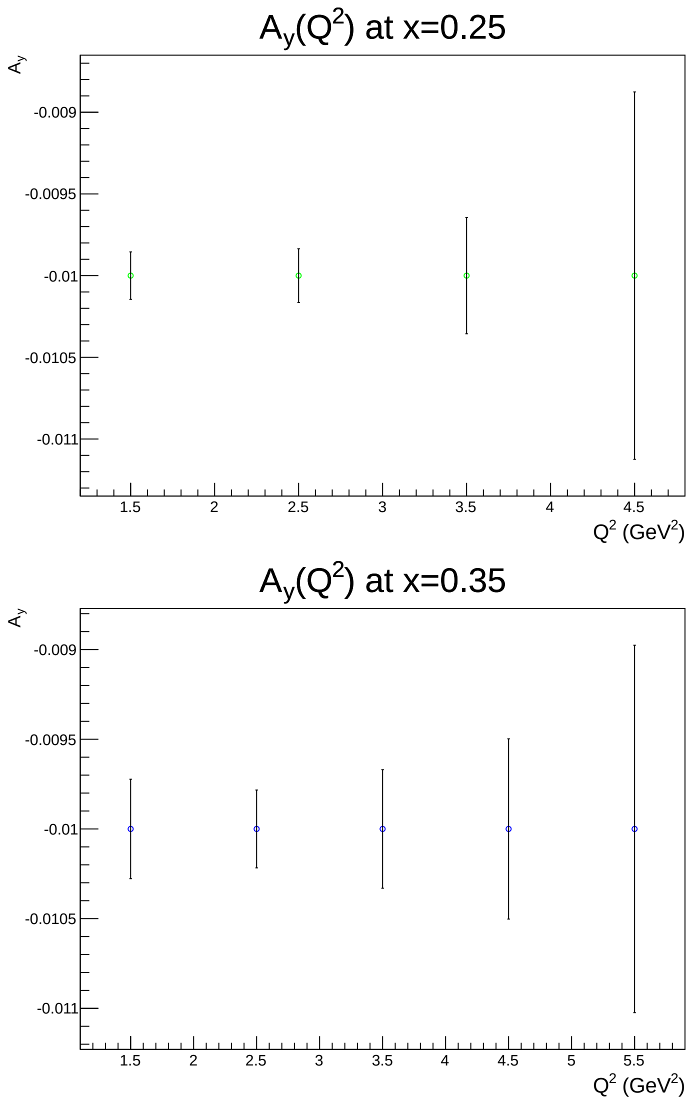

Figure 43: A_y vs Q^2 at $x = 0.25$ and 0.35 for the NH_3 target at 11 GeV.

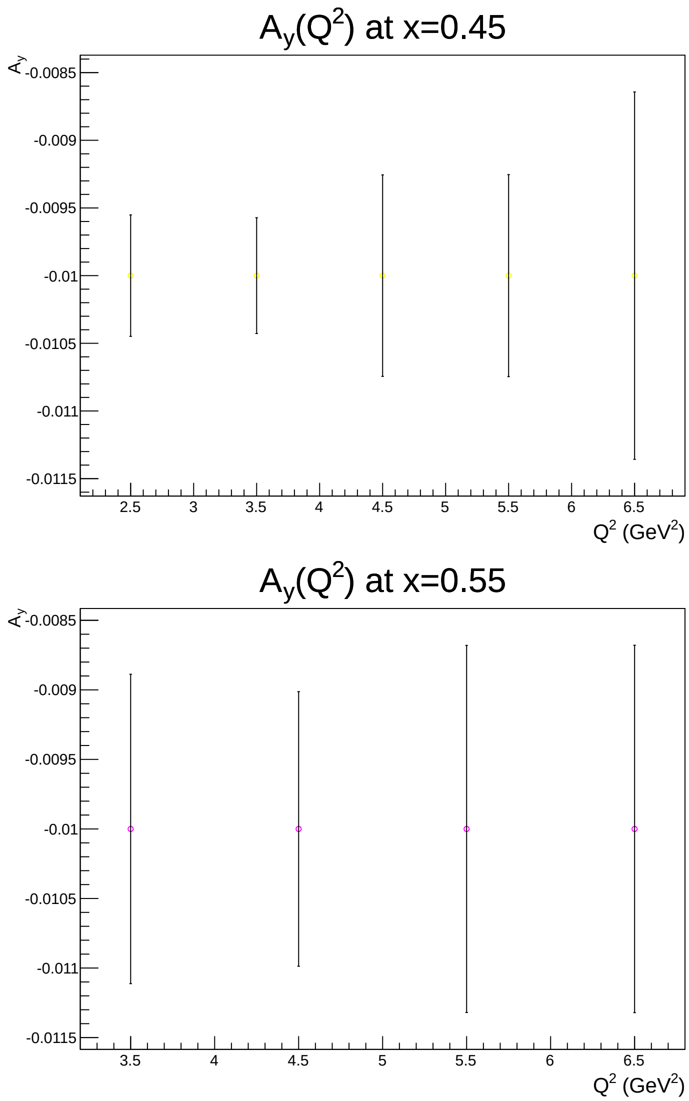

Figure 44: A_y vs Q^2 at $x = 0.45$ and 0.55 for the NH_3 target at 11 GeV.

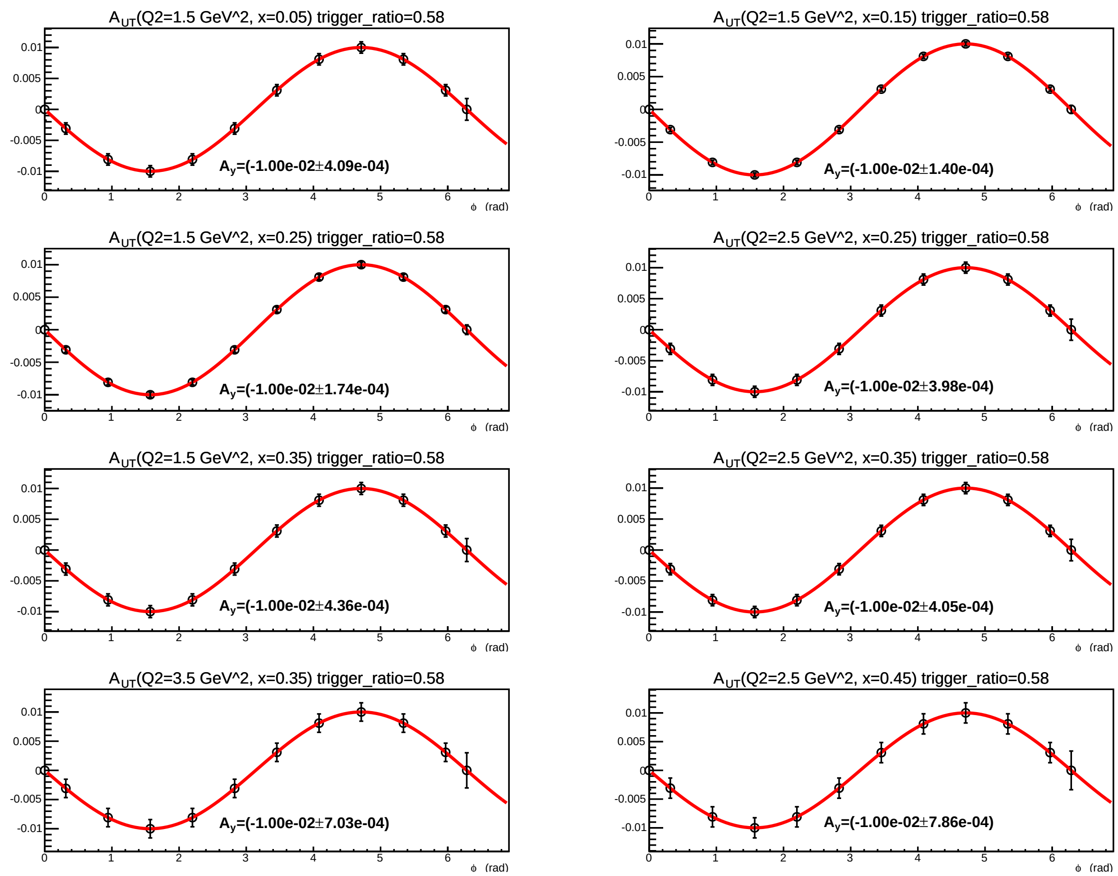

Figure 45: A_{UT} at different Q^2 and x for the NH_3 target at 8.8 GeV. Here $0.05 < x < 0.45$.

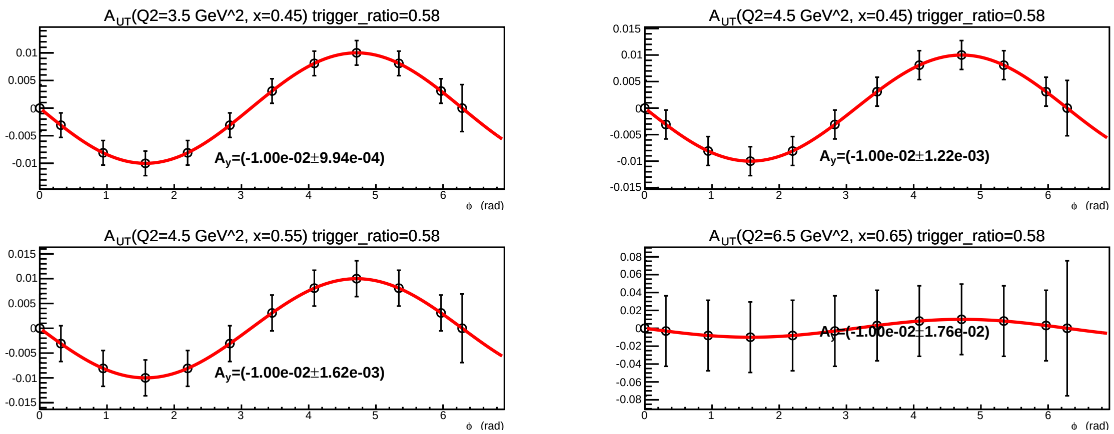

Figure 46: A_{UT} at different Q^2 and x for the NH_3 target at 8.8 GeV. Here $0.45 < x < 0.65$.

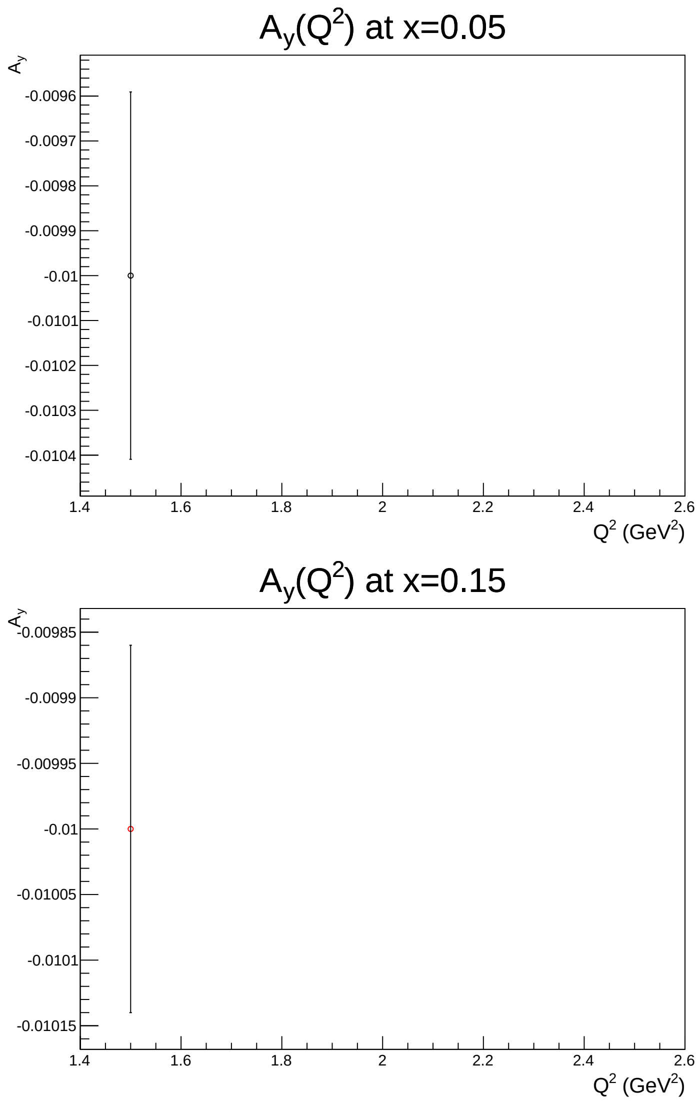

Figure 47: A_y vs Q^2 for $x = 0.05$ and 0.15 for the NH_3 target at 8.8 GeV.

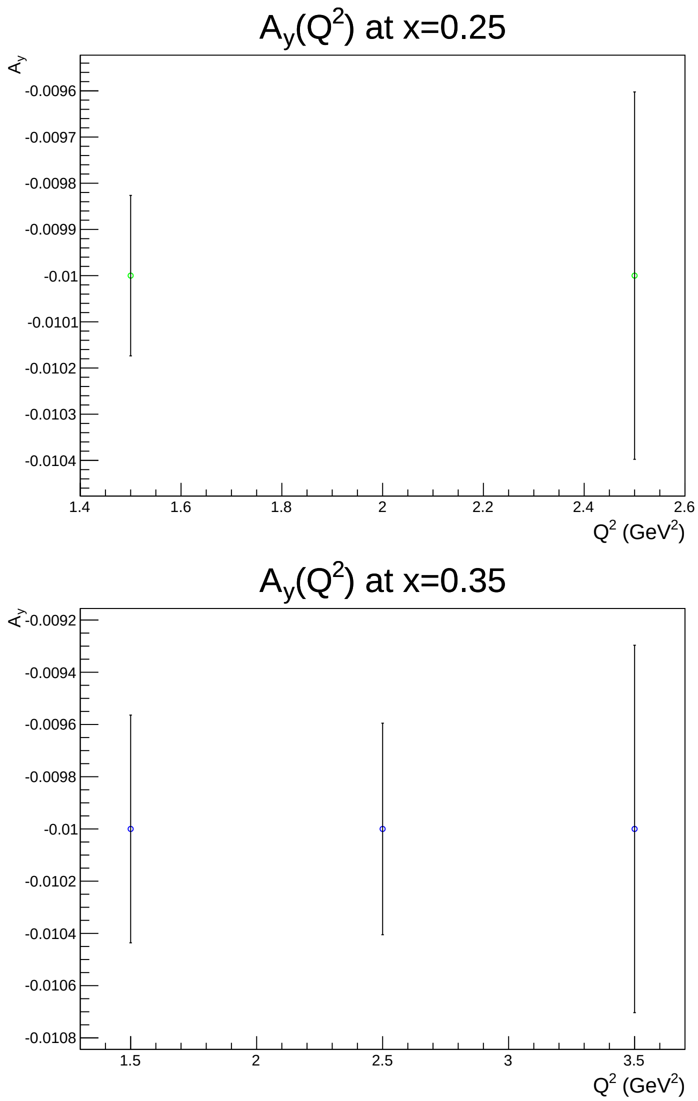

Figure 48: A_y vs Q^2 for $x = 0.25$ and 0.35 for the NH_3 target at 8.8 GeV.

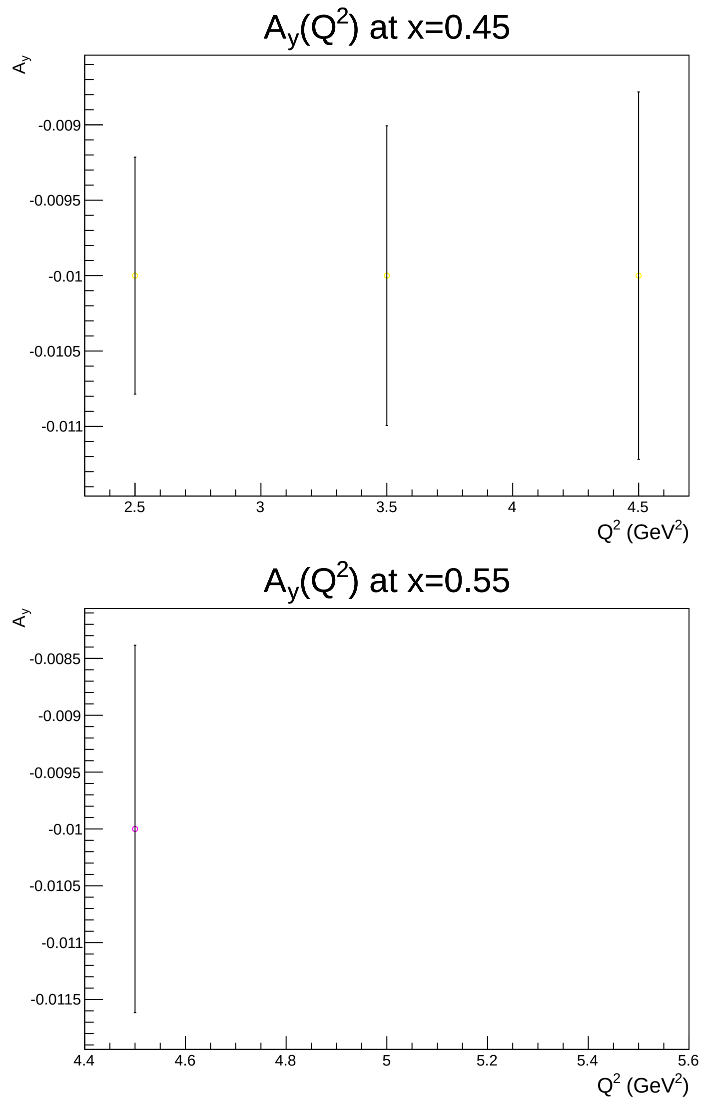

Figure 49: A_y vs Q^2 for $x = 0.45$ and 0.55 for the NH_3 target at 8.8 GeV.

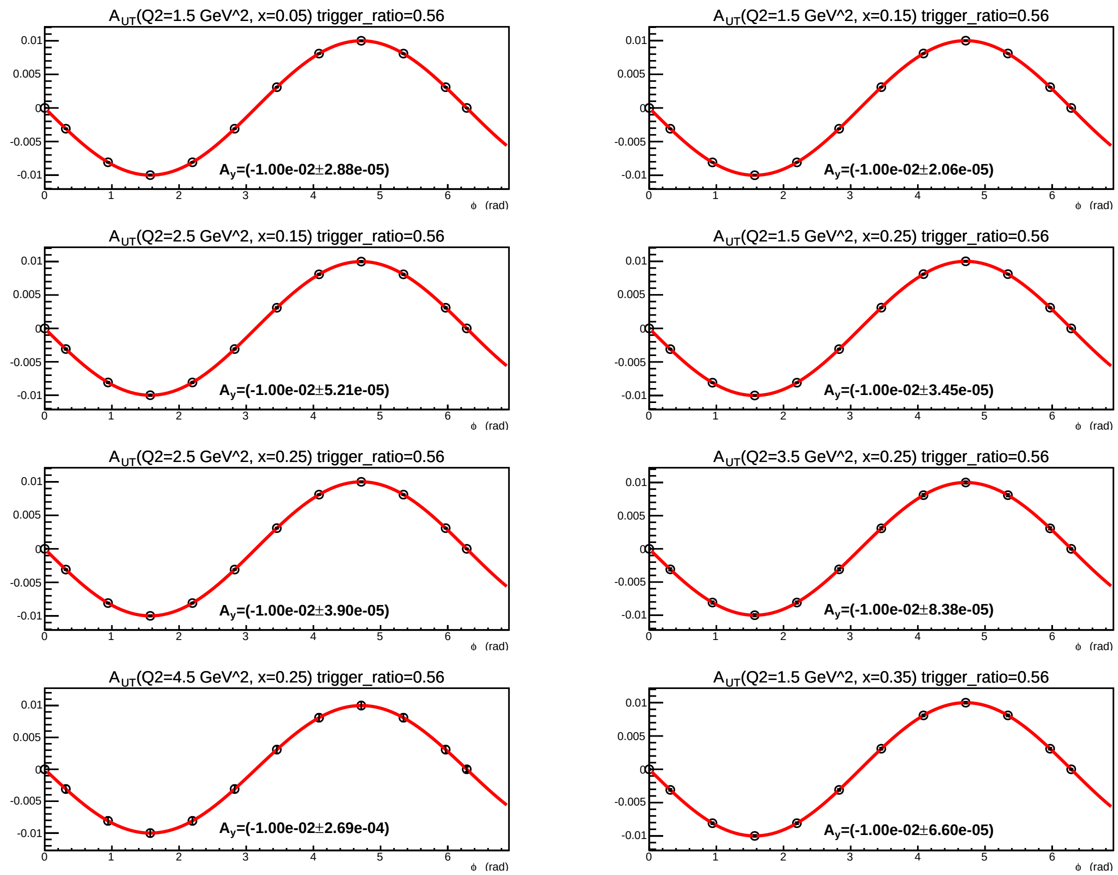

Figure 50: A_{UT} at different Q^2 and x for the ^{3}He target at 11 GeV. Here $0.05 < x < 0.35$.

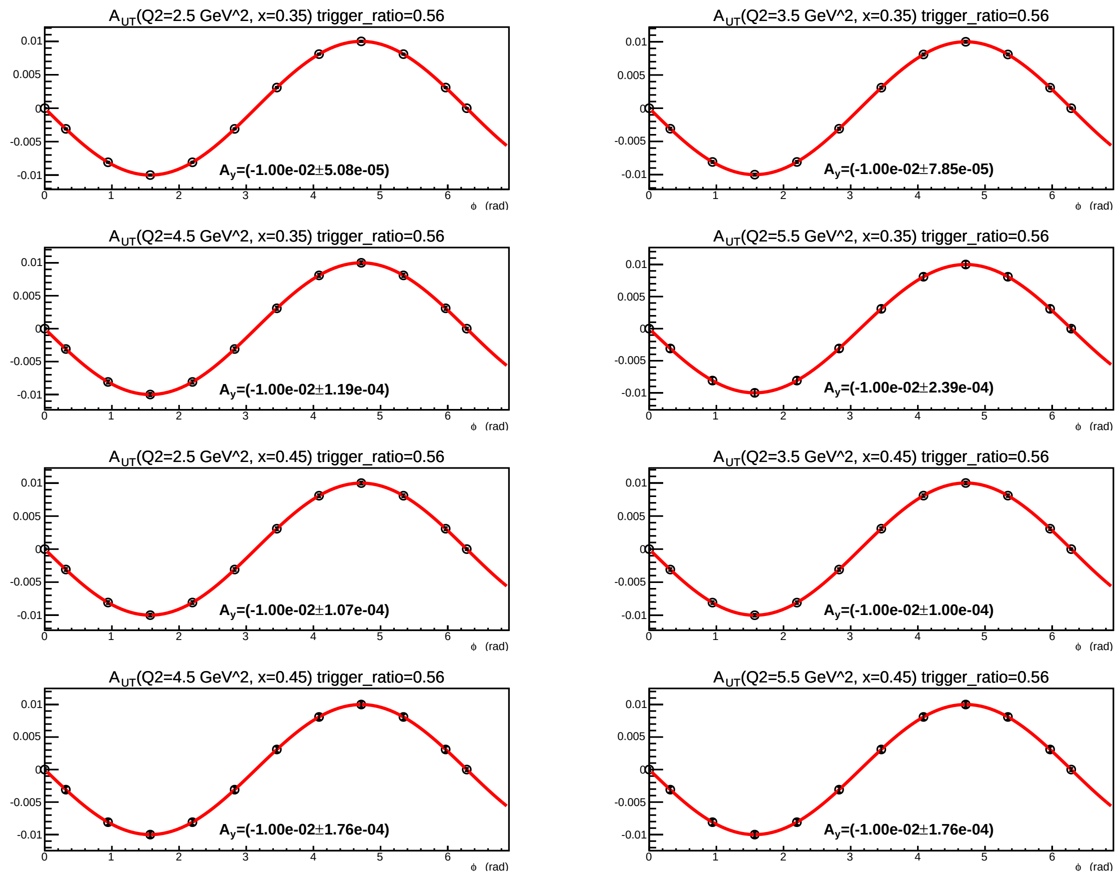

Figure 51: A_{UT} at different Q^2 and x for the ^{3}He target at 11 GeV. Here $0.35 < x < 0.45$.

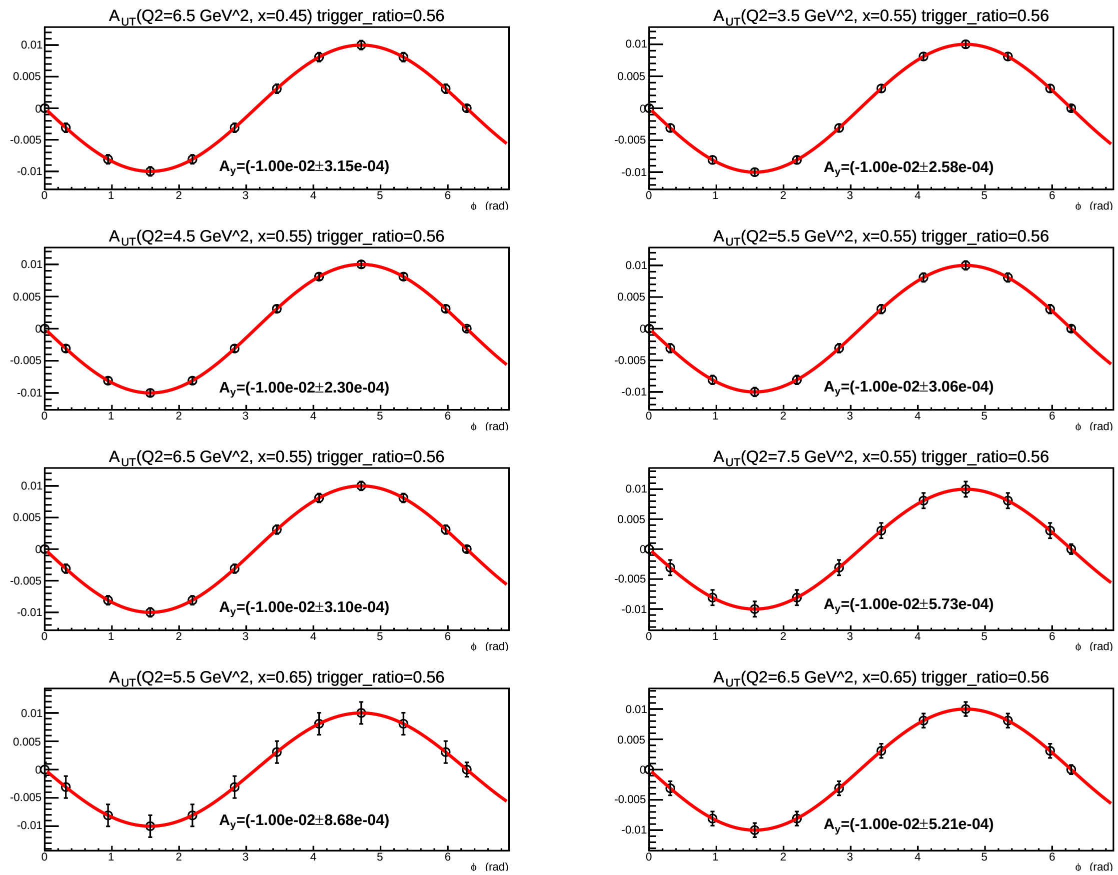

Figure 52: A_{UT} at different Q^2 and x for the ^{3}He target at 11 GeV. Here $0.45 < x < 0.65$.

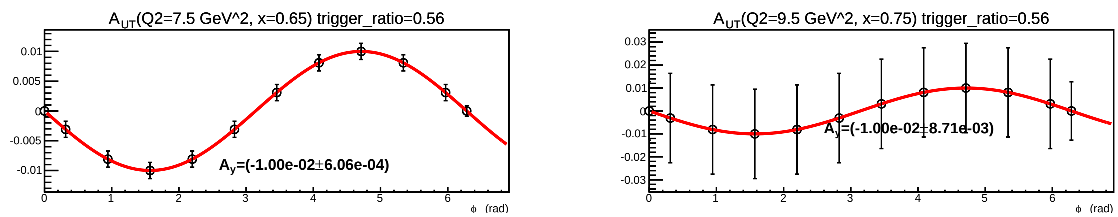

Figure 53: A_{UT} at different Q^2 and x for the ^{3}He target at 11 GeV. Here $0.65 < x < 0.75$.

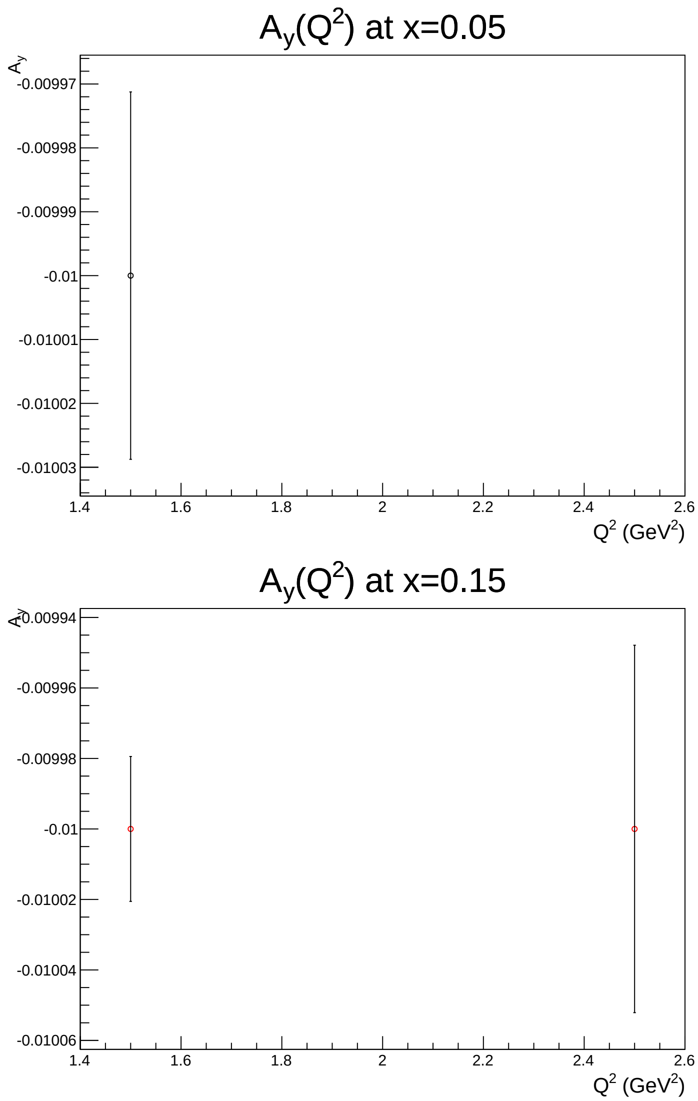

Figure 54: A_y vs Q^2 for $x = 0.05$ and 0.15 for the ^{3}He target at 11 GeV.

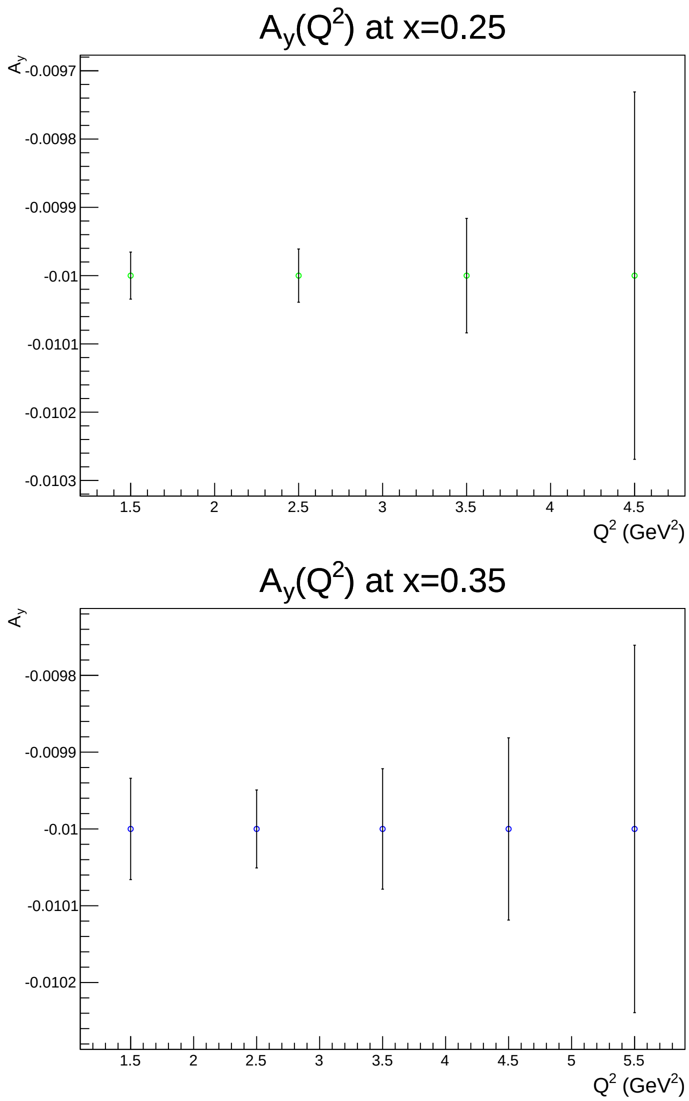

Figure 55: A_y vs Q^2 for $x = 0.25$ and 0.35 for the ^{3}He target at 11 GeV.

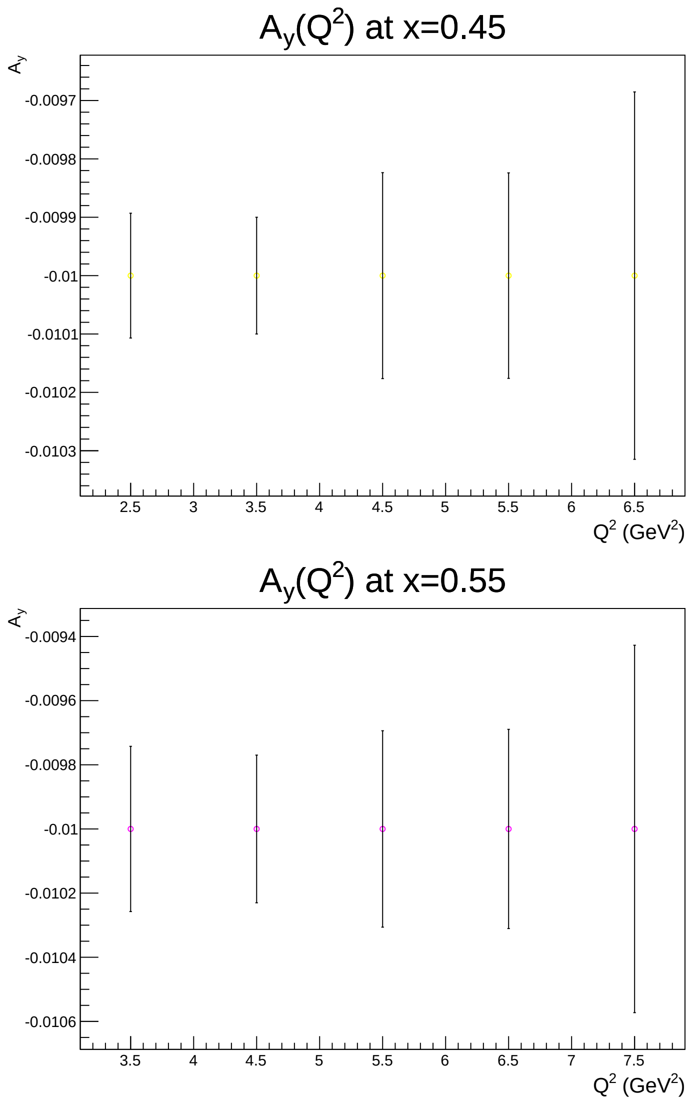

Figure 56: A_y vs Q^2 for $x = 0.45$ and 0.55 for the ^{3}He target at 11 GeV.

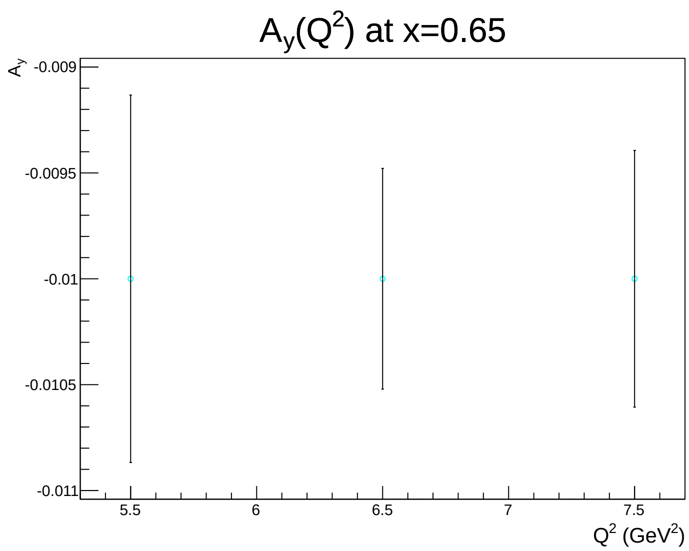

Figure 57: A_y vs Q^2 for $x = 0.65$ for the ^{3}He target at 11 GeV.

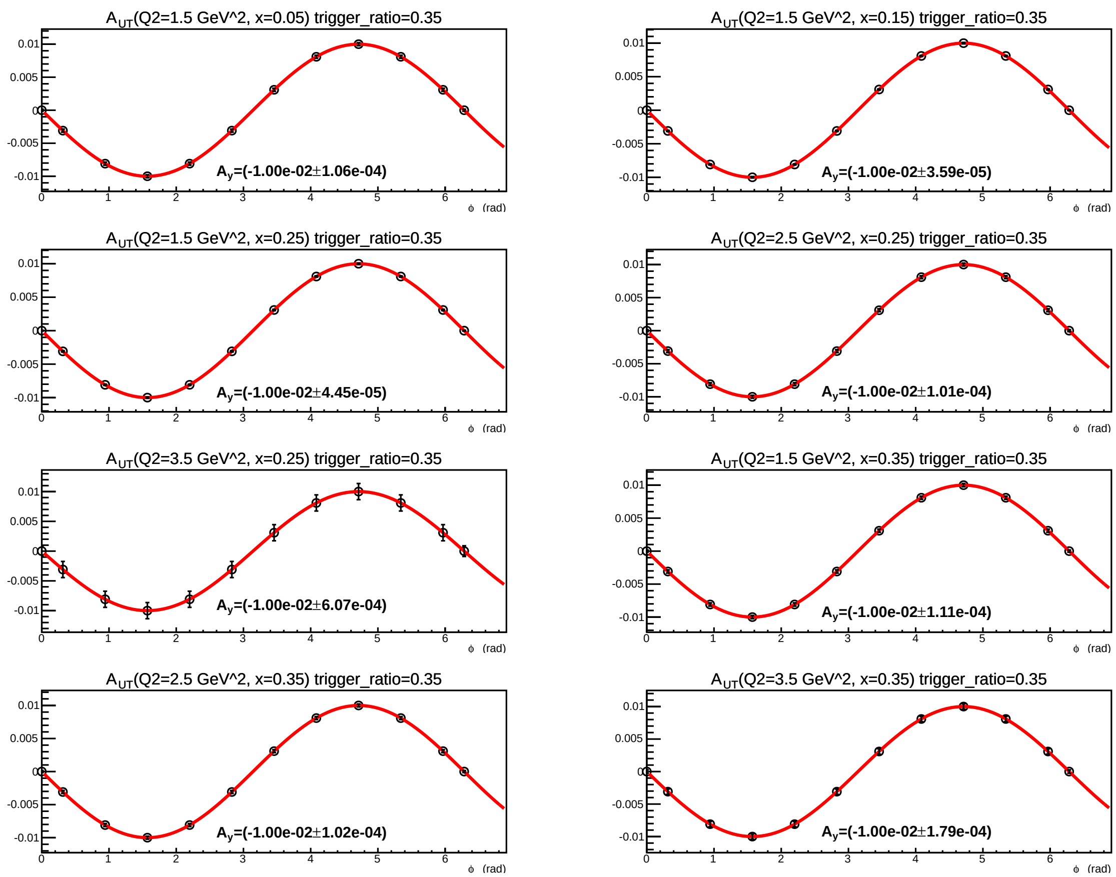

Figure 58: A_{UT} at different Q^2 and x for the ^{3}He target at 8.8 GeV. Here $0.05 < x < 0.35$.

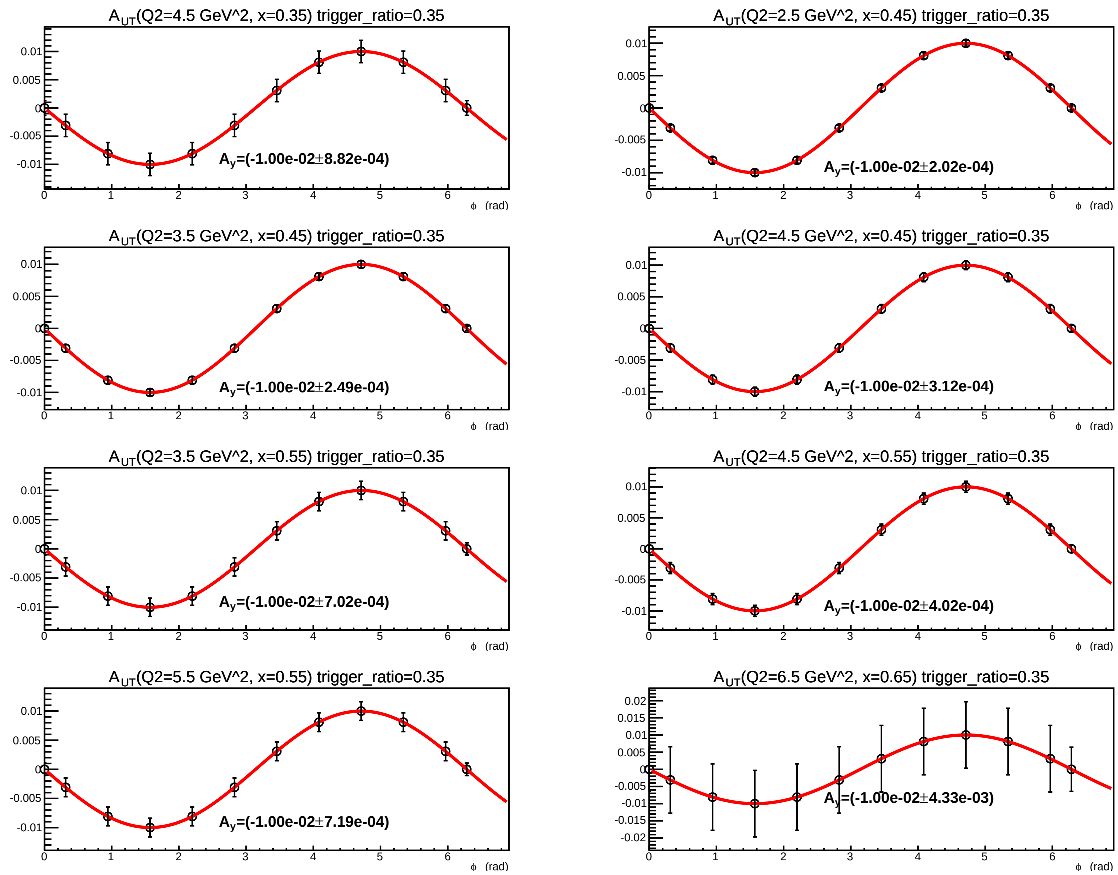

Figure 59: A_{UT} at different Q^2 and x for the ^{3}He target at 8.8 GeV. Here $0.35 < x < 0.65$.

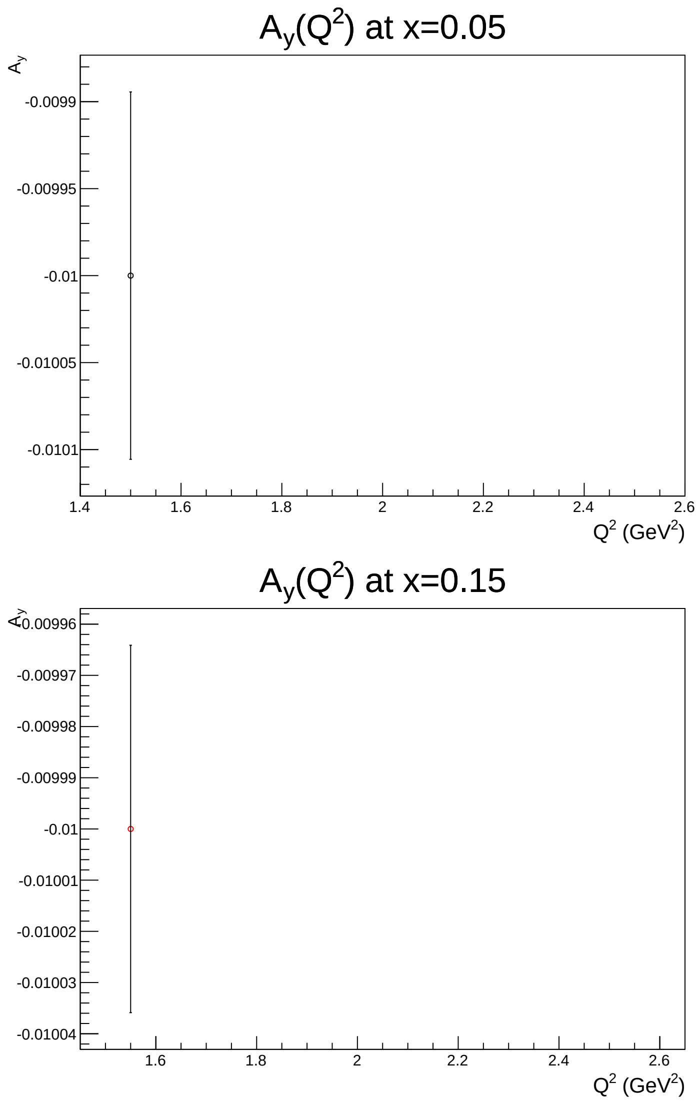

Figure 60: A_y vs Q^2 at different x for the ^{3}He target at 8.8 GeV.

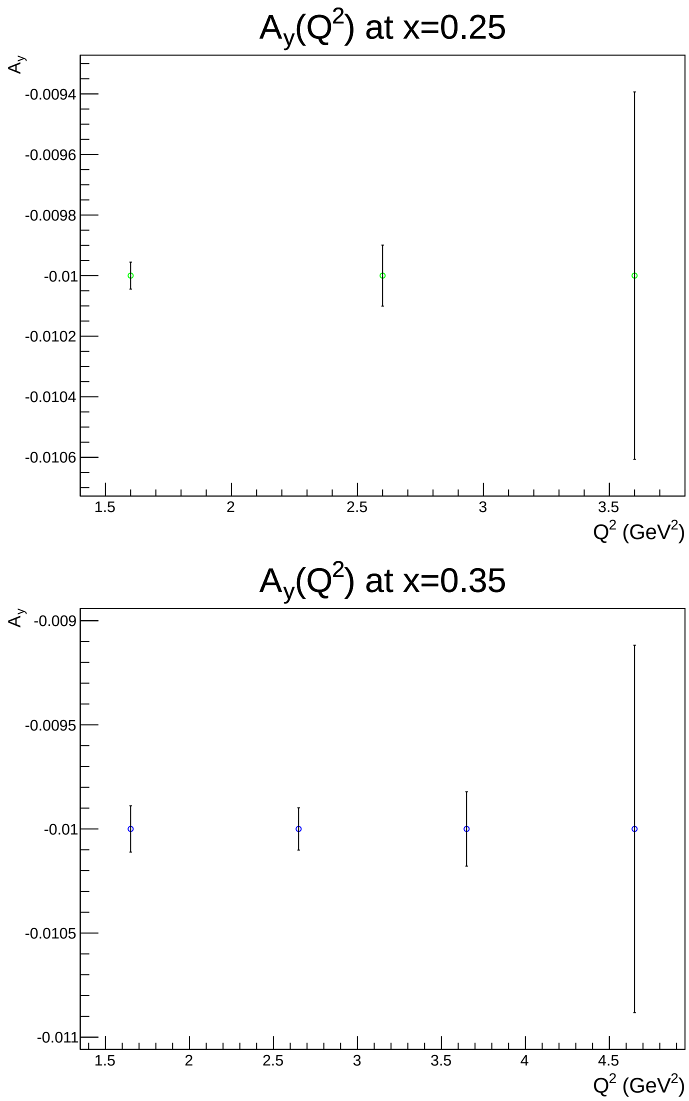

Figure 61: A_y vs Q^2 at different x for the ^{3}He target at 8.8 GeV.

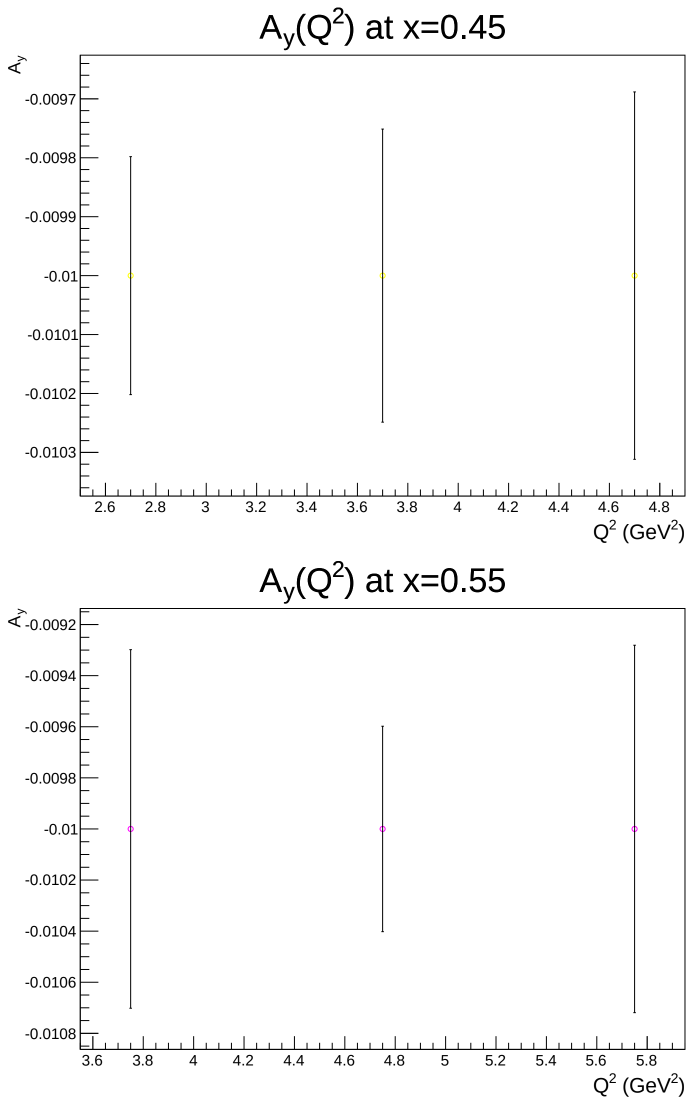

Figure 62: A_y vs Q^2 at different x for the ^{3}He target at 8.8 GeV.

References

[1] J. Arrington, Phys. Rev. **C68** (2003) 034325.

[2] J. Arrington, P. Blunden and W. Melnitchouk, Prog. Part. Nucl. Phys. 66 (2011) 782.

[3] M.E. Christy *et al*, Phys. Rev. C70 (2004) 015206.

[4] I.A. Qattan*et al*, Phys. Rev. Lett. 94 (2005) 142301.

[5] A.J.R. Puckett *et al*, Phys. Rev. C85 (2012) 045203.

[6] P.G. Blunden, W. Melnitchouk, and J.A. Tjon, Phys. Rev. Lett. 91 (2003) 142304.

[7] Y.C. Chen, A. Afanasev, S.J. Brodsky, C.E. Carlson and M. Vanderhaeghen, Phys. Rev. Lett. 93 (2004) 122301.

[8] C.E. Carlson and M. Vanderhaeghen, Annu. Rev. Nucl. Part. Sci. 57 (2007) 171.

[9] N. Christ and T.D. Lee, Phys. Rev. 143 (1966) 1310.

[10] R.N. Cahn and Y.S. Tsai, Phys. Rev. **D2** (1970) 870.

[11] A. Afanasev, M. Strikman and C. Weiss, Phys. Rev. **D77** (2008) 014028.

[12] Alessandro Bacchetta, Umberto D'Alesio, Markus Diehl, C. Andy Miller, Phys. Rev. **D70**, 117504 (2004).

[13] A. Metz *et al.*, Phys. Rev. **D86** (2012) 094039.

[14] J.R. Chen, J. R. *et al.*, Phys. Rev. Lett. 21 (1968) 1279.

[15] S. Rock *et al*, Phys. Rev. Lett. 24 (1970) 748.

[16] M. Schlegel, Phys.Re*et a.*, Phys. Rev. **C70** (2004) 065207.

[17] A. Airapetian *et al*, Phys. Lett. **B682** (2010) 351.

[18] J. Katich *et al.*, `http://arxiv.org/abs/1311.0197`.

[19] E. Babcock *et al.*, Phys. Rev. Lett. 91 (2003) 123003.

[20] M.V. Romalis and G.D. Cates, Phys. Rev. **A58** (1998) 3004.

[21] M. Mihovilovic *et al*, Nucl. Instrum. Meth. **A686** (2012) 20.

[22] J. Alcorn *et al*, Nucl. Instrum. Meth. **A522** (2004) 294.

[23] S. Scopetta, Phys. Rev. **D75** (2007) 054005.

[24] X. Zheng *et al.*, Phys. Rev. **C70** (2004) 065207.

[25] E12-10-006, "Target Single Spin Asymmetry in Semi-Inclusive Deep-Inelastic $(e, e'\pi^{\pm})$ on a Transversely Polarized ^{3}He Target at 8.8 and 11 GeV", Spokesperson: J.-P. Chen, H. Gao (contact), X. Jiang, J.-C. Peng, and X. Qian.

[26] E12-11-108 "Target Single Spin Asymmetry in Semi-Inclusive Deep-Inelastic $(e, e'\pi^{\pm})$ on a Transversely Polarized Proton Target", Spokespersons: K. Allada, J.-P. Chen, H. Gao (contact), Z.-E. Meziani, and X.-M. Li.

[27] The SoLID Collaboration, `http://hallaweb.jlab.org/12GeV/SoLID/download/doc/solid_precdr.pdf`.

[28] E12-11-007, "Asymmetries in Semi-Inclusive Deep-Inelastic $(e, e'\pi^{\pm})$ Reactions on a Longitudinally Polarized ^{3}He Target at 8.8 and 11 GeV", Spokesperson: J.-P. Chen, J. Huang (contact), Y. Qiang, and W.-B. Yan.

[29] L. W. Whitlow, SLAC-Report-357 (1990).

[30] J. W. Lightbody and J. S. O'Connell, Computers in Physics 2, 57 (1988).

[31] D. E. Wiser, Ph. D. thesis, Univ. of Wisconsin (1977).

[32] GEANT4, `http://geant4.cern.ch/`.

[33] Gemc, `https://gemc.jlab.org/`.

[34] Poisson superfish, `http://laacg1.lanl.gov/laacg/services/download_sf.phtml`.

[35] Tosca,
http://www.chilton-computing.org.uk/inf/eng/electromagnetics/p001.htm.

[36] J.Huston H.L. Lai P. Nadolsky W.K. Tung J. Pumplin, D.R. Stump. *JHEP*, 0207:12, 2002.

[37] D.E. Wiser. PhD thesis, University of Wisconsin-Madison, 1977.

[38] X. Qian *et al.*, Phys. Rev. Lett. 107, (2012) 072003. J. Huang *et al.*, Phys. Rev. Lett. 108 (2012) 052001.

[39] T.D. Averett, *et al.*, Nucl. Instr. and Meth. A 427 (1999) 440.

[40] J. Maxwell *et al.*, to be submitted to Nucl. Instr. and Meth. A.

[41] D.G. Crabb, C.B. Higley, A.D. Krisch, R.S. Raymond, T. Roser, and J.A. Stewart, Phys. Rev. Lett. 64, (1990) 2627.

[42] C.D. Keith, *et al.*, Nucl. Instr. and Meth. A 684 (2012) 27.

[43] C.D. Keith, *et al.*, Nucl. Instr. and Meth. A 501 (2003) 327.

[44] Design Report rfq 14231, Oxford Instruments Nanotechnology Tools Ltd.

[45] S. Riordan, https://hallaweb.jlab.org/wiki/index.php/Solid_eventgenerator.

[46] P. Hautle *et al.* Proceedings of the Workshop on the Polarized Drell-Yan Process, Sante Fe, New Maxico, 2010 (to be published).

[47] L.W. Mo and Y.S. Tsai, Rev. Mod. Phys. 41 (1969) 205.